I.O.S.

A NUMERICAL MODEL OF THE TURBULENT BOUNDARY LAYER BENEATH SURFACE WAVES AND TIDES

BY

H. L. KING, A. G. DAVIES

AND R. L. SOULSBY

REPORT NO. 196

1985

NATURAL ENVIRONMENT RESEARCH COUNCIL

INSTITUTE OF OCEANOGRAPHIC SCIENCES

INSTITUTE OF OCEANOGRAPHIC SCIENCES

Wormley, Godalming,
Surrey, GU8 5UB.
(0428 - 79 - 4141)

(Director: Dr. A.S. Laughton FRS)

Bidston Observatory,
Birkenhead,
Merseyside, L43 7RA.
(051 - 653 - 8633)

(Assistant Director: Dr D.E. Cartwright FRS)

Crossway,
Taunton,
Somerset, TA1 2DW.
(0823 - 86211)

(Assistant Director: M.J. Tucker)

When citing this document in a bibliography the reference should be given as follows:-

KING, H.L., DAVIES, A.G. & SOULSBY, R.L. 1985 A numerical model of the turbulent boundary layer beneath surface waves and tides.
Institute of Oceanographic Sciences, Report, No. 196, 90pp.

IOS Report 196, 1985

Errata

p 11, Eq (7a)	$z_o b_1^{-\frac{1}{2}}$ instead of $z_o b^{-\frac{1}{2}}$
p 86, Figure 22	The heights indicated in the ellipses are correct. The order of printing of the ellipses has been accidentally reversed.

INSTITUTE OF OCEANOGRAPHIC SCIENCES

TAUNTON

A numerical model of the turbulent boundary layer beneath surface waves and tides

by

H.L. King, A.G. Davies

and R.L. Soulsby

I.O.S. Report No. 196

1985

This study was supported financially by the Department of the Environment

Contents

List of Symbols

a	Semi-major axis of the tidal ellipse
$A=U_c/\omega$	Excursion amplitude of the wave oscillation
b	Turbulent energy
b/a	Ellipticity of the tidal ellipse (=semi-minor/semi-major axis)
c_o, c_1	Empirical constants used in the turbulent closure scheme
f_w	Wave friction factor
K	Eddy viscosity
$k_s=30z_o$	Equivalent roughness of the bed surface
l	Mixing length
m	Index for the computational levels in the model
n	Time-step number
R_z	The ratio z_1 / z_o
t	Time, $t'=\omega t$ gives the phase angle
u,v	Horizontal velocity components
U,V	Horizontal components of the forcing flow
U_c, V_c	Amplitudes of U and V
$W_x=u-U$ $W_y=v-V$	Components of defect velocity
z	Height above the bed
z_o	Roughness length
z_1	Height of the water surface above the bed
z_*	Constant in the depth transform
ζ	Transformed height above the bed
α_b	Constant governing the diffusion of turbulent energy
γ	Orientation angle of the tidal ellipse
δ	Boundary layer thickness (δ_1, δ_b, etc.)
$\delta\zeta'$, $\delta t'$	Discretisation intervals for height and time ($t'=\omega t$), respectively
Δ_z, Δ_n	Difference estimates, with respect to height and time, used to compare solutions
ε	Rate of dissipation of turbulent energy
θ	Phase lead of bed shear stress over the forcing free-stream flow
κ	Von Karman's constant
λ	Coriolis parameter
μ, σ	Mean and standard deviation of a sample, respectively
ρ	Density of water
τ_u, τ_v	Components of shear stress in the directions of the velocity components u and v, respectively
ϕ	Phase of V with respect to U
Ψ	'Phase' of the tidal ellipse
ω	Frequency of the fundamental oscillation

Abstract

A numerical model is presented for horizontally uniform, turbulent, oscillatory flow above a flat rough bed. It is applied to cases of surface wave-induced and tidal boundary-layer flows. The formulation of the problem involves the governing horizontal momentum equations, and closure assumptions which relate the turbulent shear stresses to the mean velocity gradients in the flow. The closure scheme adopted, for whatever application of the model, is a fairly standard description of the turbulence field in terms of the turbulent energy equation. This equation, together with various turbulence scaling laws, allows the eddy viscosity to be determined as a function of height and phase angle in the wave cycle. The calculated eddy viscosity distribution is used in the finite difference solution of the governing momentum equations.

Although some comparisons with experimental and theoretical results are described, the main emphasis of the present report is on the capability and performance of the numerical model. Initially, the formulation and finite difference scheme is discussed. Next, results for rectilinear, 'deep', wave-induced flows are presented, for which the boundary-layer is contained within the flow region being modelled. Here comparisons are made with exact analytic solutions and with previous experimental results. Finally, results for oscillations of tidal period in shallow water, including the effects of rotation, are presented, for which the boundary layer occupies the entire flow region from the bed to the free water surface. The present model results are compared both with results from a previous numerical model and with a set of current meter observations.

It is concluded that the model is a useful tool for the study of rough turbulent oscillatory boundary-layers, and that it predicts quite well the gross features of both surface wave-induced and tidal flows.

1. Introduction.

Previous studies of oscillatory rough turbulent boundary-layer flow have been based on both analytic and numerical models. Such models have been developed principally to determine the velocity and shear stress fields in surface wave-induced and tidal flows. The results have been used to quantify, for example, drag coefficients, boundary-layer thicknesses and phase leads of bed shear stress over the oscillating free-stream flow or pressure gradient. Ultimately, model results may be used to calculate energy dissipation rates in turbulent oscillatory flows, and to estimate sediment transport rates.

The formulation is very similar for the wave and tidal cases, but while the earth's rotation can be ignored in the wave problem and, hence, only one velocity component need be considered, in the tidal case rotation is important and two horizontal velocity components must be included. In addition, of course, the oscillation periods are very different in the two cases.

Analytical models of the oscillatory boundary-layer are necessarily based on simplified representations of the turbulent flow above the bed. The solutions obtained have generally been based on simple prescriptions for the eddy viscosity. For example, for oscillatory turbulent flow above a flat rough bed, the assumption of an eddy viscosity which is constant in both time and space gives rise to a turbulent 'shear wave' solution, akin to the solution presented by Lamb (1932, Art. 345) for laminar flow. A much more realistic description, based on standard scaling arguments for turbulent flow, involves the eddy viscosity increasing linearly with height above the bed. An analytical solution has been obtained on this basis by Smith (1977) for the wave case, and by Prandle (1982) and Soulsby (1983) for the tidal case. Similar solutions based upon rather more elaborate, though steady, representations for the eddy viscosity have been obtained by Kajiura (1968), Johns (1969), Brevik (1981) and Long (1981).

More realistic time-varying formulations for the eddy viscosity, based upon representations of the Reynolds' stress in terms of Prandtl's mixing length hypothesis, have been adopted by Bakker (1975) and Johns (1975). However these approaches have relied, ultimately, on numerical computations in the solution of the problem. More recently, Johns (1977) has used finite-difference methods to solve the momentum and turbulent energy equations for oscillatory boundary-layer flow. In particular, he has calculated the bed shear stress, and has derived an expression for the wave drag coefficient in terms of the bottom roughness.

The present report is also concerned with a numerical (finite-difference) model of rough turbulent oscillatory boundary-layer flow, and results have been obtained for the cases of surface wave-induced and tidal flows. It has not been the aim of the study to develop a new turbulence model. Rather, a standard formulation closely similar to that of Vager and Kagan (1969), Johns (1977) and others, has been adopted. The model is for uniform, rough turbulent, oscillatory flow above a flat bed; effects associated with variations in bottom topography and surface elevation are not treated. The early results were obtained for rectilinear (one-dimensional), 'deep', wave-induced flows for which the boundary-layer was contained within the flow region modelled. Subsequently, results were obtained for

two-dimensional oscillations of tidal period in shallow water, for which the boundary-layer occupied the entire flow region from the bed to the free water surface. The same turbulence formulation was adopted for both cases. It follows that results for the combined effects of waves superimposed on a current may be obtained on the basis of the present model, though such results are not presented in this report.

The common core of the model, for whatever application, consists of the governing horizontal momentum equations. These include acceleration, rotation, friction and forcing terms, but neglect advective terms since the flow is assumed to be horizontally uniform. The turbulence closure assumption involves the description of the turbulence field in terms of the turbulent energy equation and various turbulence scaling laws. On this basis, the eddy viscosity is determined as a function of height and phase angle in the cycle, and it is then used directly in the finite difference scheme for the solution of the horizontal momentum equations. The philosophy underlying the model is that it should provide an adequate and accurate description of the processes in the boundary-layer, while being no more complicated than can be justified by the present capability of making laboratory and field observations to verify the principal assumptions on which it is based. The turbulence model describes the generation, diffusion and dissipation of turbulence energy which, potentially at least, is a measurable quantity in the field. The relationships between the turbulence energy, eddy viscosity and mixing length are less readily verifiable, but have been found to be adequate by several previous workers. Smith and Takhar (1977), comparing three tidal models with increasing degrees of complexity of turbulence closure, found that the simplest of the three gave as good agreement with data as the more complex ones, and accordingly a model with that level of closure has been adopted here.

The central aim of the present report is to describe in some detail both the method adopted in the solution of the governing differential equations, and also the performance of the model. For potential users of such a model, the report should provide a suitable introduction to its capabilities. Initially, in Section 2, the formulation is presented, and the finite difference method of solution is discussed. Two depth transform options (logarithmic and log-linear) are discussed, and detailed comments are made about the selection of the time/space grid and about the various problems wich may arise in running the model. In Sections 3.1 to 3.7 results are presented for a series of tests carried out with a simplified version of the model, corresponding to the uniform rectilinear oscillation of a 'deep' flow above a flat rough bed. In Section 3.1 the full turbulence closure scheme is replaced by an eddy viscosity which is assumed to be constant in both time and space. The model results obtained on this basis are compared with an exact analytical solution (cf. Lamb, 1932, Art. 345). This provides a check on the finite-difference method of solution, though the unsuitabilty of a logarithmic grid for this example leads to some discrepancies. In Section 3.2 a similar comparison is made, but with an analytical solution based on an eddy viscosity which increases linearly with height above the bed (Smith, 1977). For this more appropriate assumption for use with a logarithmic grid, rather closer agreement is achieved between the analytical and numerical solutions. In Section 3.3 the full turbulence closure scheme is reinstated, and some tests are conducted with different choices for the time and space grids.

Next, in Section 3.4 the model results are compared with measurements of horizontal velocity made in an oscillating water tunnel by Jonsson and Carlsen (1976). Despite some difficulty in forming an adequate basis for comparing the model and experimental results, good agreement is found. In Section 3.5 results based upon various representations for the dissipation term in the turbulent energy equation are compared. Also, results based upon the time-varying mixing length formulation adopted in the model are compared with model results obtained with a steady mixing length which simply increases with height above the bed; the results of this comparison indicate that the model is rather insensitive to the choice of mixing length. In Section 3.6 results are presented for the wave drag coefficient, the boundary-layer thickness and the phase lead of the bed shear stress over the free-stream oscillation. Where possible, comparisons have been made with previous experimental and theoretical results, and the agreement is generally reasonable. Next, in Section 3.7 the sensitivity of the model is assessed in relation to variations in three constants in the turbulence closure scheme. In principle, these constants may be used to tune the model for particular applications. In Section 3.8 results are presented for a simple rectilinear oscillation of tidal frequency in shallow water. The emphasis here is on variations in the model results associated with different representations for the dissipation term in the turbulent energy equation. A more comprehensive examination of model results for waves of tidal frequency, including the effects of rotation, is described in Section 4. Firstly, in Section 4.1 the present model results are compared with the equivalent model results of Vager and Kagan (1969). Although the formulation is the same, the results differ somewhat, most probably due to the very different choices adopted for the grid levels. Finally, in Section 4.2 the model results are compared with a set of current meter observations made near the Scillies. In general the agreement is good, though some detailed aspects of the observations are not reproduced by the model.

2. Model Description.

The model presented here is for uniform oscillatory rough turbulent boundary-layer flow in water of finite depth. The formulation is essentially the same as that of Vager and Kagan (1969), and is similar to that of Johns (1977). The derivation of the equations and the closure scheme are discussed by these and other authors, and will not be attempted here. However, the details of normalisation and discretisation of the governing equations differ. The model is driven by the oscillatory current forcing the system, and requires values for the water depth and the bed roughness. The specified current is used to determine the horizontal level gradients driving the flow. The surface elevation does not vary in the model; in other words, depth variations associated with the forcing flow are assumed to be negligible.

The governing equations are as follows :

$$\frac{\partial u}{\partial t} - \lambda v = \frac{dU}{dt} - \lambda V + \frac{\partial}{\partial z}\left(K\frac{\partial u}{\partial z} \right) \qquad (1)$$

$$\frac{\partial v}{\partial t} + \lambda u = \frac{dV}{dt} + \lambda U + \frac{\partial}{\partial z}\left(K\frac{\partial v}{\partial z} \right) \qquad (2)$$

Terms: Acceln | Coriolis | Driving Force | Friction

with $U = U_o \cos(\omega t)$ and $V = V_o \cos(\omega t - \phi)$

where (u,v), t, z and K are the horizontal components of velocity, the time, the height above the bed and the eddy viscosity repectively; λ is the Coriolis parameter; and the components of the forcing flow (U,V) are defined by their amplitudes (U_o, V_o), their relative phase difference ϕ and the frequency ω.

The boundary conditions on (1) and (2) are of zero velocity at the bed ($z = z_o$) and zero stress at the free surface ($z = z_1$) :

$$\begin{aligned} (u,v) &= (0,0) \quad \text{at } z = z_o \text{ (roughness length)} \\ \text{and} \quad K\frac{\partial u}{\partial z} &= K\frac{\partial v}{\partial z} = 0 \quad \text{at } z = z_1 \quad \text{(free surface)}^{*}. \end{aligned} \qquad (3)$$

The components of shear stress τ_u and τ_v are defined throughout the depth by :

---

* In the earliest test runs with a one-dimensional model, an alternative surface boundary condition u = U at $z = z_1$ was used. This is appropriate when the boundary-layer is contained within $[z_o, z_1]$.

$$\frac{\tau_u}{\rho} = K\frac{\partial u}{\partial z} \quad \text{and} \quad \frac{\tau_v}{\rho} = K\frac{\partial v}{\partial z} \text{ where } \rho \text{ is the water density.} \tag{4a}$$

The bed shear stress can also be determined from the depth integrated defect equations of motion, derived from (1) and (2) :

$$\begin{aligned} \frac{\tau_{ou}}{\rho} &= -\left\{\frac{\partial \bar{W}_x}{\partial t} - \lambda \bar{W}_y\right\} \\ \frac{\tau_{ov}}{\rho} &= -\left\{\frac{\partial \bar{W}_y}{\partial t} + \lambda \bar{W}_x\right\} \end{aligned} \tag{4b}$$

where $W_x = u-U$, $W_y = v-V$ and $\bar{f} = \int_{z_o}^{z_1} f \, dz$.

The closure of Equations (1) and (2) is achieved by relating the eddy viscosity K empirically to a mixing length l and the turbulent energy b. The turbulent energy equation, incorporating the rate of dissipation of energy ε as a function of l and b, can be used together with an intrinsic relationship for mixing length to complete the system of equations. The equations which comprise the turbulence closure scheme in the model are:

$$\frac{\partial b}{\partial t} = K\left\{\left(\frac{\partial u}{\partial z}\right)^2 + \left(\frac{\partial v}{\partial z}\right)^2\right\} + \alpha_b \frac{\partial}{\partial z}\left(K\frac{\partial b}{\partial z}\right) - \varepsilon \ , \tag{5}$$

Terms: Generation | Diffusion | Dissipation

$$\varepsilon = \frac{c_1 b^{3/2}}{l} \ , \qquad K = c_o l \sqrt{b} \ , \tag{6}$$

and

$$l = -\kappa \frac{b^{1/2}}{1}\left\{\frac{\partial}{\partial z}\frac{b^{1/2}}{1}\right\}^{-1} \tag{7}$$

where κ is the Von Karman constant and α_b, c_o and c_1 are constants**.

The boundary conditions on (5) are of zero energy flux across the bed and free surface :

$$\alpha_b K \frac{\partial b}{\partial z} = 0 \quad \text{at } z = z_o \quad \text{and} \quad z = z_1 \ . \tag{8a}$$

** Constant values : $\alpha_b = 0.73$, $c_o = (0.046)^{1/4}$, $c_1 = (0.046)^{3/4}$ and Von Karman's constant $\kappa = 0.4$, taken from Vager and Kagan (1969).

The near bed condition on (7) is that 1 and z_o are related by :

$$1 \rightarrow \kappa z_o \quad \text{as} \quad z \rightarrow z_o . \tag{8b}$$

Using (8b), Equation (7) can be integrated to the form

$$1 = \kappa b^{1/2} \left\{ \int_{z_o}^{z} b^{-1/2} \, dz + z_o b^{-1/2} \right\}, \tag{7a}$$

which is more easily implemented in the model than (7) itself; an Euler-Maclaurin summation has been used to evaluate the integral in (7a).

The variables were non-dimensionalised, and then a depth transform applied to enable the difference scheme to work with depth intervals which provide adequate detail in the boundary-layer where the current is approximately logarithmic. The depth transform may be log or log-linear depending on requirements. Full details of these transformations and of the transformed equations are given in Appendix A. These equations (transformed variables : $z \rightarrow \zeta$, others $f \rightarrow f'$) apply to the depth domain $\zeta \in [0.0,1.0]$, and the motion oscillates with a period of 2π. Thus the discretization over depth and time is

$$\delta\zeta = 1 / M \quad \text{and} \quad \delta t' = 2\pi / N$$

where the number of height intervals M, and the number of time intervals per cycle N, are specified.

The tridiagonal systems for the solution of equation (1) are presented in Appendix B. The discretised variable notation is as follows :

f'^{n}_{m} is the value of f' at $\zeta_m = (m-1)\delta\zeta$ and $t' = n\delta t'$ for m = 1,M+1 and n an integer.

The boundary conditions at the bed (ζ=0.0) are implemented directly as follows :

$$\begin{aligned} & u'_1 = 0 \ , \ v'_1 = 0 \ , \\ & \text{and} \quad b'_0 = b'_2 \quad \text{implementing} \quad \frac{\delta b'}{\delta \zeta} = 0 . \end{aligned} \tag{9}$$

The free surface conditions (8) (at ζ = 1.0) can be implemented in two ways :

$$\begin{aligned} & 1) \quad u'_{M+2} = u'_M \ , \ v'_{M+2} = v'_M \ \& \ b'_{M+2} = b'_M \\ \text{or} \\ & 2) \quad u'_{M+1} = u'_M \ , \ v'_{M+1} = v'_M \ \& \ b'_{M+1} = b'_M . \end{aligned} \tag{10}$$

The use of 1) or 2) is not critical when the boundary-layer is contained within the water depth (z_1) but, if this is not the case, then only option 2) will work. (Note : Subscripts 0 and M+2 denote computational

levels outside the flow region. They are introduced in order to satisfy the gradient boundary conditions.)

The difference form of the non-linear expression for ε in Equations (6) poses problems, since ideally it should be evaluated at the half time steps. Various forms have been tried and these are described in Appendix B.

The initial conditions vary depending on what starting values are available. When none are available, a 'dead-cold start' defines values as follows :

$$u_i' \;\&\; v_i' = 0.0$$

$$u_m' = U'(\text{at } t' = t_o'), \quad v_m' = 0.0 \quad \text{for } m=2,M+1$$

$$b_m' = 0.0001 \exp\left(-20.0 \frac{(\zeta - \zeta_0)}{\zeta_1} \right)$$

$$l_m' \;\&\; K_m' \text{ calculated from equations (6) and (7a),}$$

($t_o' = -n_o \delta t'$ is chosen so that $U'(t_o')$ is approximately zero and the v momentum equation (2) is not applied until $V' \simeq 0.0$.)

If starting values are available (eg. steady current values for u, v, b, l and K) then a 'cold start' option is possible, where the values are first read by the model program and then nondimensionalised accordingly. In order to restart from a previously generated solution, the 'hot start' option allows the starting values to be read directly from a solution file.

2.1. Implementation and Behaviour

Two versions of the model are available. One, as described above, is applicable in two dimensions, the other is one-dimensional and neglects v and λ. The one-dimensional version is derived from an earlier program, so the notation and structure is very different from the two-dimensional version.

In order to run the models, the various model parameters must be set. In particular, the values of z_o, z_1 and the driving current defined by its amplitudes (U_o, V_o), period and phase difference $\emptyset$ between components** must be selected for the conditions being simulated, eg. 10s period waves in 10m of water or an M_2 tide in 20m water.

The values of M and N defining the discretisation have optimum values. If either is too small the solution misbehaves and small oscillations (of order $\delta t'$) appear, especially in the time series and vertical profiles of

---

** In the standard program a single frequency is used. For other options, eg. additional 1st harmonic terms, the software may be easily modified.

shear stress. With large values, however, the computer costs grow dramatically without any improvement in the solution. The choice of M must be influenced by both the definition of the profile structure near the bed and the value of z_* in the depth transform (see Appendix A). An empirical study of the effect of z_* on the resolution of the profiles with respect to depth is given in Appendix C. For some model parameters, the convergence of the solution (in time) may be very slow. An initial choice of N much smaller than required for an adequately behaved solution may be used from a dead-cold start to develop the flow in the upper reaches, before changing to a value of N more suitable for the near-bed layer.

When starting the model from dead cold, the dissipation term ε (Eqn. 6) is represented by (B1) of Appendix B. After a specified time, this representation is changed to a time centred one. However, there are some parameter settings for which negative energy values are produced using the time centred formulation (eg. tides in shallow water when the boundary-layer is not contained within the water depth). One point of warning when running the model from dead cold is that it sometimes requires considerable nursing through the warm-up period. The run time parameters may need adjusting and the convergence parameter should be checked every few cycles. The time series of energy and/or stress should occasionally be plotted to check for oscillations of order $\delta t'$.

In the shallow water case, finite oscillations develop in the time series, which cannot be eliminated by increasing N. However this problem can be overcome by smoothing occasionally over 3 consecutive time steps. The smoothing prevents oscillations from developing and, apparently, does not seriously affect the solution.

The model is programmed in a versatile way so that different options can be implemented simply by changing input parameters and subroutines (eg. the various start-up modes and different implementations of the free-surface boundary condition). If further tailoring is required the software can be easily modified (eg. more than one constituent for the driving current). In addition to the trials and applications mentioned in the next section, the one-dimensional model has been used successfully to study the effects in the boundary-layer of free-stream flows which are not purely sinusoidal. Also both the one- and two-dimensional models have been used to study the structure of the boundary-layer associated with the combined action of surface waves and currents.

3. Applications of the model to uniform rectilinear flow.

The model tests described in this section were carried out with a reduced set of equations and boundary conditions, corresponding to a simple, uniform, rectilinear, oscillatory free-stream flow.

3.1. Constant viscosity : 1 Dimension

In this simple case an analytic solution of the governing equations can be obtained (Lamb, 1932, Art. 345). This enables a comparison to be made with results from the 1-D numerical model, in which the full turbulence closure scheme is replaced by a constant eddy viscosity. The parameter settings used for this example are :

z_o = 0.01cm, z_1 = 1000cm, U_o = 100cm/s , $\omega = 2\pi/10s^{-1}$,

Logarithmic depth transform, M = 25 and N = 60,

Upper boundary condition: u = U at z = z_1 with $t' = n\delta t' - \pi/2$.

With K = constant (K = 100cm^2/s) the non-dimensionalised analytic solution to equations (1) and (3) (with v and λ set to zero) has the form :

$$u' = \sin(t') - \exp\left(-\beta'(z'-z_c')\right) \sin(t' - \beta'(z'-z_o')) \qquad (11)$$

where

$$\beta' = \left(\frac{1}{2K'}\right)^{1/2} .$$

The associated bottom stress is

$$\tau_o' = 2\sin(\pi/4)\, K'\beta' \sin(t' + \pi/4) .$$

The u′ profiles from the model agree very well with the analytic solution at least for z > 1.0cm (see Figure 1). Below this, the vertical gradient of u′ from the model is about 24% less than the theoretical value. This is, most probably, due to the unsuitability of the logarithmic spacing of computational levels for this comparison.

Alternative bottom stress estimates were made using :

1) two implementations of equation (4b) :

$$\tau_o' = -\frac{\partial}{\partial t'} \left\{ \int_0^1 W' \chi \, d\zeta \right\} \qquad (12)$$

and

$$\tau_o' = -\frac{\partial}{\partial t'} \left\{ \int_{z_o'}^{z_1'} W' \, dz' \right\} \qquad (13)$$

where $W' = u' - U'$ and χ is defined in Appendix A*;

and 2) exact values for u' from Equation (11) in the same difference approximation as used for the bottom stress evaluations within the model.

All the above bottom stress estimates are plotted with respect to time in Figure 2. Both estimates given by Equations (12) and (13) are in closest agreement with the theoretical values. The estimates using Equations (4a) and (B4) with u' from the model are the worst, although larger values of M and N might improve them (cf Section 3.3). It is interesting to note that using the difference equation (B4) with exact values of u' gives a curve about 13% less than the true τ_o' curve; this indicates the error due to the difference approximation to the velocity gradient.

3.2. Viscosity $K = K_o z$: 1 Dimension

In this more realistic case for rough turbulent oscillatory flow, an analytic solution (see Smith, 1977) can also be compared with a suitably modified version of the model. The input parameters used were as follows :

$z_o = 0.001\text{cm}$, $z_1 = 100\text{cm}$, $U_o = 100\text{cm/s}$, $\omega = 2\pi/10\text{s}$,

Logarithmic depth transform, $M = 25$ and $N = 60$,

Upper boundary condition: $u = U$ at $z = z_1$ with $t' = n\delta t' - \pi/2$.

For these parameter settings, with viscosity as a linear function of depth, the appropriate value of K_o is 2.2cm/s. The velocity profiles through half a cycle agree with the analytic results to within $10^{-4} U_o$. This implies that the method accurately solves the diffential equations and that a logarithmic spacing of computational levels is appropriate. Such a spacing is generally expected to be appropriate for rough turbulent boundary layer flow.

From the comparison between different bottom stress estimates (Figure 3), the velocity gradient estimates based on equation (4a) give better agreement in terms of both amplitude and phase than the estimates based on equation (12). These results are contrary to those obtained in Section 3.1.

---

* The integral for (12) was evaluated by an Euler-Maclaurin summation, while that for (13) was evaluated by summing trapezoidal areas.

3.3. Fully Turbulent Model : 1 Dimension

In the two previous sub-sections, the eddy viscosity was forced to take simple analytic forms. In this section the viscosity is computed using equations (A5) to (A7a). The parameter settings used were as follows :

z_o = 0.01cm, z_1 = 100cm, U_o = 100cm/s, $\omega = 2\pi/10s^{-1}$,

Logarithmic depth transform, M = 25 & 40, N = 60 & 120 ,

Upper boundary condition: u = U at $z = z_1$ with $t' = n\delta t' - \pi/2$.

These runs were made to assess the influence of M and N on the agreement between various estimates of bottom stress (cf. Section 3.1). As can readily be seen from the τ_o' plots in Figure 4, there is an oscillation, of order $\delta t'$, in the velocity gradient estimates for N=60 which is not present for N=120. The phase agreement of both bottom stress estimates is also improved by doubling the value of N.** The increase of M from 25 to 40, while yielding negligible difference in the velocity profiles, reduces the difference between the two bottom stress estimates. This test implies that an appropriate choice of values for M and N is one which achieves acceptable agreement between the two bottom stress estimates.

Note : During these tests, the standard convergence parameter (0.01) for the iterative loops was reduced to 0.005 with negligible effect on the agreement between the two bottom stress estimates.

3.4. Comparison with experimental data : 1 Dimension

The most suitable data set for comparison with model results in the one-dimensional case has been provided by Jonsson and Carlsen (1976). These authors have made detailed measurements of the velocity structure of rough turbulent flow in an oscillatory water tunnel. Horizontal velocities were measured at various levels above the bed through a wave cycle. These measurements were then used to determine vertical profiles of shear stress, assuming zero stress at height $z = z_1$ above the bed :

$$\frac{\tau}{\rho} = - \int_{z_1}^{z} \frac{\partial}{\partial t} (U - u) \, dz \, .$$

** In fact, the program run for N=120 had the same order of run time as did that for N=60, indicating that the iterative loops converged more rapidly.

The parameter settings to simulate Jonsson and Carlsen's Test No. 1 were as follows# :

z_o = 0.07666 cm, z_1 = 23cm, U_o = 213.36cm/s, $\omega = 2\pi/8.39s^{-1}$,

Logarithmic depth transform, M = 25, N = 120 ,

Upper boundary condition: u = U at $z = z_1$.

Although the actual water depth in the experiment was 23cm, Jonsson and Carlsen defined the free-stream flow as the region above z_f= 17.25cm, and assumed the stress to be zero at this level. However, in the absence of velocity measurements near the roof of the oscillatory water tunnel, there may be some uncertainty about the true zero-stress level.

The free-stream velocities were harmonically analysed to obtain the most significant constituents (using ω as the fundamental frequency). This gave a velocity amplitude of 213.36cm/s at frequency ω , which was used as the value of U_o in the model. After normalisation, the driving velocity used for the simulation was :

$$U' = \frac{U}{U_o} = a_o + \cos(t') + a_1\cos(2t' - \phi_1) + a_2\cos(3t' - \phi_2)$$

where $a_o = -0.39\times10^{-3}$, $t' = n\delta t' - (\pi/2 + \delta t')$,
$a_1 = 0.464\times10^{-1}$, $\phi_1 = 2.7255r$ (156.2°) ,
and $a_2 = 0.891\times10^{-2}$, $\phi_2 = 3.1091r$ (178.1°) .

Figures 5 and 6 show the results of the comparison between model and experiment, in terms of both profiles and time series of velocity and stress. Since the model gave significant stress values at z_f= 17.25cm, the values of shear stress calculated by Jonsson and Carlsen were adjusted at each phase angle by adding the stress value from the model at z_f. The agreement is remarkably good in view of the fact that the model does not closely simulate the experiment's surface condition.

The model was also run with z_1 = 100cm which allowed the boundary layer to develop fully. The free-stream velocity was attained at a height of about 50cm, significantly greater than the value assumed by Jonsson and Carlsen. To some extent, this calls into question the basis for comparing the numerical model and experimental results.

Jonsson and Carlsen's height above the 'theoretical' bed was taken as equivalent to the model's z values.

3.5. Alternative Dissipation and mixing length formulations : 1 Dimension.

The tests described below, relating to the dissipation term ε in Equation (6) and mixing length in Equation (7), were carried out using a slightly irregular, non-sinusoidal, free-stream flow. The parameter settings were as follows :

$z_0 = 0.01cm$, $z_1 = 100cm$, $U_0 = 100cm/s$, $\omega = 2\pi/10s^{-1}$,

Logarithmic depth transform, M=25, N=120
and non-standard upper boundary condition:

$U' = \cos(t') + 0.1\cos(2t'-3\pi/2)$ with $u' = U'$ at $z = z_1$ ($t' = n\delta t'-\pi/2$).

Dissipation formulation :

Since there was a choice of representations for the dissipation term, it was thought prudent to make an assessment of their relative effects on the solution. The model was run with the above input values for options B1, B2 and B3 (Appendix B). To give an objective assessment of the comparison, an algorithm was devised to define, numerically, the overall difference between two solutions. This algorithm is as follows :

For a particular time t_n, let the relative percentage difference between two solutions S1 and S2 be

$$\Delta_z = 100 * \frac{(f(S1) - f(S2))}{D_f}$$

where $D_f = \max_z \{f(S1)\}$ ie. D_f is the maximum f value in the profile.

Then the difference at time level t_n can be defined as

$$\Delta_n = \max_z (\Delta_z) .$$

For the solution as a whole, the difference may be defined by the mean (μ) and standard deviation (σ) of the series Δ_n, throughout the time span of the solution.

Table 1. below gives the values of (μ,σ) for each variable, comparing the options B1, B2 and B3.

The values of μ for all variables are less than 2%. This indicates fair agreement between the three methods, though the difference between B1 and B2, and B1 and B3, is rather greater than between B2 and B3.

For some input parameters, only method B1 maintains energy values that are always positive. However, on the assumption that centrally differenced methods are 'better', B2 and B3 should be used whenever possible. There is little to choose between methods B2 and B3, but on a computer cost basis, B3 is marginally more economical.

S1	S2	Variables									
		u		b		K		l		τ	
		μ	σ	μ	σ	μ	σ	μ	σ	μ	σ
B1	B2	0.21	0.11	1.47	0.64	0.59	0.16	0.13	0.02	0.75	0.25
B1	B3	0.21	0.16	1.03	0.56	0.61	0.17	0.17	0.01	0.66	0.23
B2	B3	0.06	0.05	0.41	0.28	0.14	0.01	0.07	0.01	0.33	0.18

Table 1 : The percentage means and standard deviations of Δ_n for each variable from solutions with the dissipation formulations B1, B2 and B3.

The above tests were conducted purely on modelling considerations, and the conclusion should be reconsidered when adequate field data is available. However, the agreement between the various options is probably closer than that which could be achieved with real data, so an absolute preference for the form of the dissipation term may not be feasible.

Mixing Length

Instead of using equation (7a) to represent the mixing length, the time independent expression

$$l = \kappa z$$

was used to generate a solution (LL) using the parameters listed above and with option B3 for the dissipation term. This solution was then compared with that obtained with the same parameter settings but the standard expression (Eqn. 7a) for l (LS), using the technique described above. The (μ, σ) values are given in Table 2. Some values are artifically high due to the large difference in l from the two solutions in the upper flow, in conjunction with the definition adopted for Δ_z. Included in Table 2 are revised values for μ, selected subjectively from the individual values of Δ_z and Δ_n.

The main difference between the K and l values in this comparison occurs in the flow above about z = 1.0cm. Comparative plots of these profiles are shown in Figure 7. The agreement between u, b and τ values is fair, as is shown in the time series plotted in Figure 8. From these, it is readily seen that, when the linear expression for the mixing length is used, the amplitudes of b and τ are slightly increased by amounts (<5%) which vary with depth, and that phase shifts are introduced. It is also clear that u, b and τ are fairly insensitive to the large changes in mixing length near the surface. Unless some real eddy viscosity profiles were available for

S1	S2	Variables									
		u		b		K		l		γ	
		μ	σ	μ	σ	μ	σ	μ	σ	μ	σ
LS	LL	3.1	3.0	9.6	3.1	91.	2.	82.	0.1	14.6	5.7
LL	LS	3.1	3.1	9.4	2.4	185.	15.	442.	0.2	13.7	3.7
Revised		2.0		8.0		<10.		<5.		10.?	

Table 2 : The percentage means and standard deviations of Δ_u for each variable from solutions using different mixing length formulations.

comparison, it would not be easy to justify the preference for the mixing length formulation (7a), apart from the fact that it introduces time dependency. The test indicates that the results from the model are relatively insensitive to the formulation chosen for the mixing length.

3.6. The boundary layer thickness and wave drag coefficient : 1 Dimension

Rather than using individual parameter settings as the input to the model (as in Sections 3.1-3.5), the one-dimensional version of the model was modified to accept the two non-dimensional parameters which uniquely define the solution of the problem. These two parameters are the ratio of water depth to roughness length, and the 'relative roughness' A/k_s, where A is the excursion amplitude defined by $A = U_o/\omega$ and k_s is the equivalent bed roughness defined by $k_s = 30z_o$:

$$R_z = \frac{z_1}{z_o} \qquad \text{and} \qquad \frac{A}{k_s} = \frac{U_o}{30\omega z_o} \tag{14}$$

The other parameters needed by the program can be derived from R_z and A/k_s, namely :

$$z_o' = \frac{1}{30\ A/k_s} \qquad z_1' = z_o' R_z .$$

The free-stream flow was defined as

$$U' = \cos(t') \quad \text{where } t' = n\delta t' - \pi/2.$$

This modified version of the model was run with the following parameter settings :

for R_z = 10000 :-

A/k_s = 1, 5, 10, 50, 100, 530 and 1000;

for R_z = 300 (as for the Jonsson & Carlsen (1976) experiment) :-

A/k_s = 100 .

Various estimates of the boundary layer thickness were made for each solution :

from the velocity profile corresponding to the peak free-stream flow :

1. δ_1 ~ the lowest z value at which the velocity attains the value U' (cf. Figure 1. of Jonsson, 1978).
2. δ_2 ~ the highest level at which the computed profile differs by less than 1% from a logarithmic profile.
3. δ_3 ~ the highest z value at which $u' - U'$ is greater than 0.01.

from the energy profile corresponding to the peak value of turbulent energy at the bed :

4. δ_b ~ the level at which the energy is 1% of its value at the bed.

These values, normalised by A, the excursion amplitude, are plotted against A/k_s, the relative roughness, in Figure 9. Whatever definition is adopted, the normalised boundary layer thickness δ /A decreases with increasing A/k_s. The largest values are for δ_b/A, which indicates the presence of turbulent energy in the region of free-stream flow as defined in terms of velocity. Energy is diffused into this region, and there it is dissipated; the absence of velocity shear ensures no energy generation. The total boundary layer thickness δ_3/A, as defined in terms of velocity, is almost an order of magnitude greater than the maximum thickness of the logarithmic layer in the wave cycle (δ_2/A), whatever the value of A/k_s. The close agreement between (δ_2/A) and (δ_1/A) indicates that, when the pressure gradient is zero, the logarithmic layer extends upwards to approximately the height at which the velocity first attains its value in the free-stream flow. Finally, the discrepancies which exist between the experimental values of Jonsson and Carlsen for δ_1/A and the model results are probably due to the lack of an adequate basis for comparing the respective results (see Section 3.4).

Following Jonsson (1978), the drag coefficient (or friction factor) f_w is defined by :

$$\tau_{o\,max} = 0.5\, \rho\, f_w\, U_{max}^2 .$$

In Figure 10, f_w is plotted against the relative roughness. It can be seen that the curves produced by the model are enclosed by previous empirical and semi-empirical curves for the physically interesting range A/k_s (>50). The divergence of the results for $A/k_s < 50$ is probably due to the inadequate representation of the turbulent energy system by the model for these

values of relative roughness.

Another parameter which can be obtained from the solution is the phase lead (θ) of τ_c' ahead of the free-stream velocity U'. Figure 10 shows θ as a function of A/k_s and compares it with analytic values obtained from Smith's (1977) model (described in Section 3.2) which is based on a linear expression for K ($K = K_c z$). There is little difference between the phase leads predicted by the present model and Smith's model, but both give underestimates when compared with the experimental values of Jonsson and Carlsen (1976). However this comparison may be unreliable for the reason given in Section 3.4.

3.7. Sensitivity of the model to variations in α_b, c and κ : 1 Dimension

In the turbulence closure scheme there are three constants (α_b, c and κ) to which values must be assigned (note : $c_c = c^{1/4}$, $c_l = c^{3/4}$). Here we are concerned with the sensitivity of the solution to variations in each of these constants. The parameter settings used for this investigation were as follows :

z_c = 0.01cm, z_l = 100cm, U_o = 100cm/s, $\omega = 2\pi/10s^{-1}$,

Logarithmic depth transform, M = 25, N = 120,

Upper boundary condition: u = U at $z = z_l$ with $t' = n\delta t' - \pi/2$.

In order to determine the model's sensitivity to the three constants the value of each was altered by $\pm$50%, and the solutions were compared using the technique described in Section 3.5. The results are tabulated in Table 3.

The solutions were also compared qualitatively by plotting time series and profiles, and looking at the intermediate values Δ_z of the algorithm for comparing two solutions. Considering each constant individually, the effects of changing the constant's value were as follows :

Sensitivity to α_b

The effect of a change of α_b on u is negligible and will not be discussed further.
The plots of energy profiles and time series in Figure 11 indicate amplitude and phase differences above about z = 0.8cm. For heights greater than 5cm, b is less when α_b is lower, while below the reverse is true. This means that the boundary layer thickness (δ_b) increases with increasing α_b. The differences in shear stress for $\alpha_b = 0.73 \pm 50\%$ are slight. Below z = 0.28cm, the agreement is good. Above this level, there are small amplitude and phase differences which vary with depth. The boundary layer thickness based on shear stress (ie. the level where $|\tau|$ drops to 1% of $|\tau_o|$) is slightly reduced by decreasing α_b by 50%. These effects are illustrated in Figure 12.

S1	S2	Variables									
		u		b		K		l		τ	
		μ	σ	μ	σ	μ	σ	μ	σ	μ	σ
BS	A+	0.6	0.4	6.3	2.0	59.	5.	45.	3.	4.0	1.3
BS	A-	1.0	0.8	8.7	3.5	56.	5.	42.	2.	6.4	3.0
A+	A-	1.5	1.1	15.	5.	90.	3.	60.	1.	9.8	3.9
BS	C+	0.5	0.3	18.	1.	11.	1.	4.2	0.4	1.8	0.3
BS	C-	0.4	0.3	41.	1.	20.	2.	7.0	0.5	2.2	0.7
C+	C-	0.8	0.5	72.	2.	31.	4.	11.	1.0	3.7	1.0
BS	K+	14.	8.	92.	20.	494.	46.	224.	15.	104	28.
BS	K-	26.	15.	74.	15.	99.	1.	58.	3.	78.	16.
K+	K-	37.	20.	86.	10.	100.	0.	86.	1.	89.	11.

Table 3 : The means and standard deviations of Δ_n for each variable from solutions obtained with different values of the constants α_b, c and κ.
Solution BS uses $\alpha_b = 0.73$, $c = 0.046$ and $\kappa = 0.4$; A+, A- use $\alpha_b = 0.73 \pm 50\%$; C+, C- use $c = 0.046 \pm 50\%$; and K+, K- use $\kappa = 0.4 \pm 50\%$, respectively.

Sensitivity to c

A 50% change in c has a negligible effect on u, a slight effect on τ but a significant one on b. The explanation for this is that, if Equation 6 is to be satisfied, no change in u and τ implies that b must change.

Reducing c by 50% decreases the amplitude of τ slightly, as is shown in Figure 13 where profiles and time series are plotted for $c = 0.046 \pm 50\%$.
The energy comparisons for $c = 0.046 \pm 50\%$ are shown in Figure 14. Increasing c by 50% decreases the energy b by about 20%, while decreasing c by 50% increases b by 40%. Thus the effect of changing c is not linear. The profiles of b show that the boundary layer thickness δ_b is only marginally affected by a change in this constant.

Sensitivity to κ - Von Karman's constant

Changes in Von Karman's constant significantly alter the solution. Profile and time series comparisons for u, b and τ for the three values $\kappa = 0.4$ and $0.4 \pm 50\%$ are shown in Figures 15-17.
The u profiles are altered so that the boundary layer thickness increases with κ. This effect applies also to b and τ but here the magnitudes of the changes are much larger. Table 4 gives an indication of these changes.

Table 4:
Ratios of the maximum values of b and τ at the bed for $K = K_a$ to those for $K = K_b$, using the values K = 0.2, 0.4 and 0.6.

K_a / K_b	0.6 / 0.4	0.4 / 0.2	0.6 / 0.2
b	1.8	2.6	4.6
τ_o	1.8	2.7	4.7

Conclusions

1. Velocity is the least sensitive of the variables u, b and τ, to changes in the constants, while energy is the most sensitive. Von Karman's constant affects the solution more significantly than either α_b or c.
2. The constants may be adjusted to obtain better agreement between a solution and real data. The choice of constant and size of adjustment depend on what change in the solution is required.
3. It can be seen from the diagrams that, for some values of the constants, the model is less stable and finite oscillations appear in the time series of b and τ at the lowest levels. (For this analysis, it was not considered worthwhile removing these oscillations.)

3.8. Tidal oscillation in shallow water : 1 Dimension

The test now considered is for a simple reversing, uniform, oscillation of tidal period, for which the boundary layer occupies the entire water depth. This produces numerical modelling difficulties not encountered if the flow is 'deep', ie. the boundary layer is contained within the depth. The parameter settings were as follows :

z_o = 0.1cm, z_1 = 2000cm, U_o = 100cm/s,

$\omega = 2\pi/44700 s^{-1}$ (M_2 tide),

Log-linear depth transform : $z_* = 1000$cm, M = 50 and N = 120.

As a suitable free-surface boundary condition, Equation 3 was selected. This implies zero stress at the free surface. Initial attempts to obtain a solution using option 1) of equation 10 at the free surface, together with dissipation term option B2, never succeeded because the energy values soon became negative and the solution misbehaved drastically at the surface. Using option B1 for the dissipation term and free-surface option 2) of equation 10, the solution converged rapidly but with finite oscillations (order $\delta t'$) in the time series.

At this stage, a modification to the mixing length formula was considered. This consisted of a scaling coefficient (a function of depth) which would reduce the mixing length to zero at the surface namely :

$$\left(1.0 - 0.99 \frac{(z-z_c)}{(z_1-z_c)}\right) \text{ with } z_c = \frac{2}{3} z_1 \ .$$

However this had an adverse effect on the solution, introducing an oscillation of order $3\delta t'$ above about z = 560cm and affecting the velocity profiles in a way which made them increase suddenly above this height before being drawn back towards U. It is relevant to point out here that the modified mixing length procedure was also applied to a surface wave simulation. In that case, the effect of modifying the mixing length scarcely influenced the solution at all.

A reasonably well-behaved solution was eventually obtained by smoothing each variable over three consecutive time levels, 2 to 4 times a cycle. Since oscillations were found to develop whenever the bottom stress changed sign, this fact was used to determine when to apply the smoothing function :

$$f(t') = 0.25 \ (2f(t') + f(t'+\delta t') + f(t'-\delta t')) \ .$$

The centrally differenced dissipation term, option B3, was implemented satisfactorily provided it was replaced by option B1 whenever the energy values turned negative. To dampen numerical oscillations, more frequent smoothing was required, especially after option B1 had been implemented, that is near phase angles corresponding to minimum energy levels.

Table 5 gives the results of the comparison of these two solutions, using the method described in Section 3.5. The 7th half-cycle of the solution using B1 is compared with the 5th half-cycle using B3. In each case, the energy profiles appeared to have converged. The high σ values are due to large Δ_n values during the low energy part of the half-cycle. The results indicate that the solutions agree to within about 5%. The difference in energy consists of small amplitude and phase changes, as shown in Figure 18.

		Variables									
S1	S2	u		b		K		l		τ	
		μ	σ	μ	σ	μ	σ	μ	σ	μ	σ
B1	B3	0.8	2.0	4.1	8.3	2.0	2.0	0.7	1.0	2.4	6.2
B3	B1	0.8	2.0	4.1	8.6	2.0	2.0	0.7	1.0	2.4	6.1

Table 5 : The percentage means and standard deviations of Δ_n for each variable from tidal solutions in shallow water using different dissipation formulations B1 and B3 (see Appendix B).

From Figure 18b, it is apparent that there are still some oscillations left in the solution. These could have been eliminated by smoothing at additional strategic points. Since for the phase angles of interest (those close to the occurence of peak free-stream velocity) the solution was well-behaved, this was not necessary.

The main reason for attempting the present exercise was to use the profiles corresponding to near-peak velocity as a 'steady' current on which suitable wave oscillations could be superimposed. This development was part of a combined wave/current interaction study, which is described elsewhere.

4. Applications of the model to uniform rotating flow

The tests described in this section were carried out with the full set of boundary-layer equations and boundary conditions. The equations are applicable to a uniform rotating flow, driven by a forcing current (U,V) (see equations (1) and (2)).

4.1. Comparison with the results of Vager and Kagan's model : 2 Dimensions

Vager and Kagan (1969) obtained a numerical solution for turbulent tidal boundary-layer flow, starting with the formulation described in Section 2, but using a different discretisation and computational scheme. In order to make a comparison with their results, the following parameter settings were used in the present model :

z_o = 1.0cm, z_1 = 10000cm, U_o = 141.56cm/s ,

V_o = 281.12cm/s , $\phi = -\pi/2$,

$\omega = 2\pi/44700 s^{-1}$, $\lambda = 0.998 \times 10^{-4} s^{-1}$, M = 40 and N = 60.

Dissipation term represented by B3. Logarithmic depth transform.

The two-dimensional version of the model was run using parameters that were compatible with the non-dimensional ones used by Vager and Kagan (V&K), namely :-

$\frac{z_1}{z_o} = 10^4$, $\frac{V_o}{U_o} = 2$, $f_x - f_y = \frac{\pi}{2}$ where f_x & f_y are the phases of U & V,

$\frac{\lambda}{\omega} = 0.71$, and $\mathcal{N} = \frac{U_o}{\omega z_1} = 100.$

The settings above do not yield quite the same values for V_o/U_o and $\mathcal{N}$ as those of V&K, but since they agree to within 1%, the solution was not rerun for the present comparison. This discrepancy was due simply to a typing error, made when the parameters for the program run were being set up, which remained undetected until recently. The depth discretisation used by V&K has 50 linearly-spaced intervals below $z/z_1 = 0.05$ and 200 above, which is very different from the 40 logarithmically spaced intervals used in the present model.

In order to provide values for comparison with the present model solution, the time series plotted by Vager and Kagan were enlarged 2-3 times and values, at phase intervals of $\pi/4$, were transferred directly to the model's time series plots. These values were then joined by 'smooth' curves. It was estimated that this procedure for transferring V&K's results was accurate to within about 5%. The model solution was plotted at z levels which

were in closest agreement with those adopted by V&K.

The comparisons for the defect velocity components, turbulent energy and eddy viscosity show reasonable agreement in view of the differences in the computational schemes of the two methods (see Figures 19-21). The differences mostly amount to variations in amplitude, with the overall behaviour of the curves being very similar. The defect velocities (Figure 19) are in poorest agreement at the higher levels, which is probably due to the different depth discretisations. The energy series (Figure 20) agree very well except at the bed, which is not readily explained. The most significant differences are those for viscosity (Figure 21). Once again however, despite amplitude differences, the behaviour of the viscosity with respect to time and depth is similar for both solutions.

The comparison illustrates that even when the same closure scheme is used, the solution can be quite sensitive to the method of implementation. Although the qualitative agreement between the results of the present model and V&K's model is reasonable, it tells us nothing about the ability of the models to reproduce natural phenomena. The next section seeks to fulfil this need by comparing a model solution with data from a current meter string.

4.2. Comparison with current meter string data : 2 Dimensions

The parameter settings for this comparison were as follows :

$z_o \in [0.1,1.0]$cm, z_1 =120m, $\omega = 2\pi/44100s^{-1}$,

U, V defined by various constituents,

Log-linear depth transform. $z_* = 2000$cm, $\lambda = 1.112\times10^{-4}s^{-1}$, M = 40, N = 147,

Dissipation term represented by B3 after warm-up.

A string of 8 Aanderaa RCM4 current meters was deployed at a 120m deep site in the Celtic Sea about 60nm west of the Scilly Isles. The area was selected because it has a flat, horizontal, uniform bed which is featureless except for ripples in the silty sand. The measurements were made in March 1983 in order to avoid thermal stratification (an XBT profile confirmed that the water column was isothermal). Seven of the meters provided data, from which 11 tidal cycles, over a 6 day period during the peak of spring tides, were used to obtain ensemble-averaged velocity profiles over one cycle. The 10 min values thus obtained were further averaged to give profiles every 30 min. (In the remainder of this section, 'data' will refer to these ensemble-averaged velocity profiles.) The series of values for the top meter gave cycles of 12hr 15min which was the period adopted for the model solution. A harmonic analysis of each series showed that there was a non-zero mean of about 2cm/s at each level, possibly due to the wind, which averaged about 10 knots over the 6 day period. Since the model is designed for purely oscillatory flow, these means were subtracted from

each velocity value. The resulting profiles, given in Table 6, have been used in this comparison.

Height above bed Means removed hr	90.0 -2.62	70.0 -1.63	50.0 -2.15	30.0 -2.05	15.0 -1.32	2.5 -1.55	1.0 -1.68
0.0	-14.52	-13.48	-8.37	-5.81	-7.59	-2.88	-1.96
0.5	-3.11	-2.12	2.15	3.79	2.30	4.18	4.53
1.0	6.96	8.83	13.46	13.86	11.35	12.04	10.91
1.5	20.42	18.68	21.79	22.92	21.29	19.86	16.55
2.0	29.04	27.60	31.18	31.25	28.29	23.52	19.95
2.5	35.65	35.86	37.55	38.02	34.44	26.77	22.56
3.0	40.45	40.05	41.96	41.54	37.44	28.60	24.32
3.5	41.35	42.15	43.74	42.81	38.23	28.90	24.20
4.0	41.39	42.00	42.71	40.24	35.16	27.34	23.10
4.5	38.01	39.54	38.99	36.09	31.06	23.96	20.82
5.0	32.56	34.36	32.99	29.63	25.80	19.87	17.97
5.5	25.05	27.88	24.77	21.82	19.18	14.72	13.40
6.0	16.70	19.31	13.34	11.55	10.52	7.21	6.14
6.5	6.58	8.59	3.33	1.57	1.92	0.09	-1.03
7.0	-2.72	-3.15	-6.80	-9.34	-7.25	-7.49	-7.11
7.5	-13.02	-11.71	-18.08	-20.87	-16.83	-15.70	-13.84
8.0	-22.51	-23.22	-27.84	-29.54	-25.73	-21.72	-18.91
8.5	-29.91	-31.96	-36.57	-37.17	-32.12	-26.82	-22.92
9.0	-36.95	-39.61	-42.60	-42.44	-36.70	-29.21	-25.57
9.5	-42.82	-44.24	-45.34	-44.53	-39.39	-31.67	-26.80
10.0	-44.87	-46.69	-46.00	-43.64	-37.50	-31.02	-26.06
10.5	-42.98	-45.48	-43.14	-39.21	-34.33	-27.63	-23.40
11.0	-38.59	-40.04	-36.77	-32.50	-29.74	-22.63	-19.59
11.5	-30.66	-31.18	-27.06	-22.79	-22.38	-15.46	-13.57
12.0	-20.49	-20.51	-15.62	-11.80	-12.64	-7.42	-5.80

Table 6a : The ensemble average profiles for the u component (cm/s) of the current meter data.

The z_o values estimated from the velocities at 1m and 2.5m ranged between 0.1 and 1.0cm during the cycle. The model was run initially with z_o = 0.4cm, the geometric mean of the calculated values, but later with z_o = 0.1 and 1.0cm to determine whether alternative values would improve the agreement between the predictions and data.

Choices of M and z_* were made as described in Appendix C, so that the number of computational levels between each meter level was about equal and greater than two. The meter levels with usable data were : 90, 70, 50, 30, 15, 2.5 and 1.0m. For convenience, the u- and v-components of velocity were identified with the measured easterly and northerly components respectively.

Neither the pressure gradients nor the true geostrophic currents were available to drive the model so, as a first attempt, four constituents from

Height above bed	90.0	70.0	50.0	30.0	15.0	2.5	1.0
Means removed	0.98	1.67	1.86	2.71	0.84	0.32	0.61
hr							
0.0	18.91	20.50	20.84	19.06	18.15	15.55	13.24
0.5	25.58	26.74	26.14	24.17	25.22	20.73	17.64
1.0	31.03	31.56	30.30	29.14	30.81	25.13	20.49
1.5	34.52	35.36	34.09	32.99	34.37	27.74	22.42
2.0	35.30	37.29	34.91	34.06	36.37	27.55	22.67
2.5	34.53	36.09	33.23	31.33	33.25	25.12	21.15
3.0	30.43	33.42	29.13	28.17	29.62	21.94	18.13
3.5	26.66	27.87	22.98	21.57	23.77	17.98	14.97
4.0	20.24	21.40	15.17	14.44	16.65	13.85	10.91
4.5	11.19	11.94	7.38	5.71	9.34	7.27	6.10
5.0	1.78	1.85	-1.36	-3.27	0.20	0.22	-0.05
5.5	-8.78	-8.73	-12.95	-13.03	-8.93	-7.44	-6.87
6.0	-17.32	-18.93	-22.08	-21.86	-17.96	-14.47	-13.31
6.5	-24.70	-27.40	-28.72	-27.87	-25.41	-20.22	-17.97
7.0	-29.80	-33.19	-32.85	-31.55	-30.56	-25.17	-21.24
7.5	-33.64	-37.42	-34.81	-32.56	-33.32	-28.55	-23.03
8.0	-35.25	-38.10	-34.62	-33.03	-34.42	-28.52	-22.38
8.5	-35.48	-37.53	-31.75	-30.68	-33.18	-26.08	-21.47
9.0	-32.99	-33.59	-27.21	-25.40	-29.03	-23.89	-19.27
9.5	-26.98	-28.71	-22.48	-19.91	-23.97	-18.84	-15.50
10.0	-20.01	-21.43	-15.48	-13.20	-18.93	-13.38	-10.68
10.5	-12.76	-11.55	-7.51	-5.90	-10.76	-8.09	-6.15
11.0	-4.22	-1.24	1.58	2.11	-2.97	-0.37	0.02
11.5	5.51	6.89	8.76	8.70	5.46	6.55	5.52
12.0	14.51	16.10	16.55	15.33	14.19	12.33	10.63

Table 6b : The ensemble average profiles for the v component (cm/s) of the current meter data.

the 90m level data were used to synthesise a possible driving current. In order to control the $\delta t'$ oscillations that developed in the energy series, smoothing 3 times per cycle was required. Convergence of the solution was achieved by the 25th cycle. This solution was analysed at the 90 and 70m levels and the harmonic constituents compared with those from the equivalent current meter. Since the data at the 90m level might have been influenced by surface wave conditions not included in the model, the 70m level was also considered for matching purposes. On the assumption that at the upper levels the model affects each constituent independently and linearly with depth, the forcing current constituents were adjusted to match the model with the data at either the 90m or the 70m level, and the model was re-run with the adjusted inputs. Because the linearity assumption is not completely valid, the agreement at the matching level is still not exact, but it was felt that further iterations were not warranted. The solutions from the 90m match and the 70m match were compared at each meter level by plotting the velocity ellipses from the model over one cycle. The solution which was matched at the 90m level gave poor agreement with the data for all the other meter levels and was not considered further.

However the agreement of the solution matched with the data at 70m is quite good at all levels (see Figure 22). All subsequent comparisons were made using profiles of the following properties of the tidal ellipse corresponding to the fundamental constituent :

- the semi-major axis (a)
- the ellipticity : semi-minor / semi-major axes (b/a)
- the ellipse orientation : the angle the first semi-major axis makes with the positive x axis (γ)
- the ellipse phase : the angle between the vector of the first point in the ellipse to γ (Ψ).

Since these last two values depend on the arbitrary direction of north and the arbitrary time origin of the series, it is relative differences over the depth that are of interest and not the absolute values. Hence for particular comparisons, the profiles of γ and Ψ are matched at 70m and an appropriate angle added/subtracted from the remaining values in the profile. Agreement between the model and the data is quite good for the semi-major axis a, though the modelled profile has less curvature near the bed than the data (Figure 23a). The modelled b/a profile (Figure 23b) shows the same general trend as the data, but does not display as much variation top-to-bottom. The modelled phase (Ψ) profile (Figure 23c) also trends the same way as the data, but shows only about half as much variation top-to-bottom. The orientation (γ) data (Figure 23d) shows reasonable ageement with the model at most heights, but the measured values of γ at 30 and 50m are out of line with the other values. The reason for this is not known, but might be due to an as yet untraced error in the compass calibrations.

Attempts were made to improve the agreement by altering the constants α_b, c, k and parameter z_o to other realistic values. The main aims were to increase the difference in Ψ between the top and bottom of the profile and to increase the curvature of the a profile below 50m.

Reducing the diffusion of turbulent energy by setting $\alpha_b = 0.01$ improved the curvature only marginally (< 0.5%), and scarcely influenced the phase at all (< 0.3%). The realistic range of values for c was taken to be [0.034,0.1], where 0.034 was estimated from atmospheric and marine boundary-layer data (Soulsby, 1983) and 0.1 is the value of c used by Dickey and Van Leer (1984). The values 0.034 and 0.1 were both used to obtain solutions, but again the ellipse properties were hardly changed (<0.3%), though c = 0.034 did at least alter the values of a in the required direction. The variations due to setting $k = 0.35$ are shown in Figure 23 (points marked with a '+'). Although not large (<1.5%), the movements of both a and Ψ were in the required directions.

Selecting z_o at the extremes of the range produced the most significant alterations in the ellipse properties (see Figure 23). A value of z_o = 0.1cm slightly improved the curvature of a below 50m; but the phase Ψ values were shifted in the wrong direction. Increasing z_o to 1.0cm slightly decreased the curvature of the a profile, but improved the near

bed Ψ by about 1^{o}.

None of these alterations produced the required 5^{o} decrease in Ψ at 1m, and the discrepancy cannot, as yet, be explained. However it is interesting to note that, as with the comparison of the model with Jonsson and Carlsen's (1976) experimental results (Section 3.4), the phase leads are underestimated by the model. For all the alterations made, the semi-major axis profiles are in reasonable agreement with the data, and the model also displays the same trends in its b/a profiles as the data. With regard to the orientations, if the suspect data values at the 50m and 30m levels are ignored, the trends of the profiles obtained from the model solutions agree well with the remaining data values.

From the comparisons made above, one may conclude that the model solution predicts the gross behaviour of the turbulent boundary-layer. However it fails to cope with the finer detail of the data, probably because the closure assumptions in the model do not represent the turbulent processes quite well enough.

5. Conclusions

The basic momentum equation is solved correctly by the model, as is shown by the one-dimensional test cases using constant K and $K = K_o z$. The use of different representations for the dissipation term did not significantly alter the solution of the full turbulence model. Although use of the expression $l = \kappa z$ for mixing length instead of the time-varying formulation (Eqn. 7a) only affected the solution at higher levels in the model, Eqn. 7a was selected to allow time variations in l. The option of 'clawing' the mixing length back to zero near the surface was examined, but not seriously considered as an alternative, since for the case where it has most relevance (ie. when the turbulent boundary layer extends to the surface) it caused the solution to behave badly.

The sensitivity of the model to changes in the constants α_b, c and κ is rather variable, changes in Von Karman's constant κ producing the most significant effects. Changes in the constants α_b, c and κ could in principle be used to tune the model for particular applications. However, varying these constants within physically realistic limits proved to be inadequate to tune the model enough to fit a measured tidal data set (see Section 4.2).

For all the various parameter settings used, the solutions of the full turbulent boundary layer equations (Eqns. 1-7) were well-behaved, though in some instances they required smoothing to keep control of finite oscillations that developed in the energy and stress values. The solutions can be used to study aspects of the vertical structure of turbulent flow. For example, a boundary layer thickness analysis has been successful with respect to a range of input parameters (Section 3.6). The prediction of drag coefficients (or friction factors) has also been considered in respect of the one-dimensional version of the model. Here, the computed values agreed well with empirical estimates for a wide range of input parameters (Section 3.6).

Although qualitative agreement of the model with Vager & Kagan's (1969) numerical results was good, the quantitative comparison was disappointing. This could be due to the different discretisation and computational schemes used in the two cases.

The absolute test of the model's capability involves comparing its predictions with real data. This is difficult since the model does not represent all the physical realities. Some of the assumptions, in addition to the formulation itself, are :

1. No change in surface elevation.
2. No surface stress, eg. due to wind.
3. Constant roughness length (z_o) through time.
4. No topographical influences on the flow.

All these factors must be taken into consideration when comparing the model's results with real data.

Despite the model not being entirely applicable to the experimental conditions in Jonsson and Carlsen's 1976 Test 1, the one-dimensional solution agreed remarkably well with their laboratory data.

The comparison of the two-dimensional model with current meter data from near the Scillies indicated that the model predicts the first order behaviour of the flow satisfactorily. It did not however reproduce the finer detail of the data, which indicates that some of the turbulence closure assumptions could be improved.

All the tests and trials completed recommend the model as a useful tool to study many aspects of the structure of oscillating, turbulent, boundary layer flow. Since velocities are easily measured, they can be used to match a solution. The solution can then be used to obtain whatever aspects of the flow need to be studied, the choice being limited only by the need to write the software to perform the analysis. The model is especially useful for studying flow properties that cannot be realistically measured, but which can be estimated from the solution. For example, an analysis of the mean values of velocity, stress and energy can be used to estimate sediment transport rates in oscillatory flow regimes.

6. References

Bakker, W.T., 1975. Sand concentration in an oscillatory flow. Proceedings of the 14th International Conference on Coastal Engineering, 1974. American Society of Civil Engineers, 1129-1148.

Brevik, I., 1981. Oscillatory rough turbulent boundary layers. Proceedings of the American Society of Civil Engineers, Journal of the Waterway, Port, Coastal and Ocean Division, 107, No. WW3, 175-188.

Dickey, T.P. and Van Leer, J.C., 1984. Observations and simulation of a bottom Ekman layer on a continental shelf. Journal of Geophysical Research, 89, No. C2, 1983-1988.

Johns, B., 1969. On the mass transport induced by oscillatory flow in a turbulent boundary layer. Journal of Fluid Mechanics, 43, 177-185.

Johns, B., 1975. The form of the velocity profile in a turbulent shear wave boundary layer. Journal of Geophysical Research, 80, 36, 5109-5112.

Johns, B., 1977. Residual flow and boundary shear stress in the turbulent bottom boundary layer beneath waves. Journal of Physical Oceanography, 7, 733-738.

Jonsson, I.G., 1967. Wave boundary layers and friction factors. Proceedings of the 10th International Conference on Coastal Engineering, 1966. American Society of Civil Engineers, 127-148.

Jonsson, I.G., 1978. A new approach to oscillatory rough turbulent boundary layers. Technical University of Denmark, Institute of Hydrodynamics and Hydraulic Engineering, Ser. Pap. 17, 87pp. (Also in Ocean Engineering, 1980, 7, 109-152).

Jonsson, I.G. and Carlsen, N.A., 1976. Experimental and theoretical investigations in an oscillatory turbulent boundary layer. Journal of Hydraulic Research, 14, 1, 45-60.

Kajiura, K., 1968. A model of the bottom boundary layer in water waves. Bulletin of the Earthquake Research Institute, 46, 75-123.

Kamphuis, J.W., 1975. Friction factor under oscillatory waves. Proceedings of the American Society of Civil Engineers. Journal of the Waterway, Port, Coastal and Ocean Division, 101 No. WW2, 135-144.

Lamb, H., 1932. Hydrodynamics (6th edition). Cambridge University Press, Cambridge, 738pp.

Long, C.E., 1981. A simple model for time-dependent stably stratified turbulent boundary layers. Dept. of Oceanography, University of

Seattle, Seattle, Wash., Special Report 95, 170pp.

Mitchell, A.R., 1969. Computational methods in partial differential equations. John Wiley and Sons Ltd., London, 255pp.

Prandle, D., 1982. The vertical structure of tidal currents. Geophysical and Astrophysical Fluid Dynamics, 22, 29-49.

Smith, J.D., 1977. Modelling of sediment transport on continental shelves, pp539-577 in The Sea, Volume 6, by E.D.Goldberg, I.N.McCave, J.J. O'Brien and J.H. Steele (Editors). Wiley-Interscience, New York, 1048pp.

Smith, T.J. and Takhar, H.S., 1977. The calculation of oscillatory flow in open channels using mean turbulence energy models. Simon Engineering Laboratories, University of Manchester, UK., Report No. HHS/77/01, 34pp.

Soulsby, R.L., 1983. The bottom boundary layer of shelf seas, pp189-266 in Physical Oceanography of Coastal and Shelf Seas, by B. Johns (Editor), Elsevier, Amsterdam, 470pp.

Vager, B.G. and Kagan, B.A., 1969. The dynamics of the turbulent boundary layer in a tidal current. Atmospheric and Ocean Physics, 5, No. 2, 168-179.

Appendix A : Transformed equations.

Normalisation

The variables are non-dimensionalised as follows :

$$u' = {}^{u}/_{U_o}, \quad v' = {}^{v}/_{U_o}, \quad t' = \omega t, \quad U' = {}^{U}/_{U_o}, \quad V' = {}^{V}/_{U_o}, \quad \Lambda = {}^{\lambda}/_{\omega},$$

$$z' = z\omega/_{U_c}, \quad l' = l\omega/_{U_c}, \quad K' = K\omega/_{U_o^2}, \quad b' = {}^{b}/_{U_c^2}, \quad \tau' = \tau/_{\rho U_o^2}, \quad \varepsilon' = \varepsilon/_{\omega U_c^2}.$$

Depth Transforms

The depth transform may be either log or log-linear depending on the value specified for z_*.

Log	Log-Linear
$\zeta = \ln(\frac{z'}{z'_o}) \,/\, XL$	$\zeta = \ln(\frac{z'}{z'_o}) + \frac{(z'-z'_o)}{z'_*} \,/\, XL$
$XL = \ln(\frac{z_1}{z_o})$	$XL = \ln(\frac{z_1}{z_o}) + \frac{(z_1 - z_o)}{z_*}$
iff $z_* = 0.0$	iff $z_* \neq 0.0$ & $z'_* = z_*(\omega/_{U_c})$
$\chi = XL\ z'_c \exp(XL\,\zeta)$	$\chi = \frac{XL\ z'\ z'_*}{(z'+z'_*)}$

where χ is a depth transform constant used in the model.

Transformed equations

The differential equations solved in the model are as follows :

$$\frac{\partial u'}{\partial t'} - \Lambda v' = P_u + A(\zeta,z')\frac{\partial^2 u'}{\partial \zeta^2} + B(\zeta,z')\frac{\partial u'}{\partial \zeta} \qquad (A1)$$

$$\frac{\partial v'}{\partial t'} + \Lambda u' = P_v + A(\zeta,z')\frac{\partial^2 v'}{\partial \zeta^2} + B(\zeta,z')\frac{\partial v'}{\partial \zeta} \qquad (A2)$$

$$\frac{\partial b'}{\partial t'} = A(\zeta,z')\left\{(\frac{\partial u'}{\partial \zeta})^2 + (\frac{\partial v'}{\partial \zeta})^2\right\} + \alpha_b\left\{A(\zeta,z')\frac{\partial^2 b'}{\partial \zeta^2} + B(\zeta,z')\frac{\partial b'}{\partial \zeta}\right\} - \varepsilon' \qquad (A3)$$

with

$$P_u = \frac{\partial U'}{\partial t'} - \Lambda V', \qquad P_v = \frac{\partial V'}{\partial t'} + \Lambda U',$$

$$K' = c_c l' \sqrt{b'} \quad , \qquad \varepsilon' = c_\varepsilon (b')^{3/2} / l' \tag{A6}$$

and $$l' = \kappa b'^{1/2} \left\{ \int_0^{\zeta} b'^{-1/2} \chi(\zeta)\, d\zeta + z_c' (b_c')^{-1/2} \right\} \tag{A7a}$$

where

$$A(\zeta, z') = \frac{K'}{\chi^2} \quad , \qquad B(\zeta, z') = \left\{ \frac{\partial K'}{\partial \zeta} - K' XL\, F_*^2 \right\} \Big/ \chi^2$$

$$F_* = \begin{cases} 1.0 & \text{if } z_* = 0.0 \\ \dfrac{z_*'}{(z' + z_*')} & \text{if } z_* \neq 0.0 \end{cases}$$

The boundary conditions

$$(u', v') = (0,0) \qquad \text{at } \zeta = 0.0$$

$$\frac{\partial u'}{\partial \zeta} = \frac{\partial v'}{\partial \zeta} = 0.0 \qquad \text{at } \zeta = 1.0 \tag{A3}$$

and

$$\frac{\partial b'}{\partial \zeta} = 0.0 \qquad \text{at } \zeta = 0.0 \quad \text{and } \zeta = 1.0$$

$$l' \rightarrow \kappa z_o' \qquad \text{as } \zeta \rightarrow 0.0. \tag{A8}$$

Appendix B : Discretised equations and the tridiagonal systems.

1. Discretised equations.

The discretisation is as follows :

N time intervals / cycle : $N * \delta t' = 2\pi$

M height intervals : $M * \delta\zeta = 1$

The differential equations are implemented at half time-steps $(n+0.5)\delta t'$ for each $\zeta_m = (m-1)\delta\zeta$ for m=1,M+1. The derivative replacements are as follows :

$$\frac{\partial f}{\partial t'} \quad \text{replaced by} \quad \frac{f_m^{n+1} - f_m^n}{\delta t'}$$

$$\frac{\partial f}{\partial \zeta} \quad \text{replaced by} \quad \frac{1}{2}\left\{ \frac{f_{m+1}^{n+1} - f_{m-1}^{n+1}}{2\delta\zeta} + \frac{f_{m+1}^{n} - f_{m-1}^{n}}{2\delta\zeta} \right\}$$

$$\frac{\partial^2 f}{\partial \zeta^2} \quad \text{replaced by} \quad \frac{1}{2}\left\{ \frac{f_{m+1}^{n+1} - 2f_m^{n+1} + f_{m-1}^{n+1}}{\delta\zeta^2} + \frac{f_{m+1}^{n} - 2f_m^{n} + f_{m-1}^{n}}{\delta\zeta^2} \right\}.$$

where f_m^n denotes the value of f at ζ_m and $t' = n\delta t'$.

Values for l, A and B (see Appendix A) are evaluated at levels m and time (n+0.5), by averaging the values at times n and n+1.

Ideally the representation for the dissipation term should be time-centred about the n+0.5 step; but this does not always generate a well behaved solution. The dissipation term of Equation (6) may implemented in various ways. The term $(b')^{3/2}$ may be expressed in one of three ways :

$$(b_m')^{3/2} \text{ at } n+0.5 \simeq \begin{cases} b_m'^{n+1}(b_m'^{n+1})^{1/2} & \text{at } n+\nu,\ \nu\in(0,1) \quad (B1) \\ 0.5\,[\, b_m'^{n+1,s+1}(b_m'^{n+1,s})^{1/2} + (b_m'^{n})^{3/2}\,] & \text{at } n+0.5 \quad (B2) \\ 0.75\, b_m'^{n+1}(b_m'^{n})^{1/2} + 0.25\,(b_m'^{n})^{3/2} & \text{at } n+0.5 \quad (B3) \end{cases}$$

where s is an iteration parameter.

The integral used to evaluate l may be approximated by the Euler-Maclaurin summation :

$$\int_{x_0}^{x_n} f(x)\,dx \simeq \delta x\,[\, f_0/2 + f_1 + f_2 + \ldots\ldots + f_{n-1} + f_n/2 \,].$$

For the evaluation of the normalised shear stress, eg. τ_u' given by

$$\tau_u' = K' \frac{\partial u'}{\partial z'} = \frac{K'}{\chi} \frac{\partial u'}{\partial \zeta} ,$$

the model uses the approximations

$$\frac{\partial u'}{\partial \zeta} \simeq \frac{u'_{m+1} - u'_{m-1}}{2\delta\zeta} \quad \text{for } m=2,M$$

$$\text{with} \quad \simeq \frac{4u'_2 - 3u'_1 - u'_3}{2\delta\zeta} \quad \text{for } m=1 \qquad (B4)$$

$$\text{and} \quad \simeq \frac{u'_{M-1} + 3u'_{M+1} - 4u'_M}{2\delta\zeta} \quad \text{for } m=M+1 .$$

Alternatively at m=M+1 : $\frac{\partial u'}{\partial \zeta} \simeq \frac{u'_{M+1} - u'_M}{\delta\zeta}$

ie. $\tau_u' = 0.0$ for free surface condition 2) of Eqn. (10)

The values of τ_v' are estimated in a similar fashion.

2. Tridiagonal System for Equations (A1) & (A2).

The approach adopted is fully discussed elsewhere (see Mitchell (1969) and others). The tridiagonal system of equations for the solution of Equations (A1) and (A2) is as follows :

$$-\alpha_m u'^{n+1}_{m-1} + \beta_m u'^{n+1}_m - \gamma_m u'^{n+1}_{m+1} = \alpha_m u'^{n}_{m-1} + (2-\beta_m) u'^{n}_m + \gamma_m u'^{n}_{m+1} + \delta t' \left[P_u + \Pi v' \right]^{n+1/2}_m$$

$$-\alpha_m v'^{n+1}_{m-1} + \beta_m v'^{n+1}_m - \gamma_m v'^{n+1}_{m+1} = \alpha_m v'^{n}_{m-1} + (2-\beta_m) v'^{n}_m + \gamma_m v'^{n}_{m+1} + \delta t' \left[P_v - \Pi u' \right]^{n+1/2}_m$$

The values of $v'^{n+1/2}_m$ and $u'^{n+1/2}_m$ on the right hand sides, are evaluated using

$$f^{n+1/2}_m = 0.5 \left(f^{n+1}_m + f^{n}_m \right)$$

where the value for f^{n+1}_m is from the previous iteration. The coefficients are defined (for notation see Appendix A) by :

$$\alpha_m = \left\{ \frac{A_m^{n+1/2}}{\delta\zeta^2} - \frac{B_m^{n+1/2}}{2\delta\zeta} \right\} \frac{\delta t'}{2}$$

$$\gamma_m = \left\{ \frac{A_m^{n+1/2}}{\delta\zeta^2} + \frac{B_m^{n+1/2}}{2\delta\zeta} \right\} \frac{\delta t'}{2}$$

and $$\beta_m = 1.0 + \frac{\delta t'}{\delta\zeta^2} A_m^{n+1/2} .$$

For a solution of this system of equations to be stable, the following conditions must be satisfied :

$$\alpha_m > 0, \quad \gamma_m > 0, \quad \beta_m > 0 \text{ and } \beta_m > \alpha_m + \gamma_m .$$

Since K>0 implies A>0, whence β>0, and since $\alpha_m + \gamma_m = \beta_m - 1$ is true, the last two conditions are always satisfied. Thus only two conditions require checking in the model.

Note: These conditions are occasionally violated while the solution is warming up. However, provided the coefficients are 'close' to zero, the program is allowed to continue.

3. Tridiagonal System for Equation (A5)

The tridiagonal system for the solution of Equation (A5) is as follows :

$$- a_m b'^{n+1}_{m-1} + \mathfrak{B}_m b'^{n+1}_m - c_m b'^{n+1}_{m+1} = a_m b'^{n}_{m-1} + (2-\mathfrak{B}_m) b'^{n}_m + c_m b'^{n}_{m+1} + \delta t' \left[AQ - \varepsilon' \right]_m^{n+1/2}$$

where $a_m = \alpha_b \alpha_m$, $c_m = \alpha_b \gamma_m$,

$$\mathfrak{B}_m = (1.0 + \alpha_b (\beta_m - 1.0))$$

and $$Q \simeq \left[\left(\frac{\partial u'}{\partial \zeta} \right)^2 + \left(\frac{\partial v'}{\partial \zeta} \right)^2 \right]_m^{n+1/2} .$$

Depending on the formulation of $[b'_m]^{3/2}$, $\mathfrak{B}_m$ and $(2-\mathfrak{B}_m)$ are modified accordingly. The present version of the model incorporates options (B1) and (B3), and the option required is selected by a model input parameter.

Appendix C : Behaviour of the log-linear Transform

This appendix describes the behaviour of the log-linear depth transform with respect to values of M and z_*. The transform of $z \rightarrow \zeta$ is defined as follows :

$$\zeta = \frac{\ln(\frac{z}{z_c}) + \frac{(z - z_c)}{z_*}}{\ln(\frac{z_i}{z_c}) + \frac{(z_i - z_c)}{z_*}}$$

ie. $z \in [z_c, z_i] \Rightarrow \zeta \in [0,1]$.

In order to compare the log-linear with the straight log transform ie

$$y = \frac{\ln(z/z_c)}{\ln(z_i/z_c)} ,$$

the z values equivalent to $\zeta_m = y_m = (m-1)/M$ (z^{ζ}_m and z^{y}_m, respectively) can be compared. The height z_p where z^{ζ}_m and z^{y}_m differ by 10% will then represent the proportion (p) of the transform which is logarithmic :

$$p\% = \frac{z_p}{(z_i - z_c)} * 100.$$

Values of z_p were determined for various values of z_c, z_i, z_* and M, and a relationship between p and z_* was found to be :

$$p = G_{z_i} z_*$$

where G_{z_i} was strongly dependent on z_i and only weakly dependent on z_c and M. G_{z_i} was estimated for five values of z_i (20000, 10000, 5000, 3500 and 2000cm) and a linear function fitted to the points (z_i, G_{z_i}) to obtain

$$z_i = \frac{9.107}{G_{z_i}} + 0.352 \times 10^{3} .$$

With some a priori knowledge of z_p (or p) these last two equations could be used to estimate a suitable value of z_*. However, since M can be selected only by a 'trial and error' approach, this method may as well be used also to obtain a value of z_*. This simply requires the computational levels z_m for a wide range of M and z_* (with the particular values for z_c and z_i) to be calculated. Thereafter, the M and z_* values which produce the most suitably spaced z_m over the water depth can be selected by observation. The selection procedure is made much simpler if certain heights are of particular interest (eg. current meter positions).

Appendix D : Iterative scheme for the solution of the model equations.

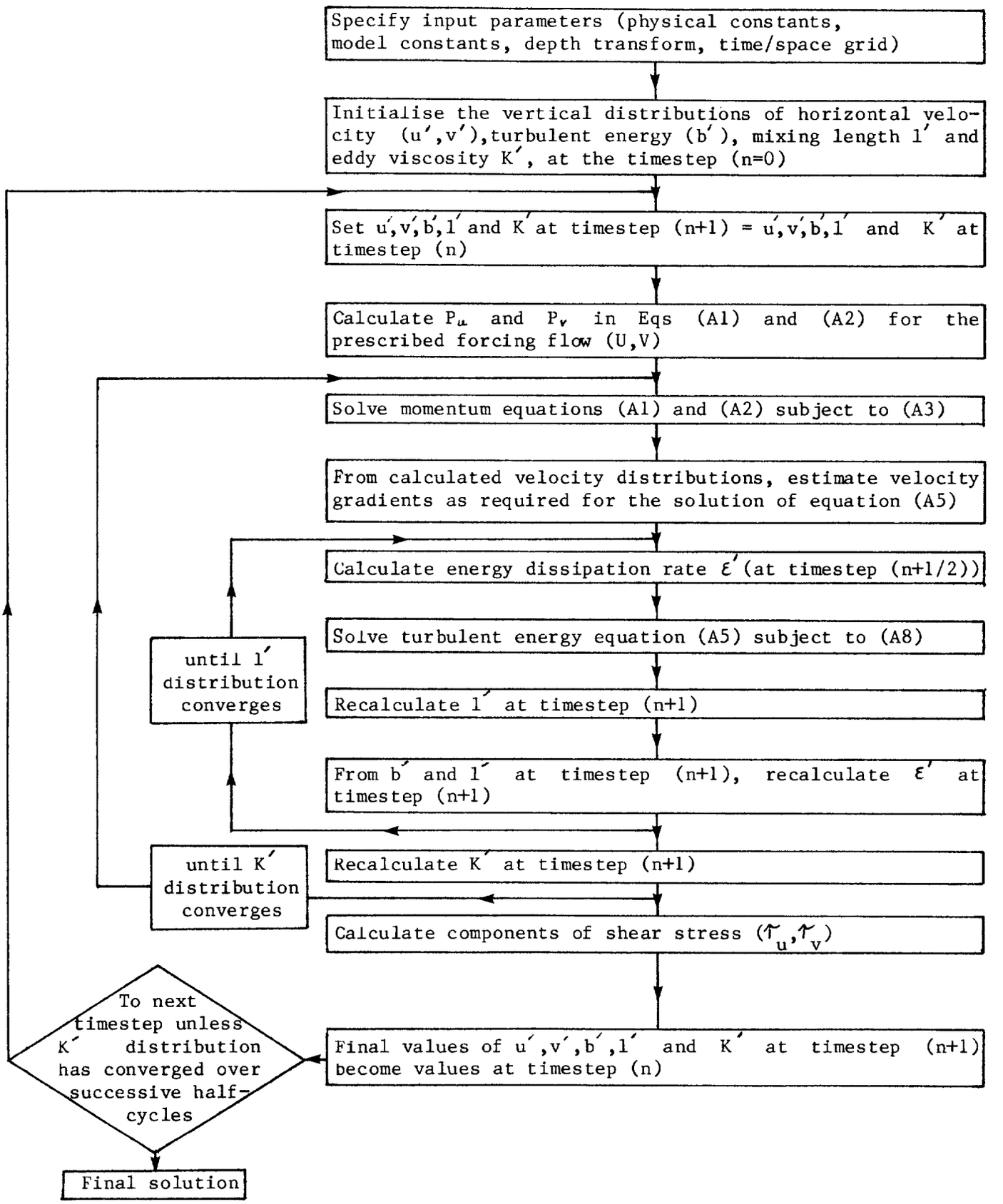

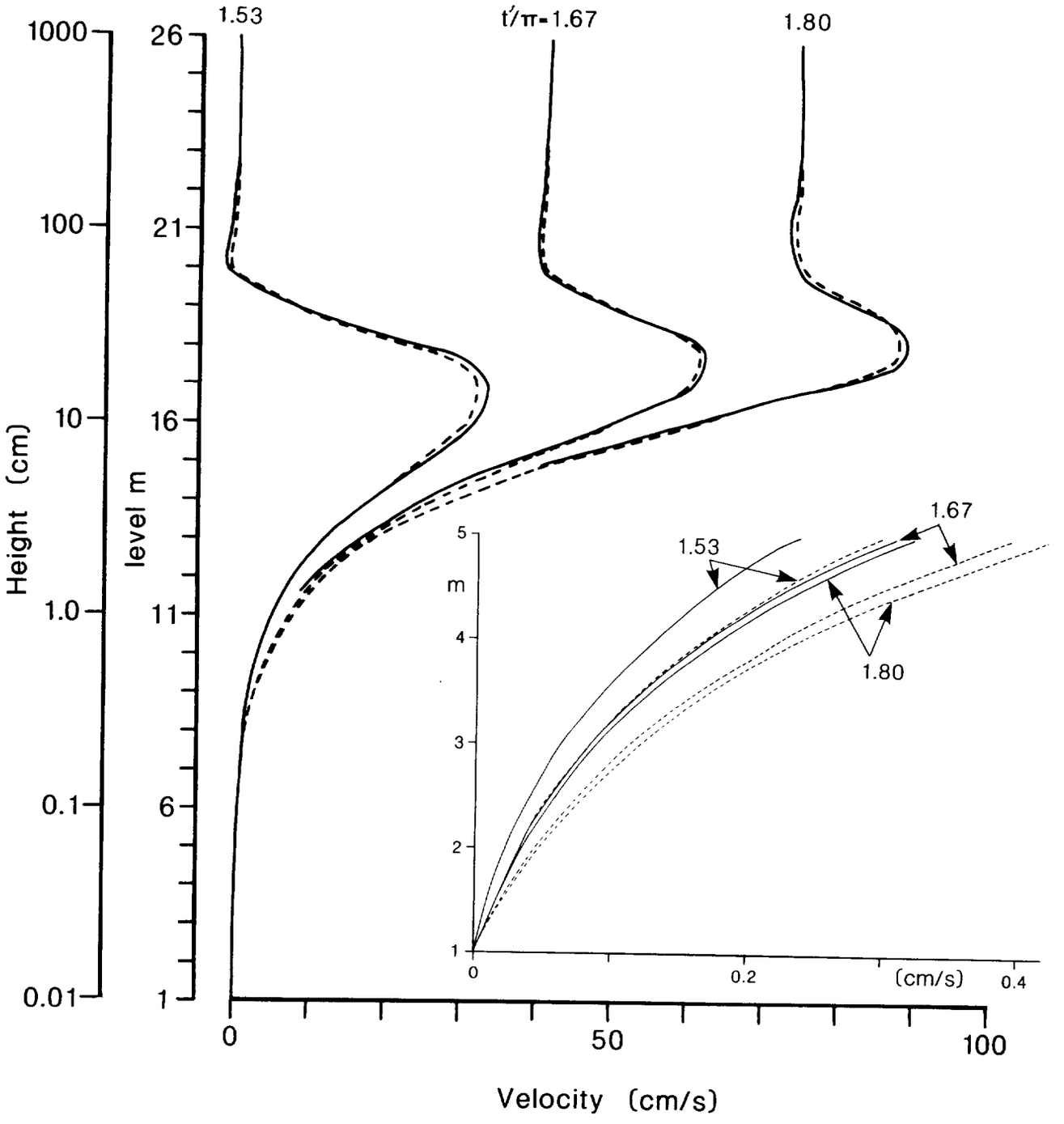

Figure 1: Comparison of velocity profiles from the model (with K=constant) and the analytic solution [Eqn. (11)]. The inset gives the detail for levels 1 to 5.

Model profiles ——————
Analytic solution - - - - - - - - -

The phase angles t' are defined by $t' = (n\delta t' - \pi/2) - 2r$ where r is chosen so that $t' \in [0, 2\pi]$.

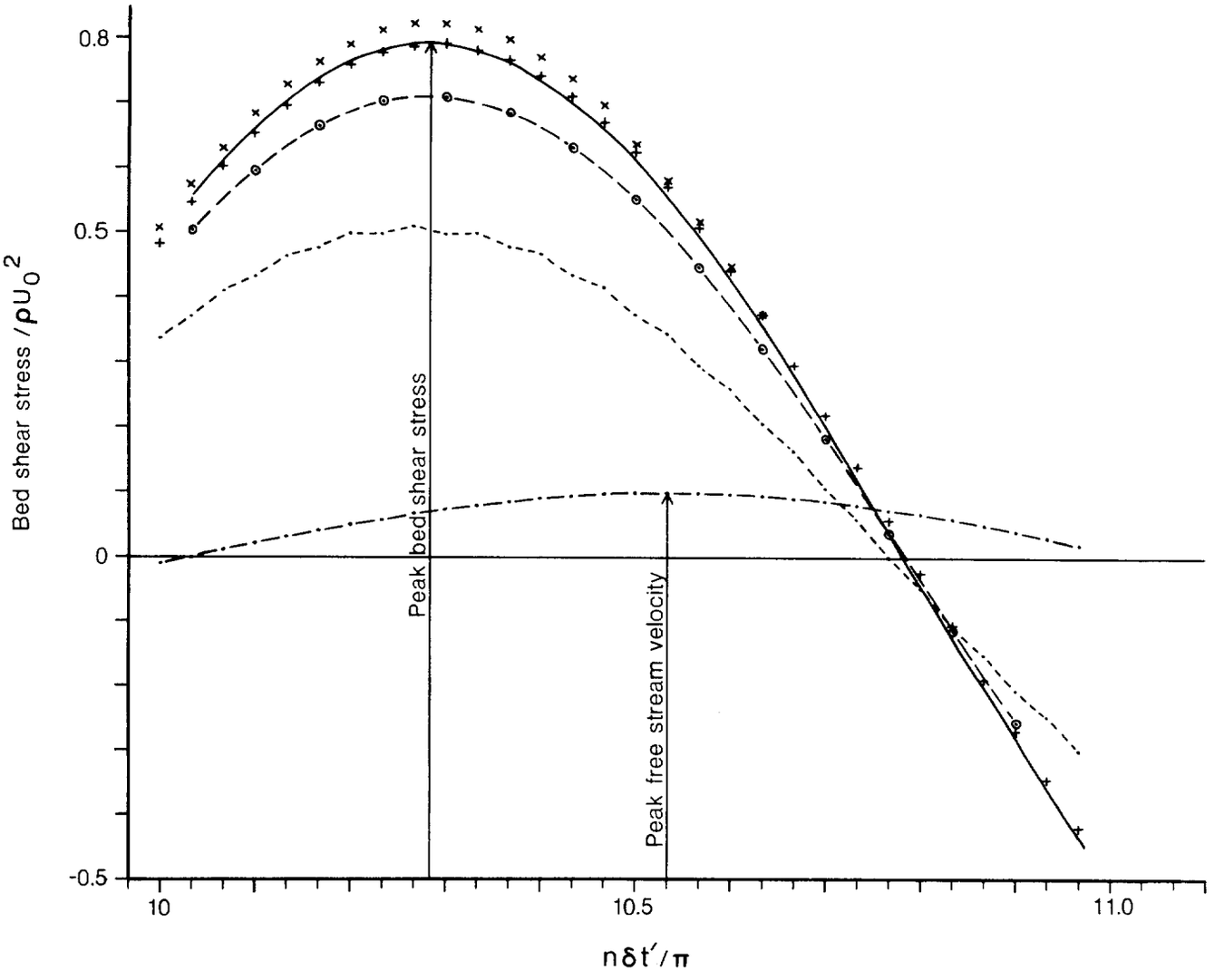

Figure 2: Comparison of bed shear stress estimates from the model (K=constant) with the analytic τ_o' values.

Exact solution for τ_o', Eqn. (10a) ——————

Difference approximations for Eqn. (4a) :

using u' from the model -·--·--·--·-

using exact u' —o— —o— —o—

Model's τ_o' estimates using Eqn. (12) + + +

Model's τ_o' estimates using Eqn. (13) × × ×

Free stream velocity ·— · — · —·

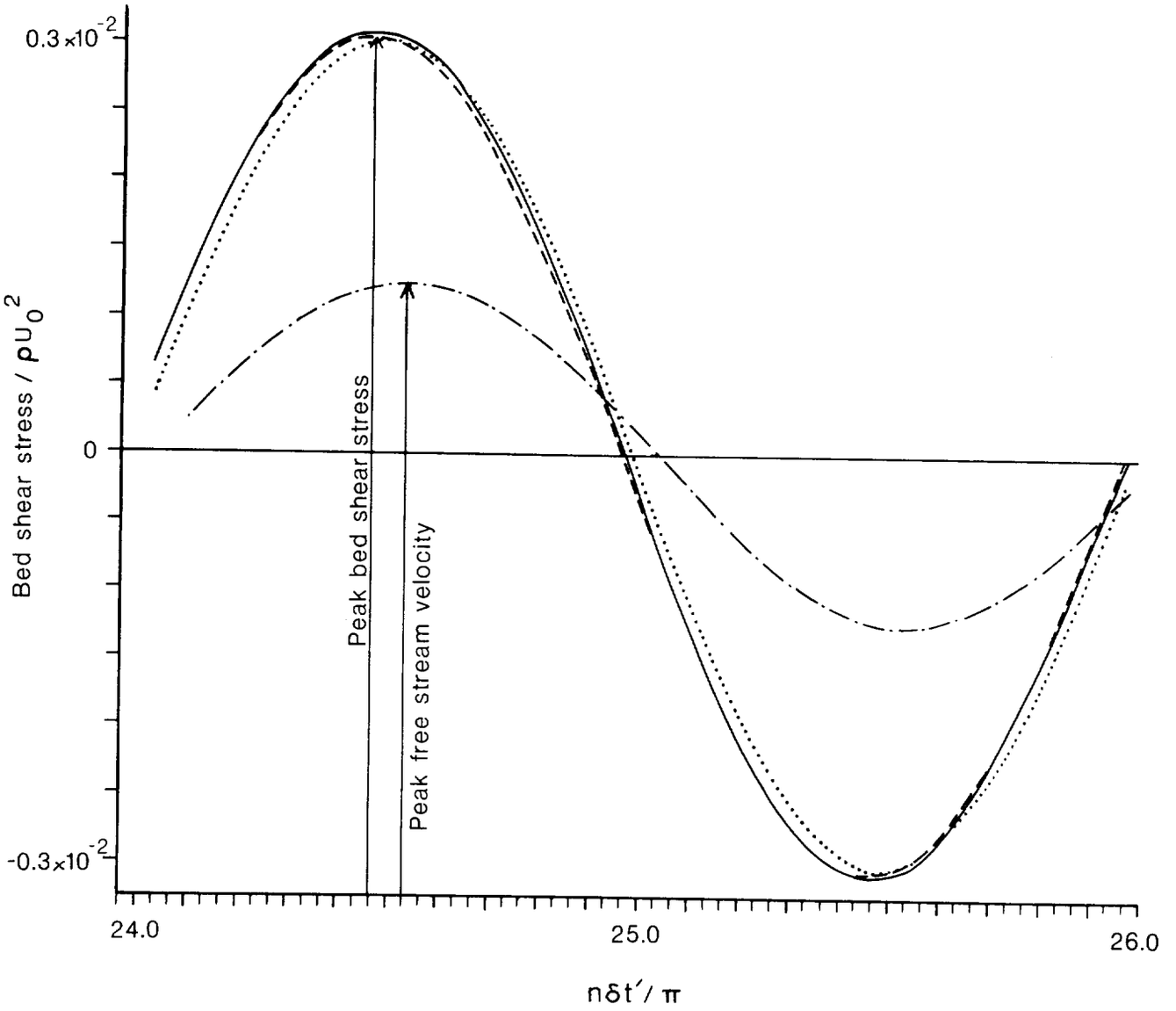

Figure 3: Comparison of bed shear stess estimates from the model with $K=K_0 z$ and the analytic solution.

Analytic solution (Smith, 1977)	————
Model's τ_o' from differenced Eqn. (4a)	– – – – – – – –
Model's τ_o' from Eqn. (12)	. . . . .
Free stream velocity	. — . — . —

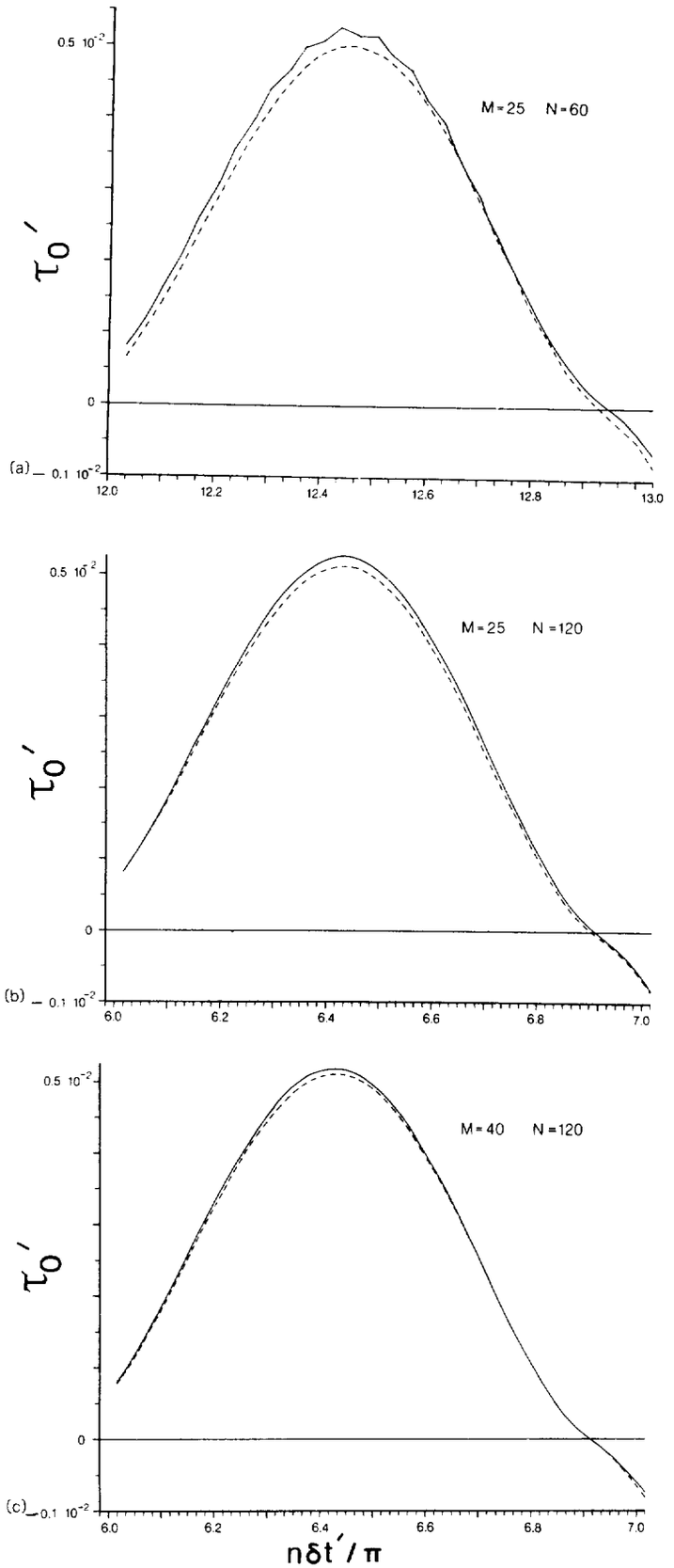

Figure 4: Comparison of normalised bed shear stress τ_o' for various values of M and N.

a) M = 25 N = 60
b) M = 25 N = 120
c) M = 40 N = 120

Model's τ_o' from differenced Eqn. (4a) ————————
Model's τ_o' from defect equation of motion, Eqn. (12) - - - - - - -

Figure 5: Comparison of the model with the results from Jonsson and Carlsen's experiment :

a) velocity profiles
b) shear stress profiles.

The free stream velocity U' is maximum at about $t' = 0.02\pi$ with $\cos(t') = 1.0$ at $t' = 0.0\pi$ where $t' = n\delta t' - (\pi/2+\delta t') - 6\pi$.

In Figure 5b, the model's τ' at z = 17.25cm has been added to the Jonsson and Carlsen values to compensate for the model's non-zero values of stress calculated at this level.

Profiles from the model ————————
Profiles of the Jonsson and Carlsen results. – – – – – – – –

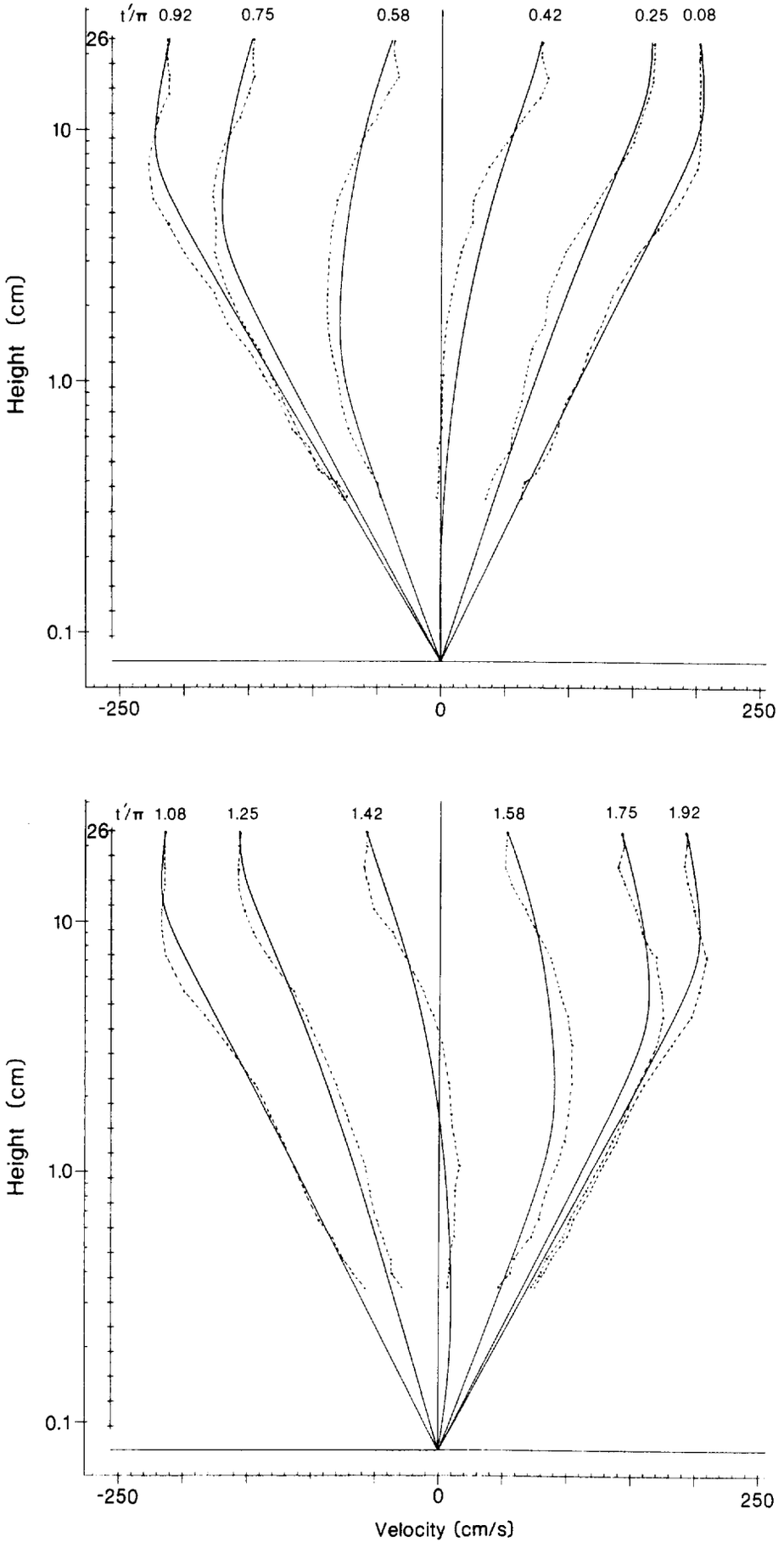

Figure 5a: Velocity profiles.

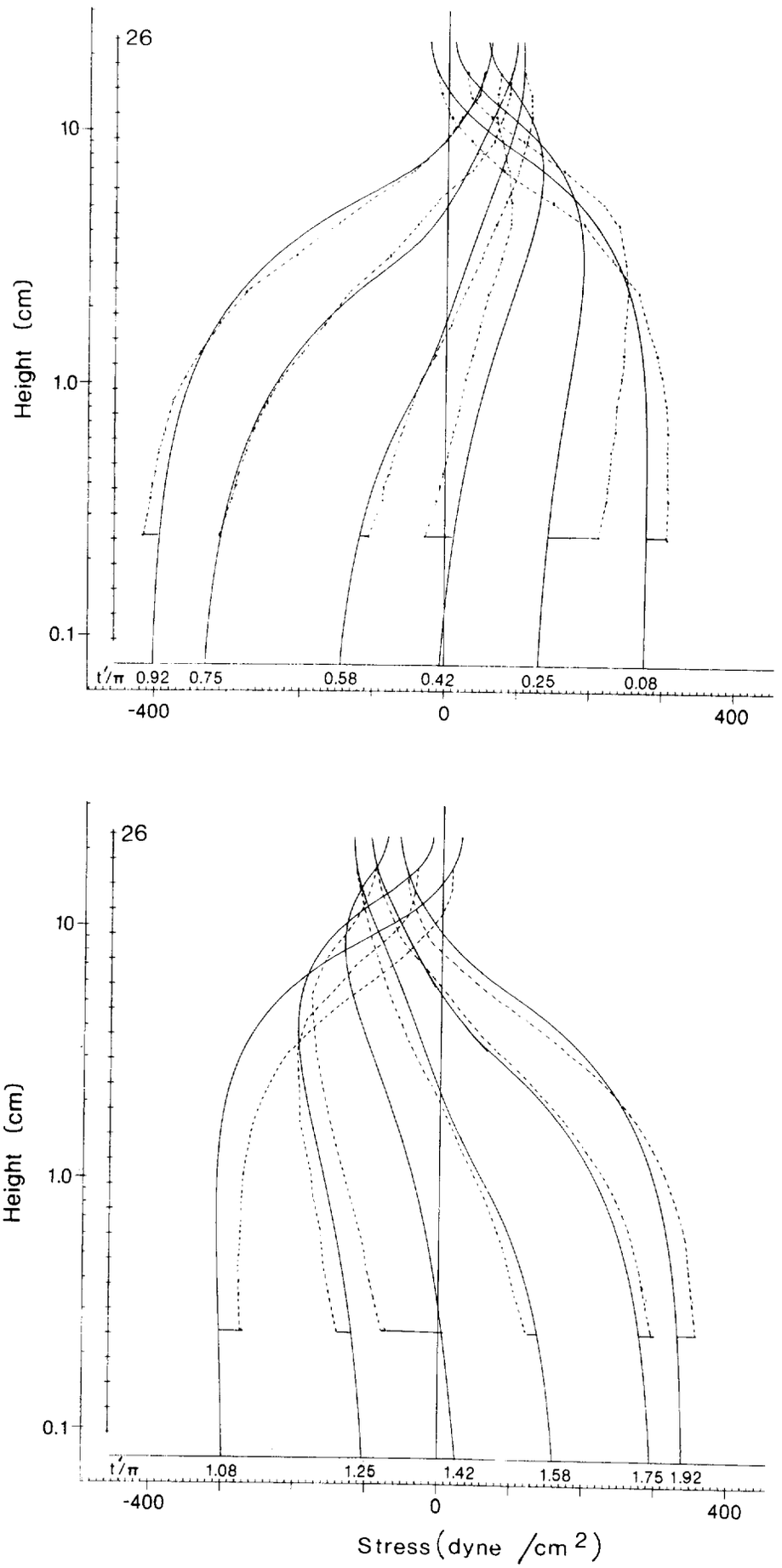

Figure 5b: Shear stress profiles.

Figure 6: Comparison of the model with the results from Jonsson and Carlsen's experiment -

6a) Velocity time series,
6b) Shear stress time series.

Each time series is drawn relative to its own origin, with the base lines indexed at the left of the graph by the corresponding computation level index. The computed series are similarly indexed at the right of the graph.

The correspondence between the model and data levels is :

z Index	Model's z cm	Data z cm
26	23.0	23.25
22	9.23	9.25
16	2.35	2.25
12	0.94	1.05
8	0.38	0.40
6	0.24	0.25

Jonsson and Carlsen's shear stress values are modified as in Figure 5.

Model's values +———+———+
Adjusted Jonsson and Carlsen results *- - -*- - -*

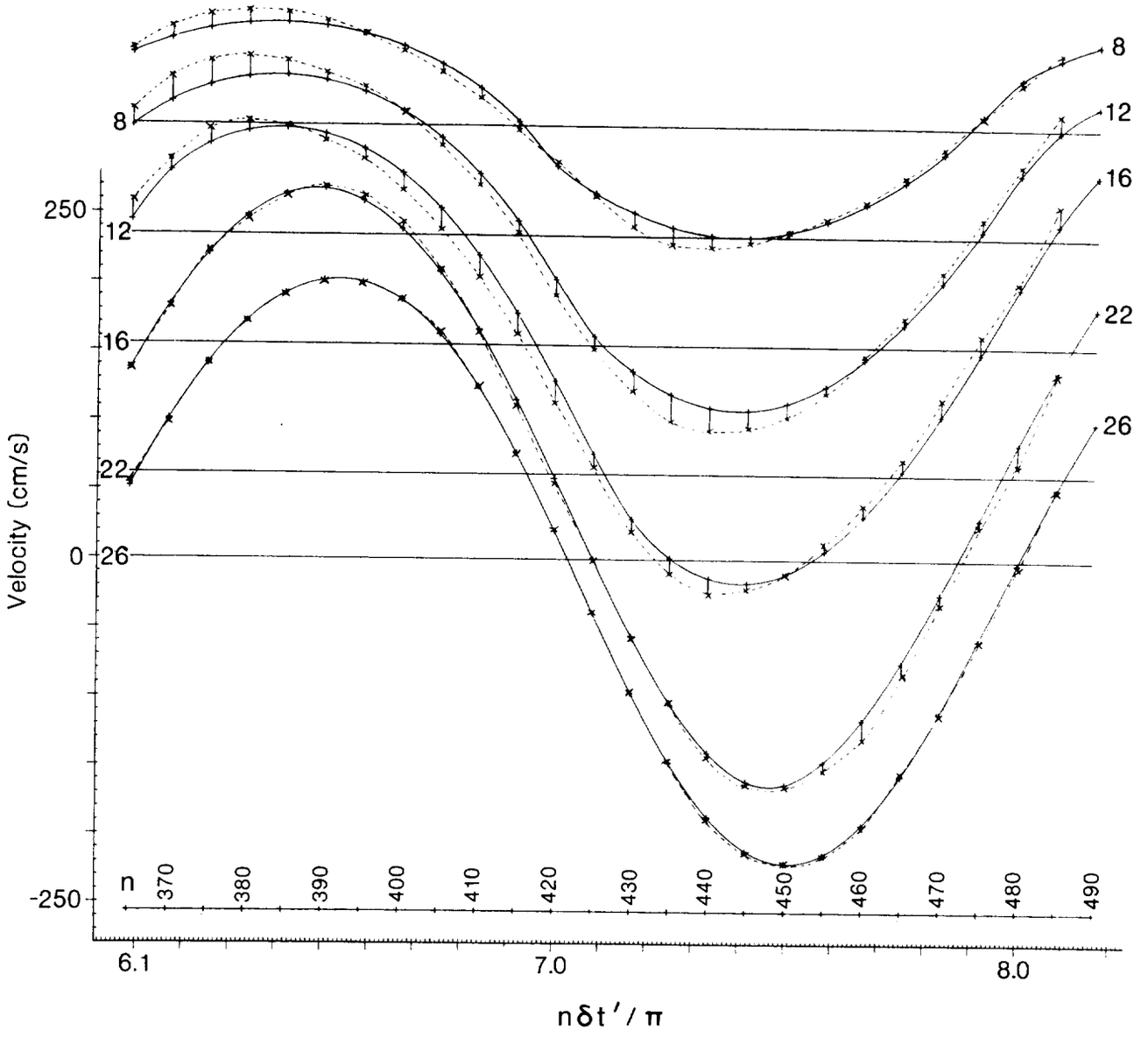

Figure 6a: Velocity time series.

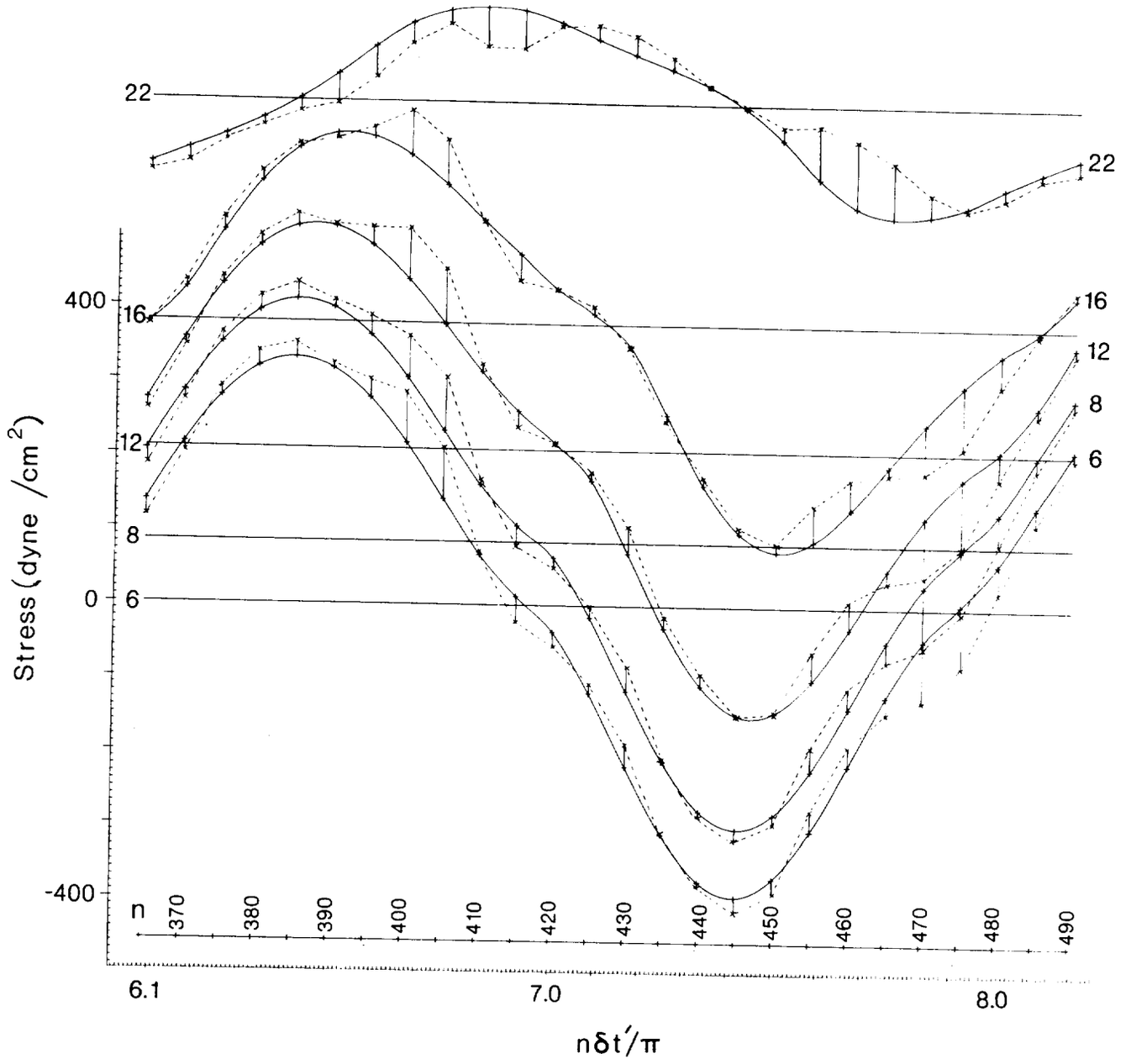

Figure 6b: Shear stress time series.

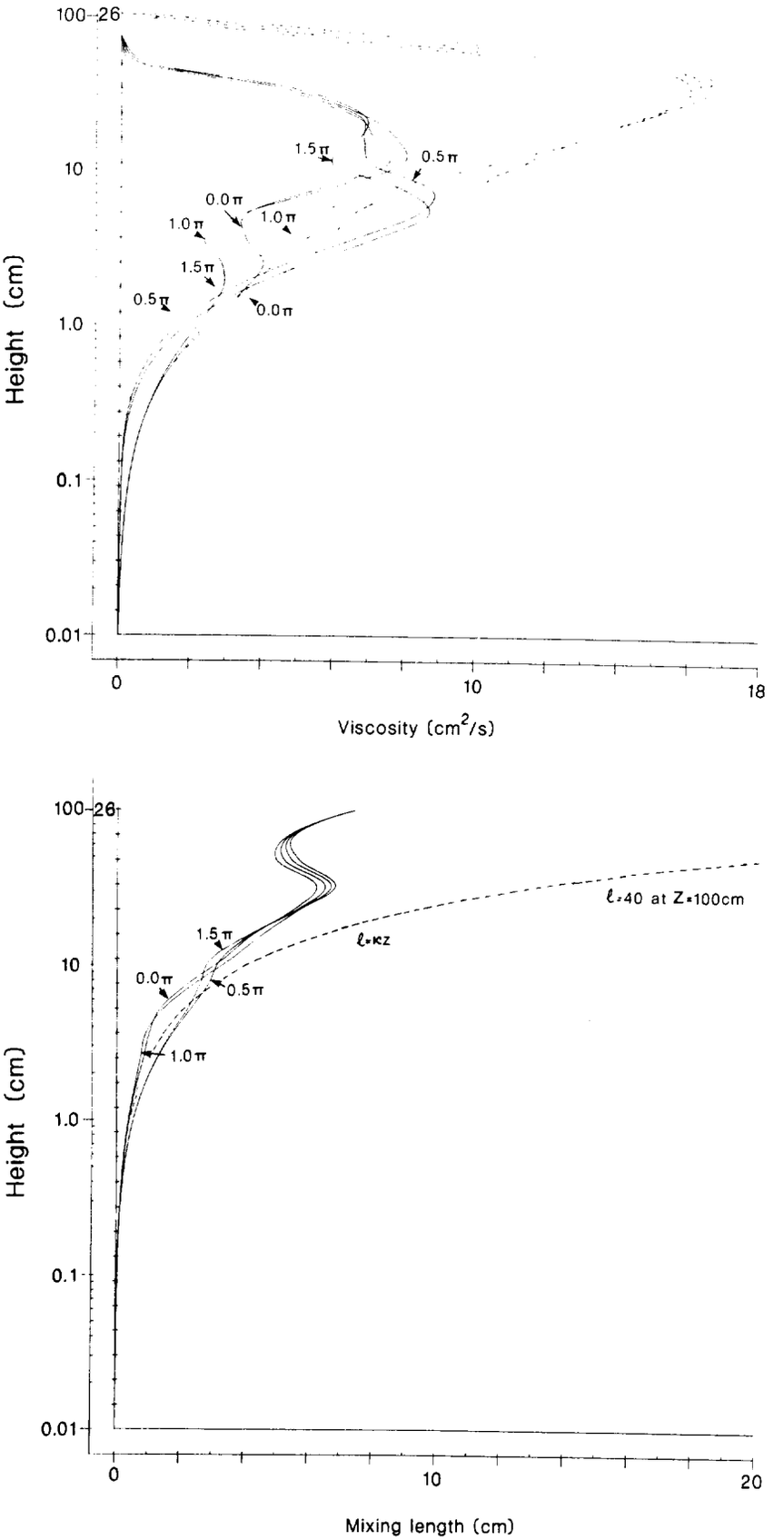

Figure 7: Comparative profile plots for viscosity and mixing length for solutions using :

i) the standard mixing length formula Eqn. (7a) ————————
ii) the linear expression $\ell = \kappa z$ – – – – – – – –

The profiles are plotted at $\pi/2$ intervals over a cycle.

Figure 8 : The comparison of time series for the solutions using different mixing length formulae -

i) Standard formula Eqn. (7a) — — — — —
ii) Linear expression $\ell = \kappa z$ ————————

For each time series, the axis is shifted vertically; the corresponding curves and base lines are indexed by their z level index :

m =	1	8	11	12	13	15	16	17	20	26	
z =	0.010	0.132	0.398	0.575	0.832	1.74	2.51	3.63	10.96	100.0	cm

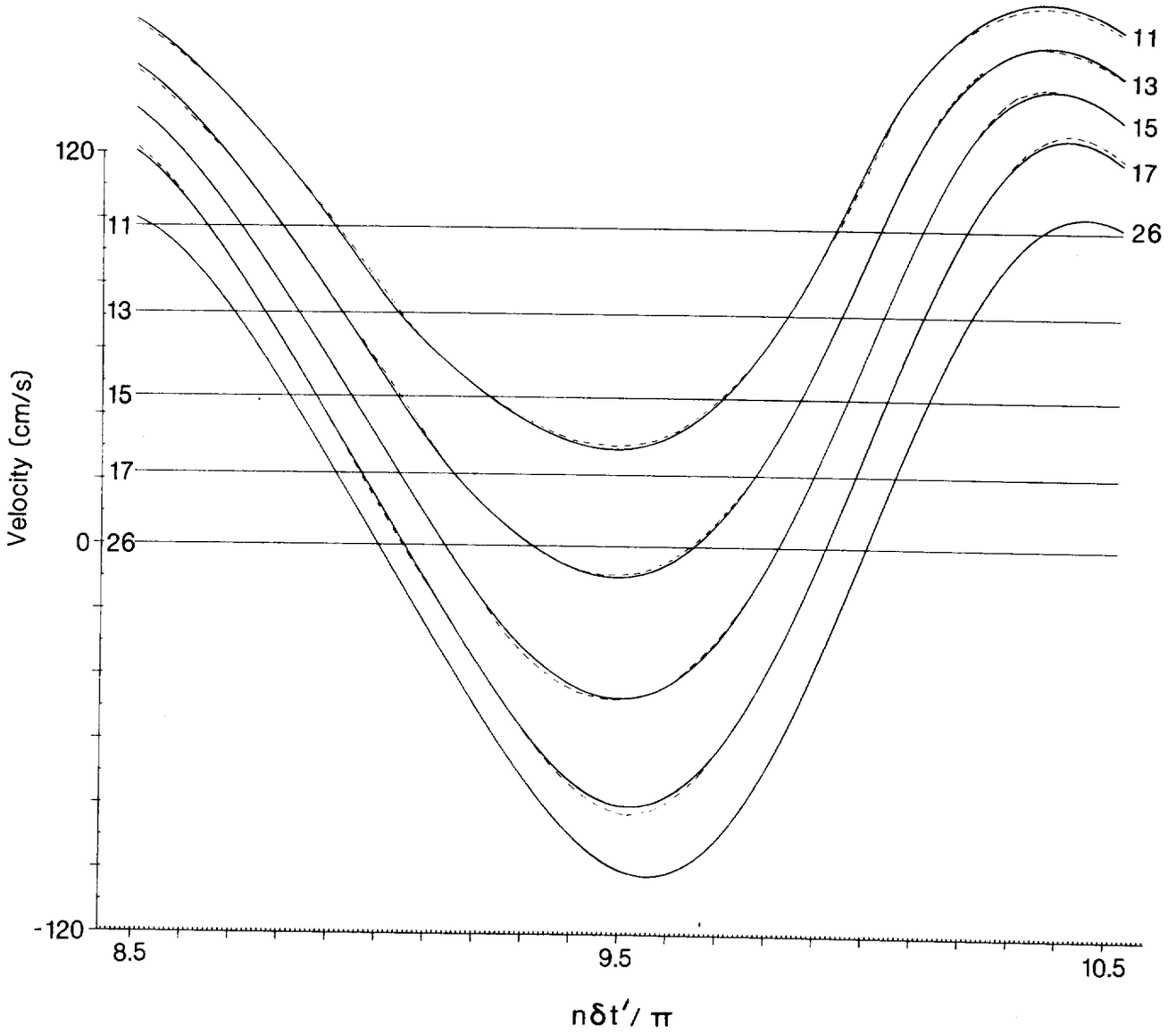

Figure 8a: Velocity time series.

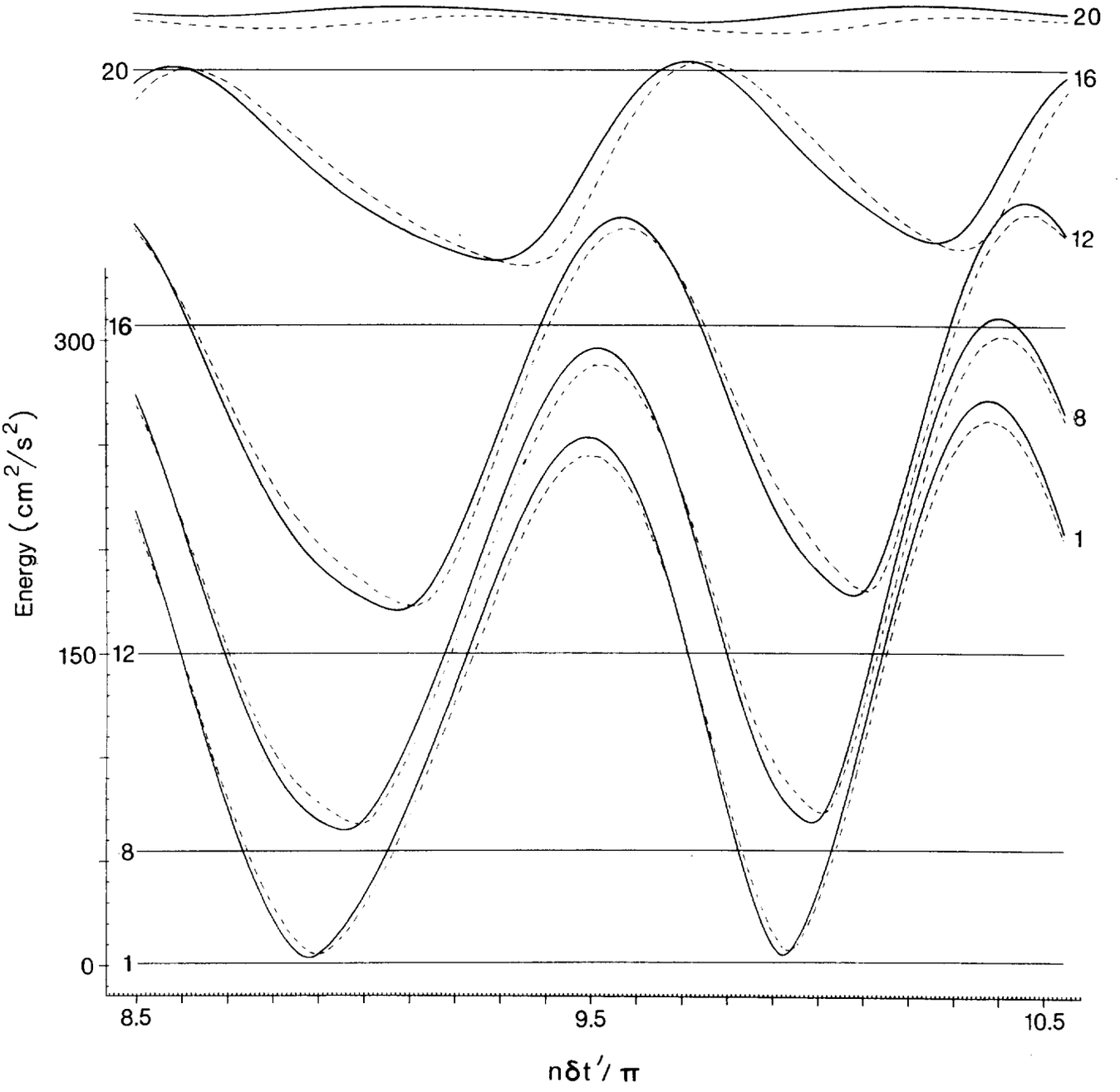

Figure 8b: Energy time series.

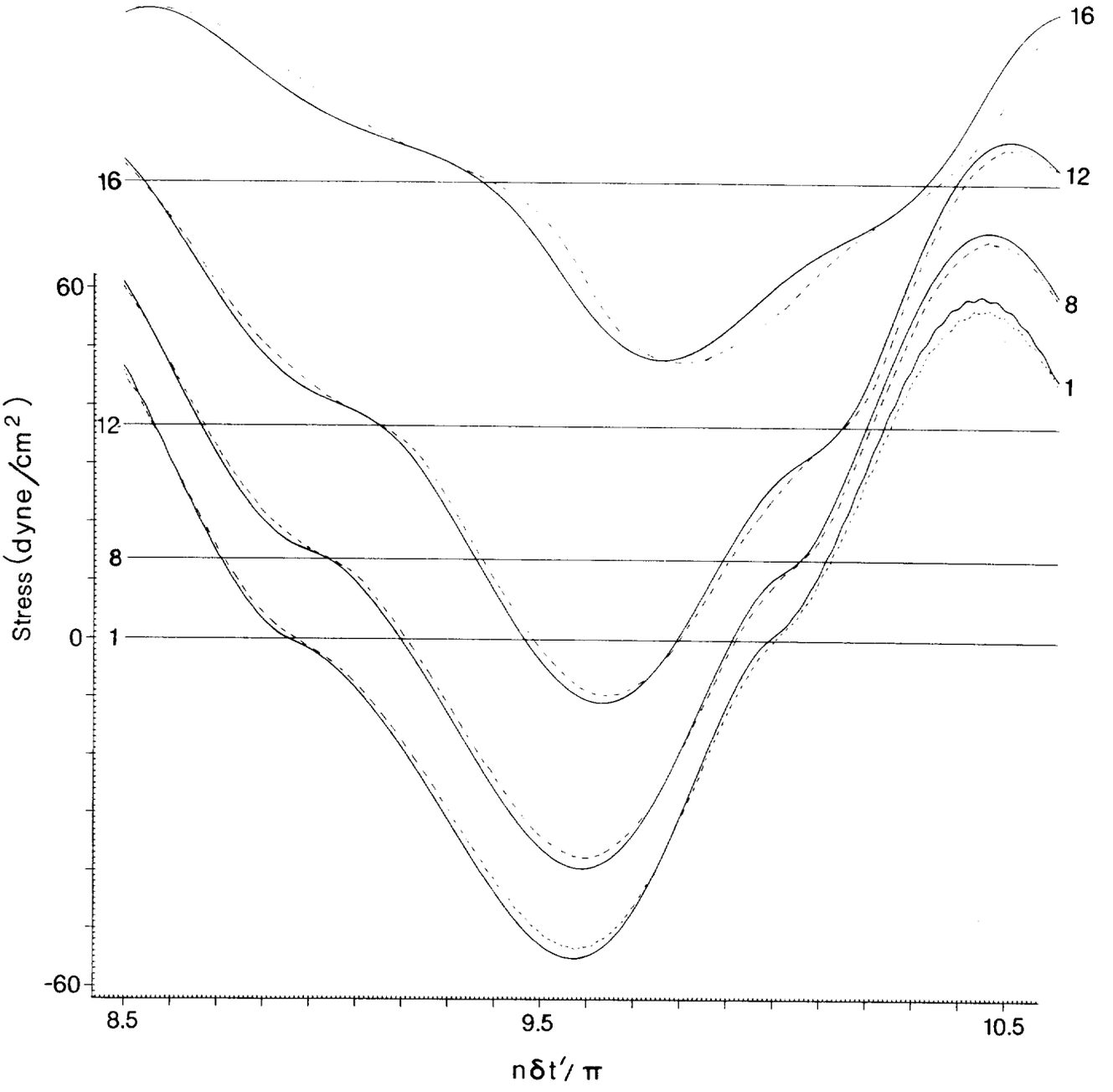

Figure 8c: Shear stress time series.

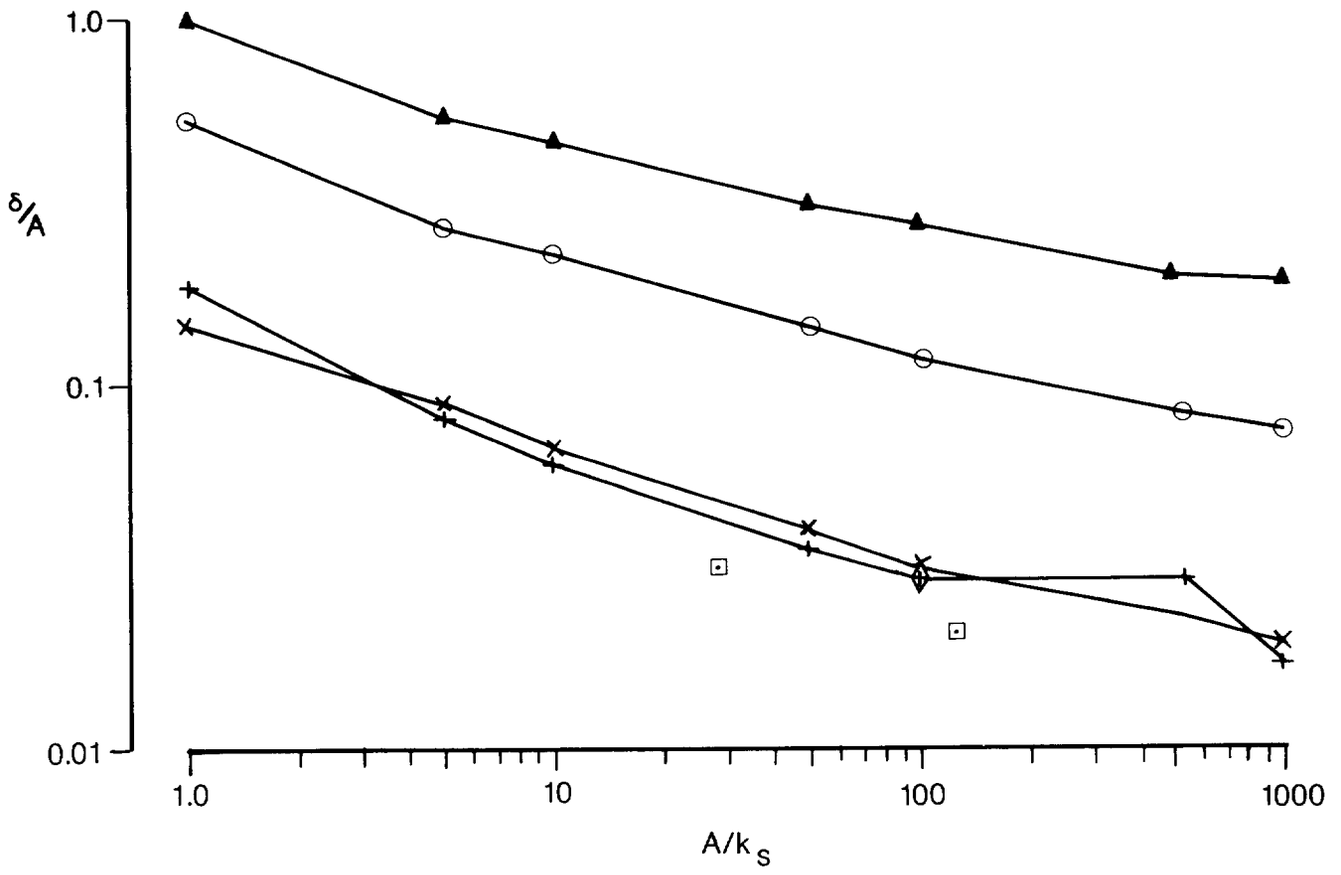

Figure 9: The normalised boundary layer thickness δ/A plotted against the relative roughness A/k_s.

For R_z = 10000 :

δ_1/A	height where peak u' = max U'	+
δ_2/A	height where peak u' profile is 1% from logarithmic	x
δ_3/A	height where peak u' - max U' = 1%	○
δ_b/A	height where (peak b') / (peak b'_0) = 1%	▲

For R_z = 300 :

δ_1/A	from model.	◊
δ_1/A	from Jonsson & Carlsen's (1976) two experiments.	⊡

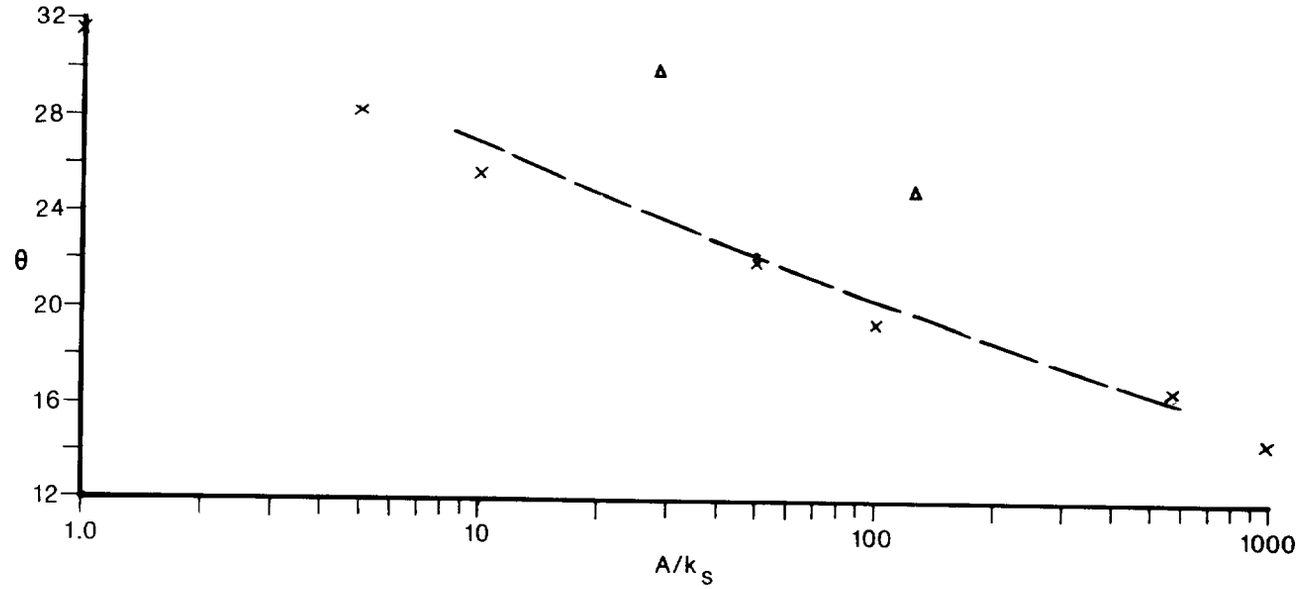

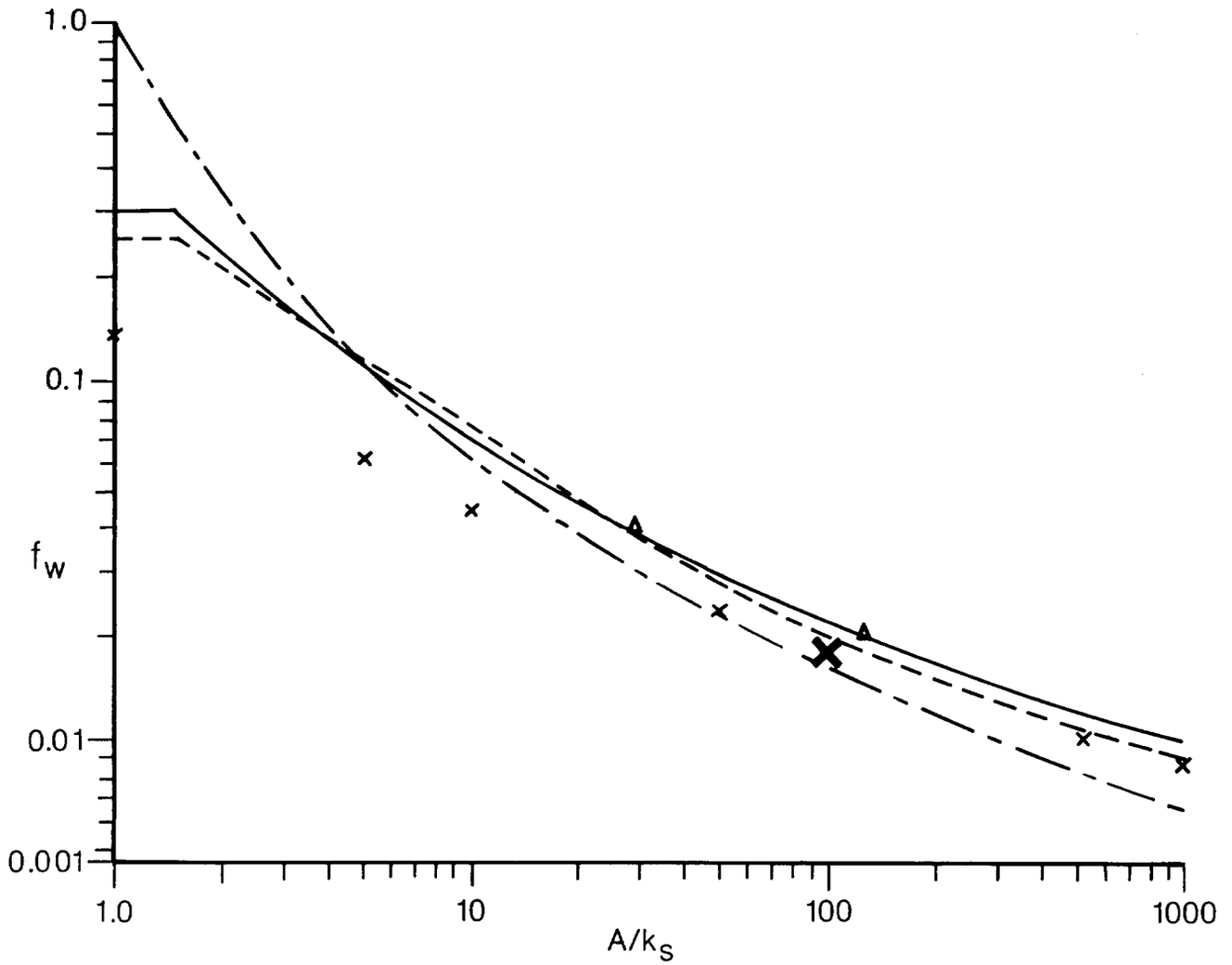

Figure 10: The drag coefficient f_w, and phase lead θ of τ_0' over U', plotted as functions of A/k_s and compared with other relationships.

Kajiura (1968) (- - - - -); Jonsson (1967,1978) (————); Kamphuis (1975) (— - — - —); Jonsson & Carlsen (1976) experimental values (Δ); Smith (1977) (—— —— ——); Model values for $R_z = 10^4$ (×) and for $A/k_s = 100$, R_z = both 10^4 and 300 (✖).

Figure 11: Sensitivity of model's energy values to a change in the constant α_b. Figure 11a compares the vertical profiles and Figure 11b the time series from solutions obtained using the values :

$\alpha_b + 50\% = 1.095$ ——————————
and $\alpha_b - 50\% = 0.365.$ – – – – – – – – –

In 11b, the heights corresponding to the z level indices are :

m	=	1	6	11	16	21
z	=	0.01	0.06	0.40	2.51	15.85 cm

The profiles in 11a are indexed by their phase angle/π where $t' = (n\delta t' - \pi/2) - 8\pi$.

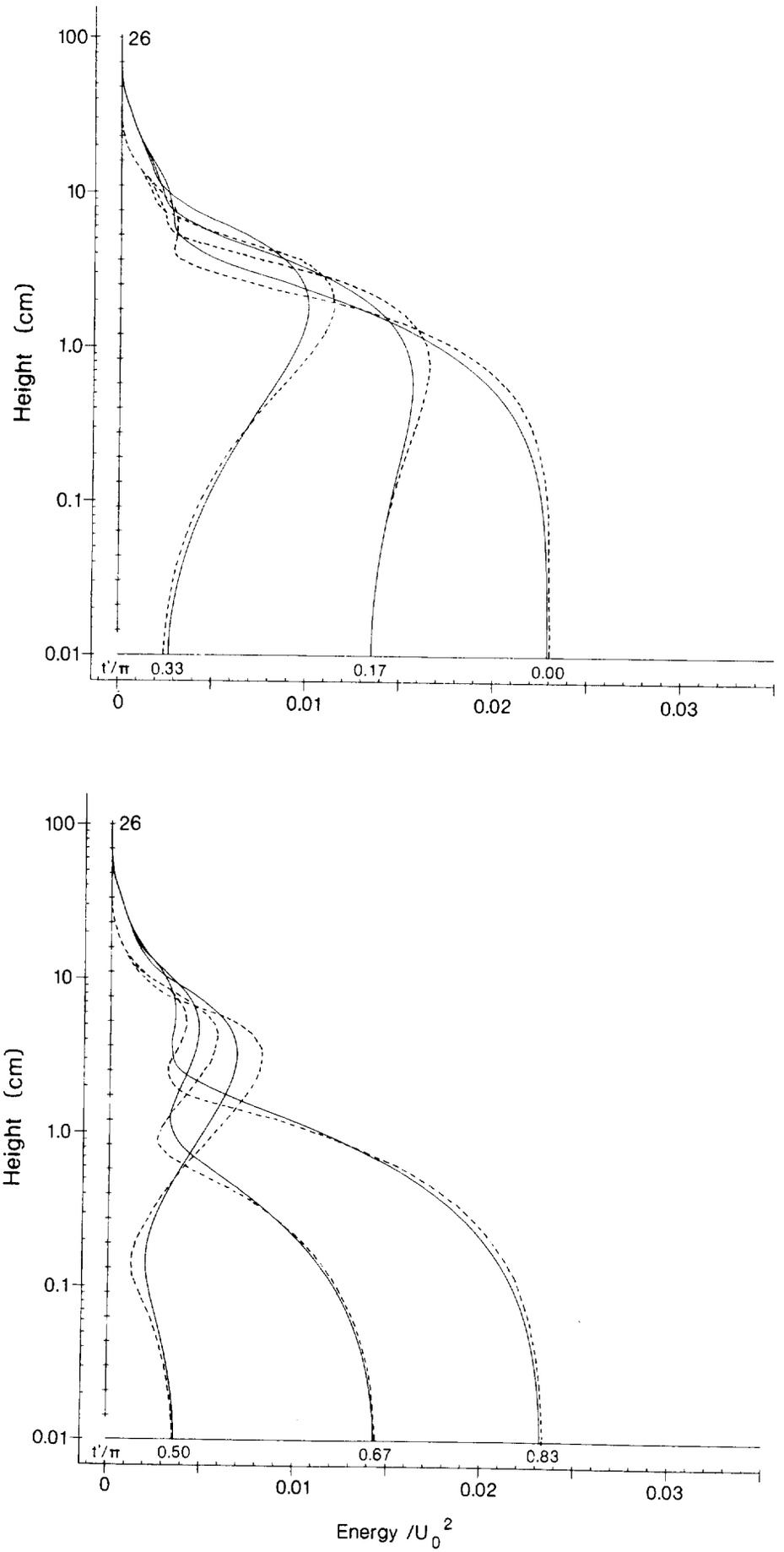

Figure 11a: Energy profiles.

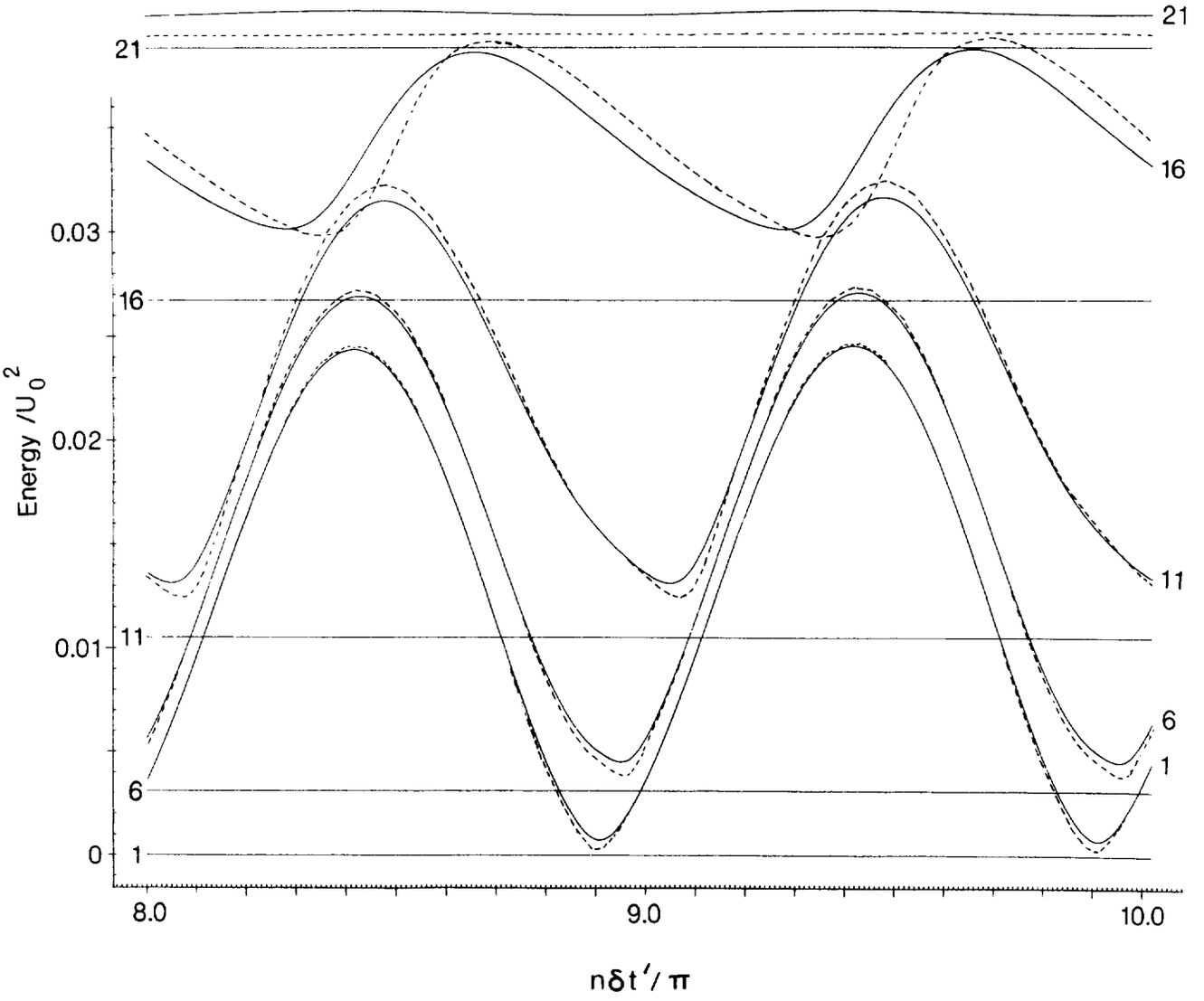

Figure 11b: Energy time series.

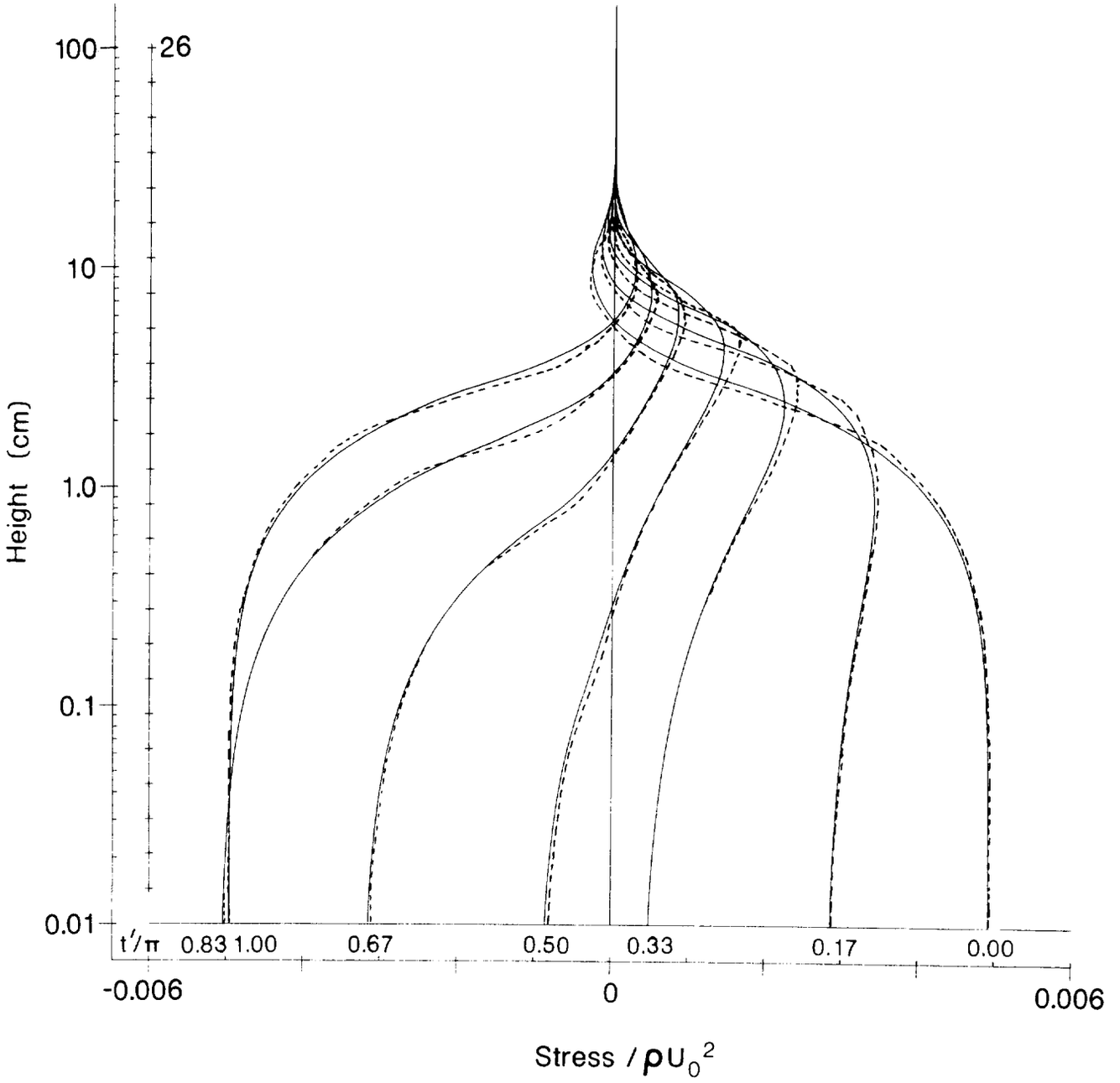

Figure 12a: Shear stress profiles.

Figure 12: The sensitivity of the model's stress values to a change in the constant α_b. The solutions were obtained with the values :

α_b + 50% = 1.095 ——————
and α_b - 50% = 0.365 - - - - - - - - -

12a compares the vertical profiles of stress and 12b the stress time series values. The details of the annotation are as for Figure 11.

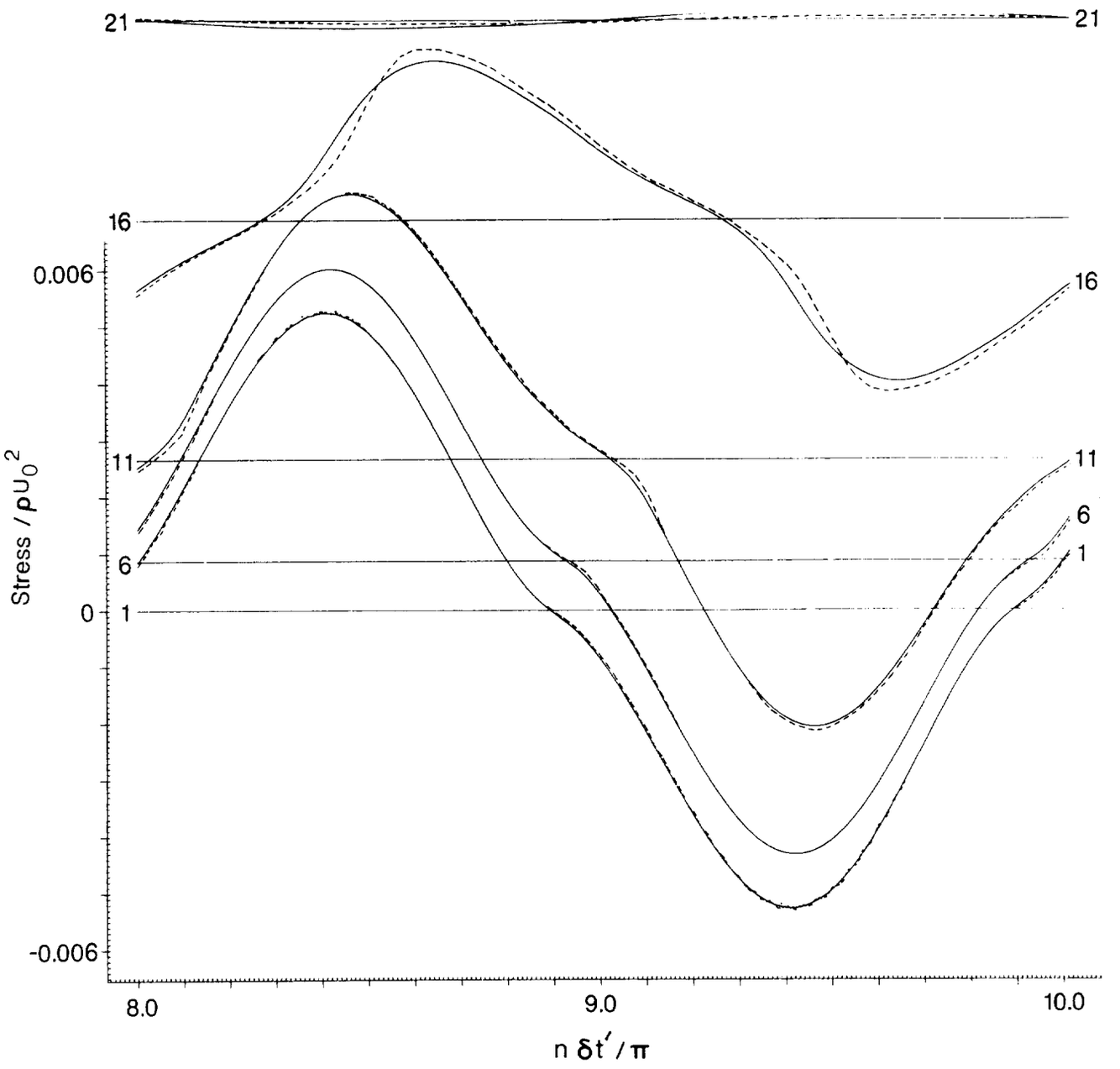

Figure 12b: Shear stress time series.

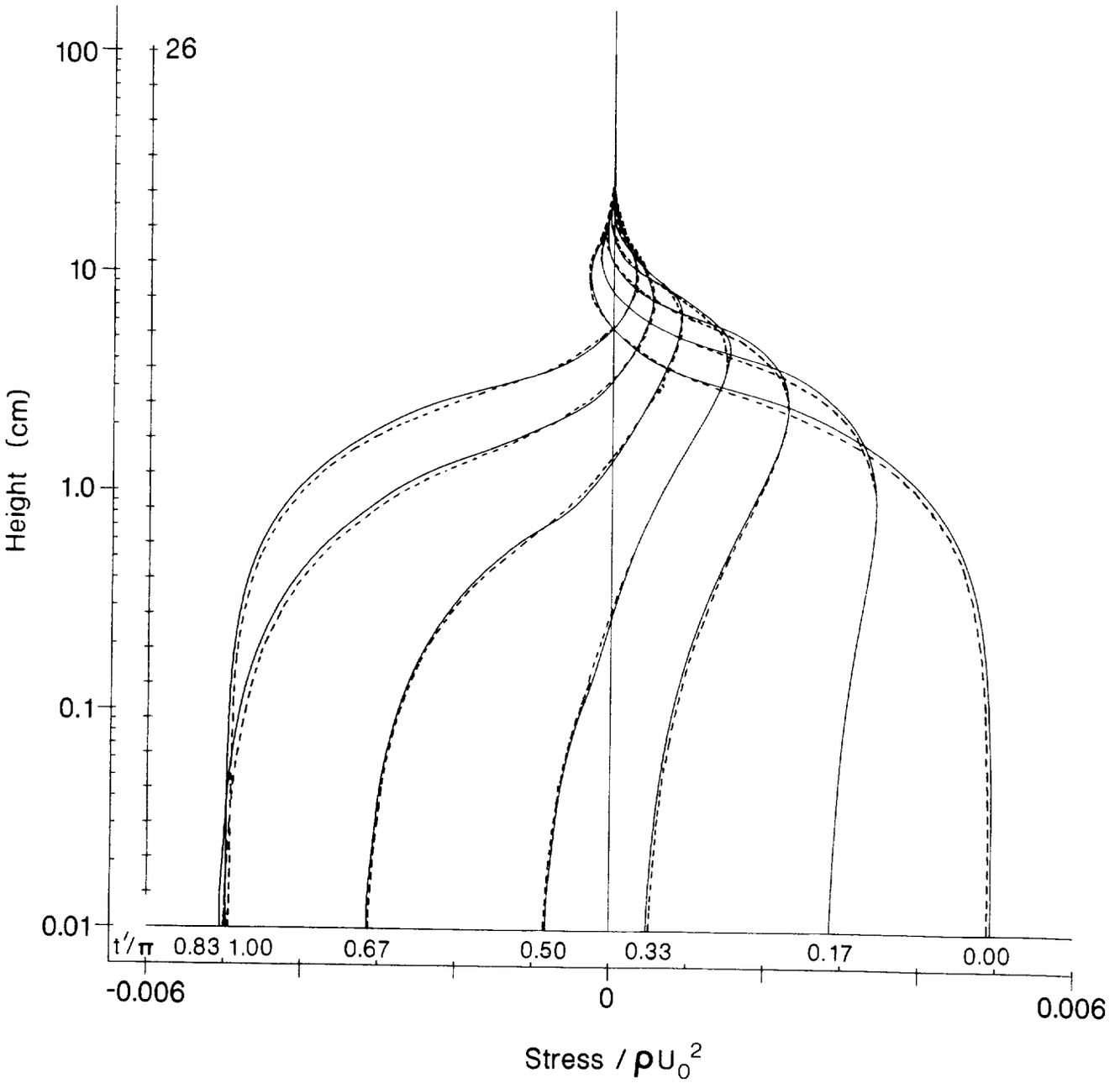

Figure 13a: Stress profiles.

Figure 13: The sensitivity of the model's stress values to a change in the constant c. Figure 13a compares the vertical profiles, and 13b the time series, from solutions obtained using :

c + 50% = 0.089 ————————
and c - 50% = 0.046. — — — — — — —

The details of the annotation are as for Figure 11.

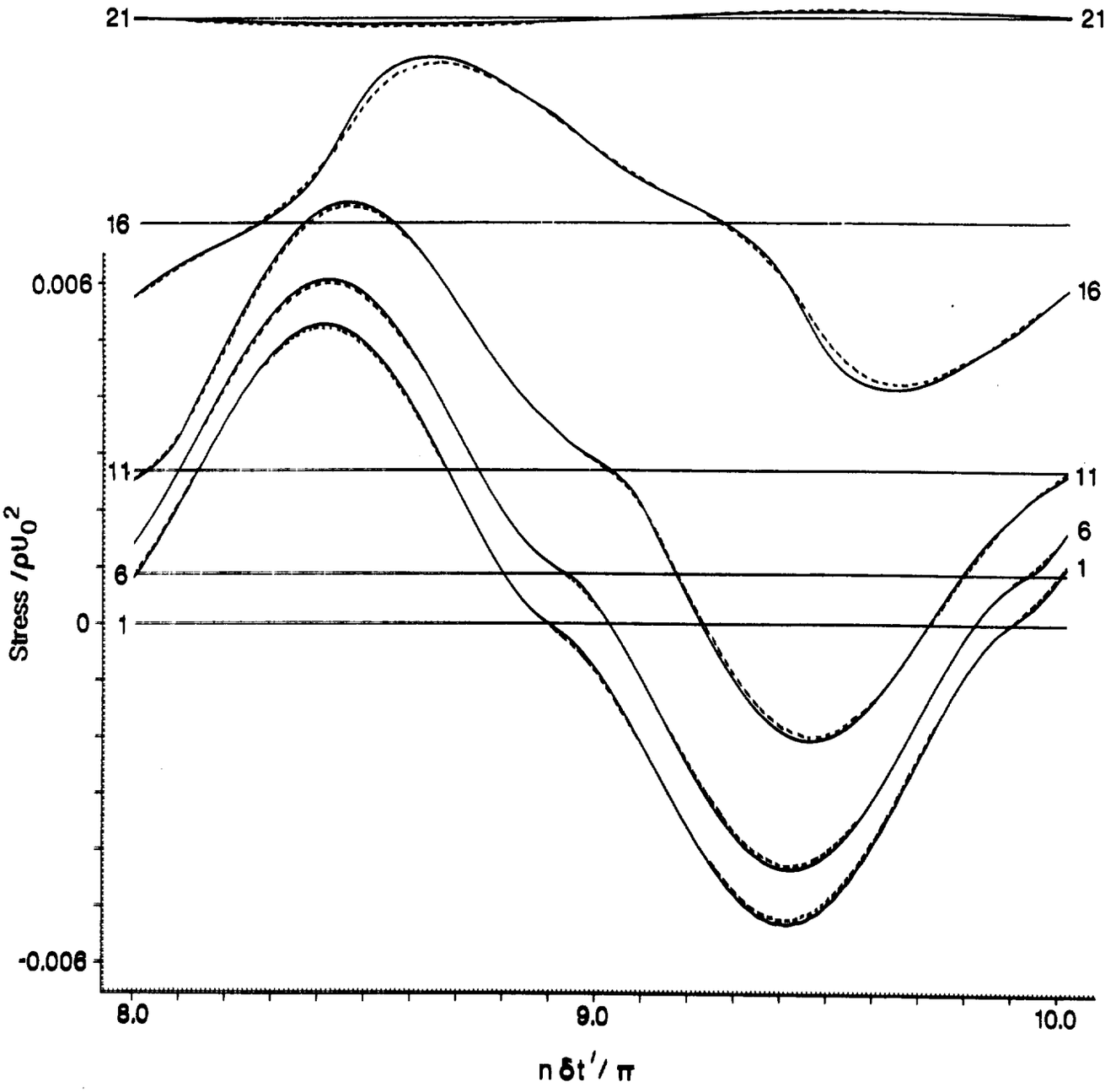

Figure 13b: Stress time series.

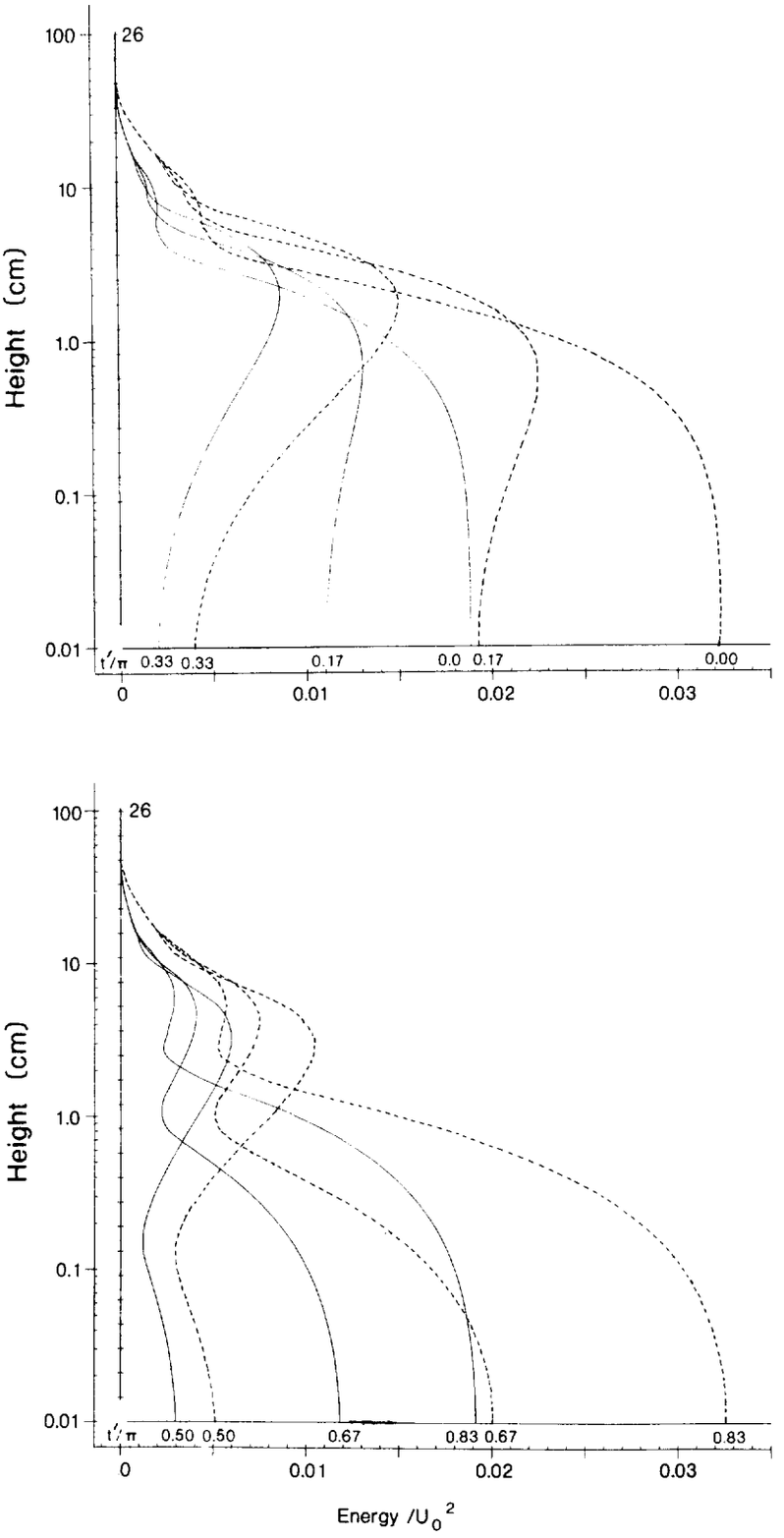

Figure 14a: Energy profiles.

Figure 14: The sensititivity of the model's energy values to a change in the constant c. Figure 14a compares profiles and 14b time series from solutions obtained using :

c + 50% = 0.089 ——————

and c - 50% = 0.023. — — — — — — —

The details of the annotation are as for Figure 11.

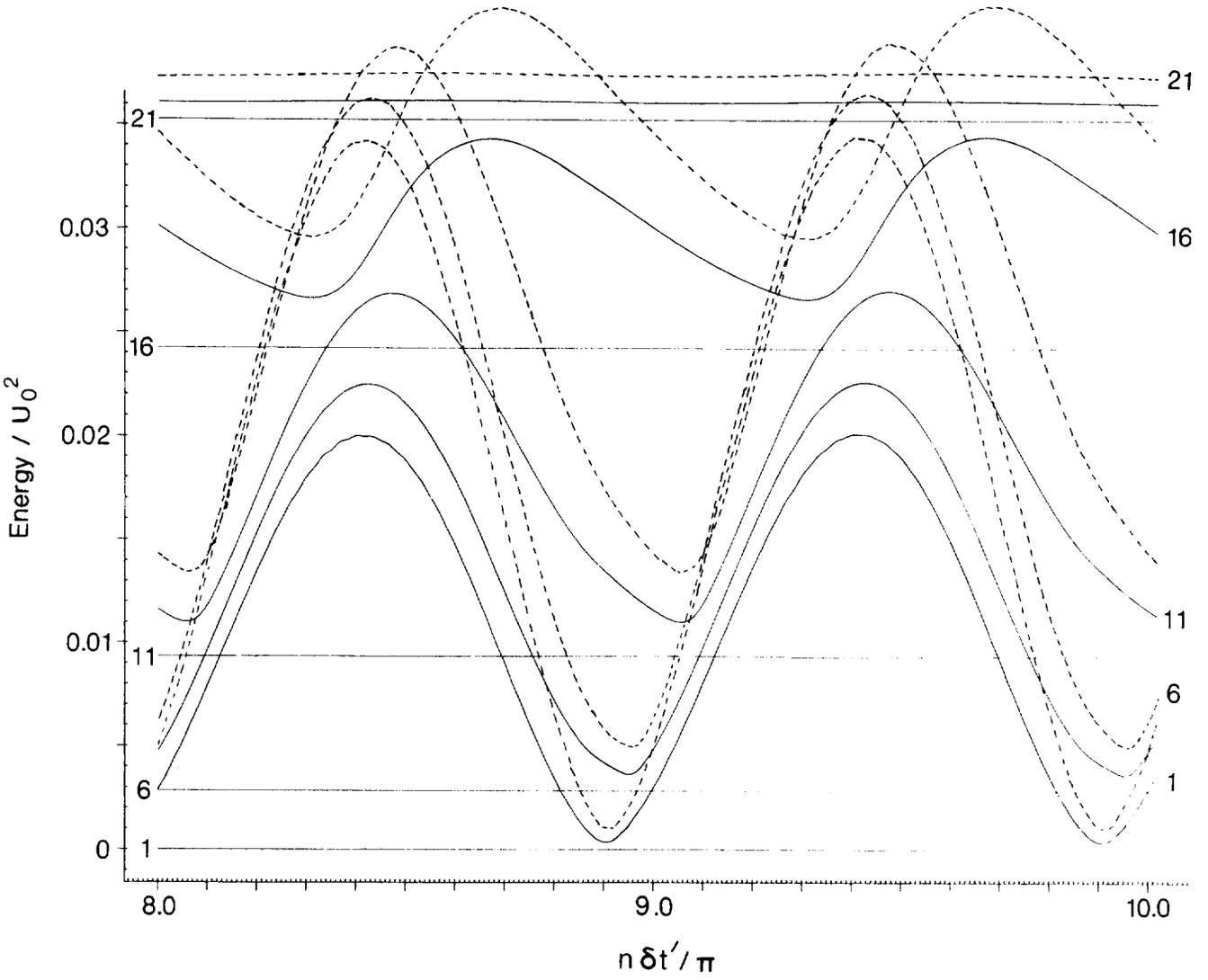

Figure 14b: Energy time series.

Figure 15: The sensitivity of the model's velocity values to a change in Von Karman's constant κ. The solutions have been obtained using the values :

$\kappa = 0.4$, ————————

$\kappa + 50\% = 0.6$, — — — — — — —

and $\kappa - 50\% = 0.2$ —— —— ——

15a compares some vertical profiles and 15b some time series of velocity.

In 15b the heights corresponding to the z level indices are :

m =	8	12	16	20	26	
z =	0.13	0.58	2.51	10.96	100.0	cm.

The phase angle annotation is the same as that for Figure 11.

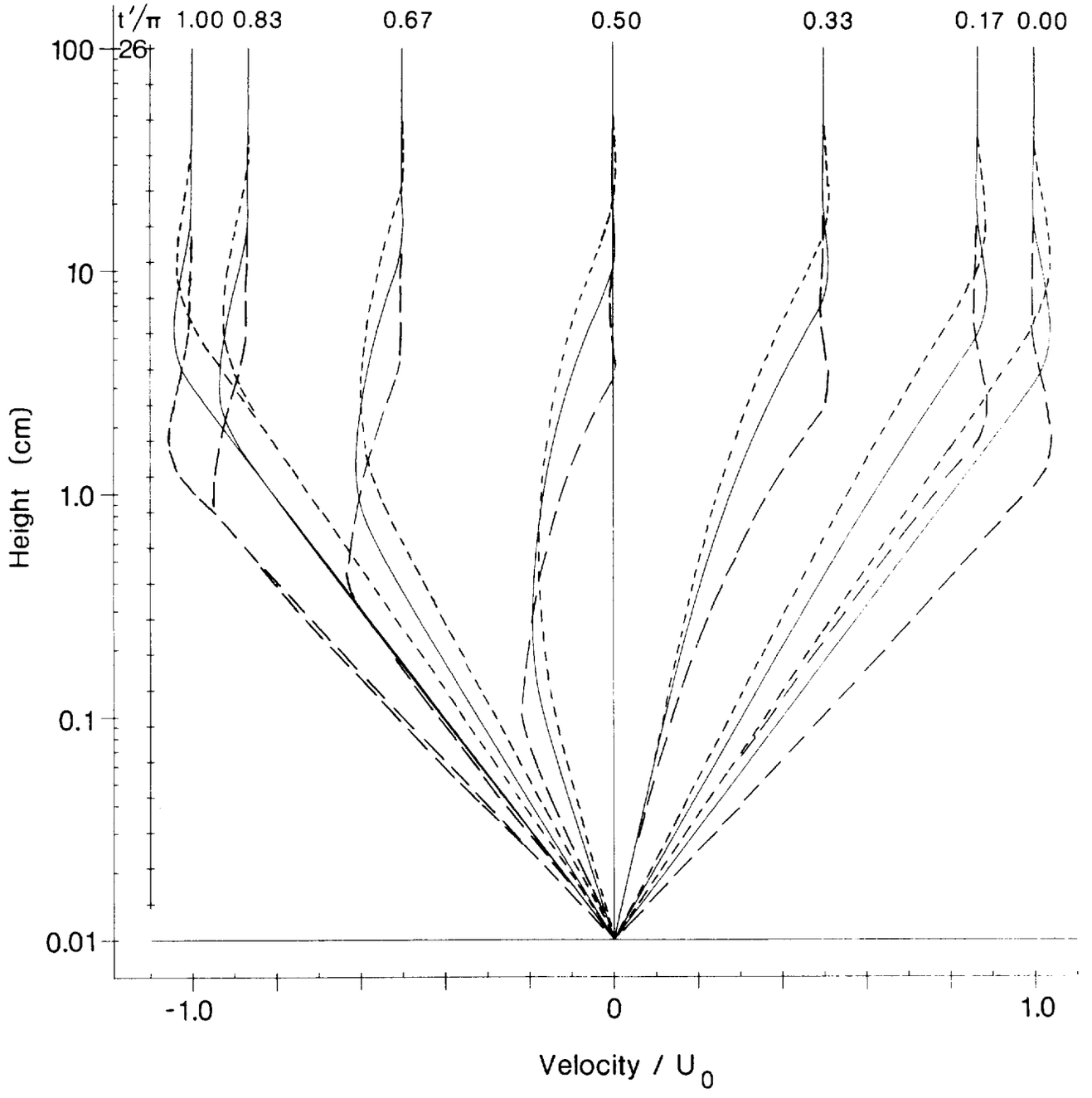

Figure 15a: Velocity profiles.

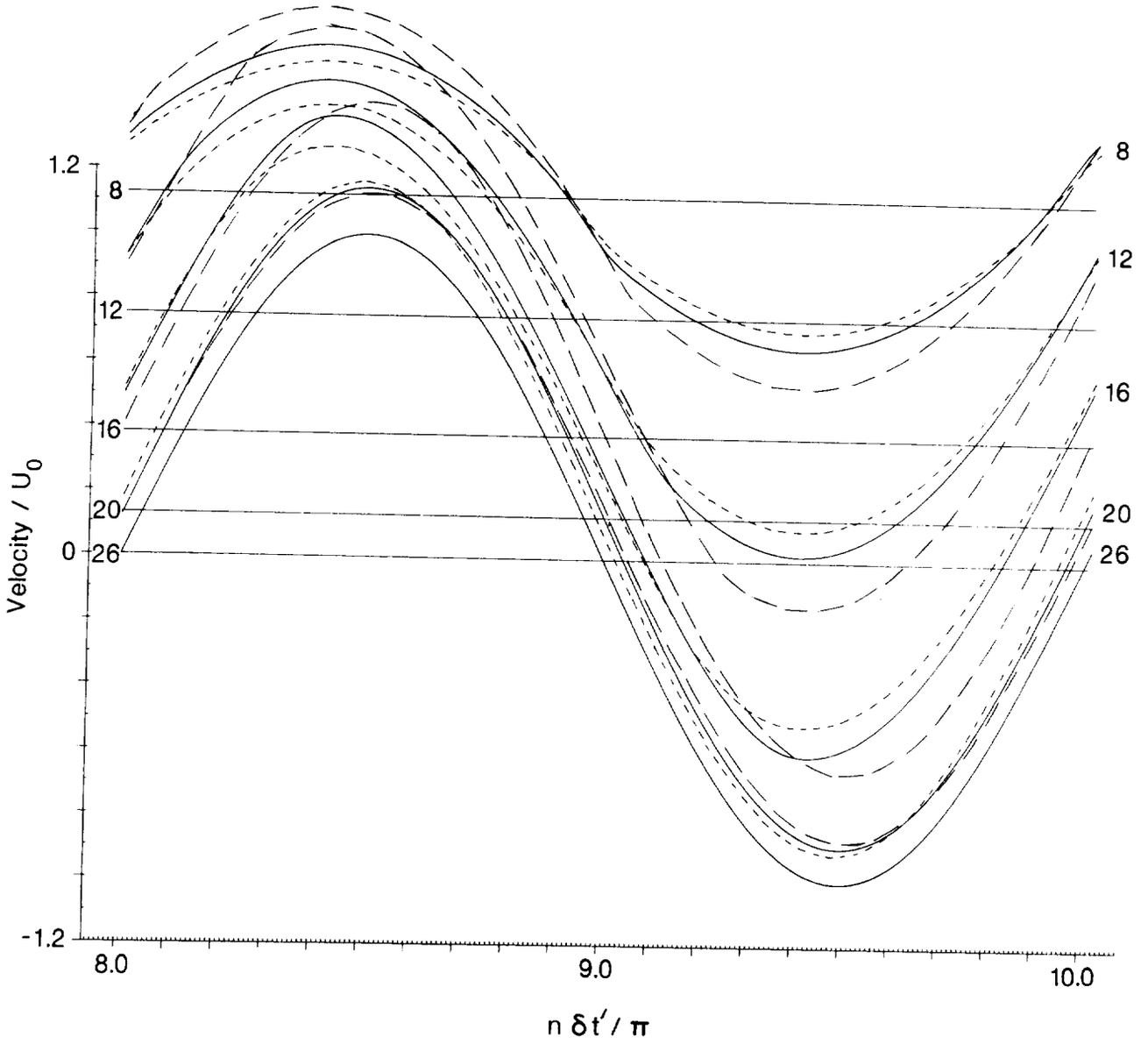

Figure 15b: Velocity time series.

Figure 16: The sensitivity of the model's energy values to changes in Von Karman's constant κ. Figure 16a compares profiles, and 16b time series, from solutions obtained with the values :

κ = 0.4, ————————————

κ + 50% = 0.6. — — — — — — — —

and κ - 50% = 0.2. —— —— —— —

For details of the annotation see Figure 15.

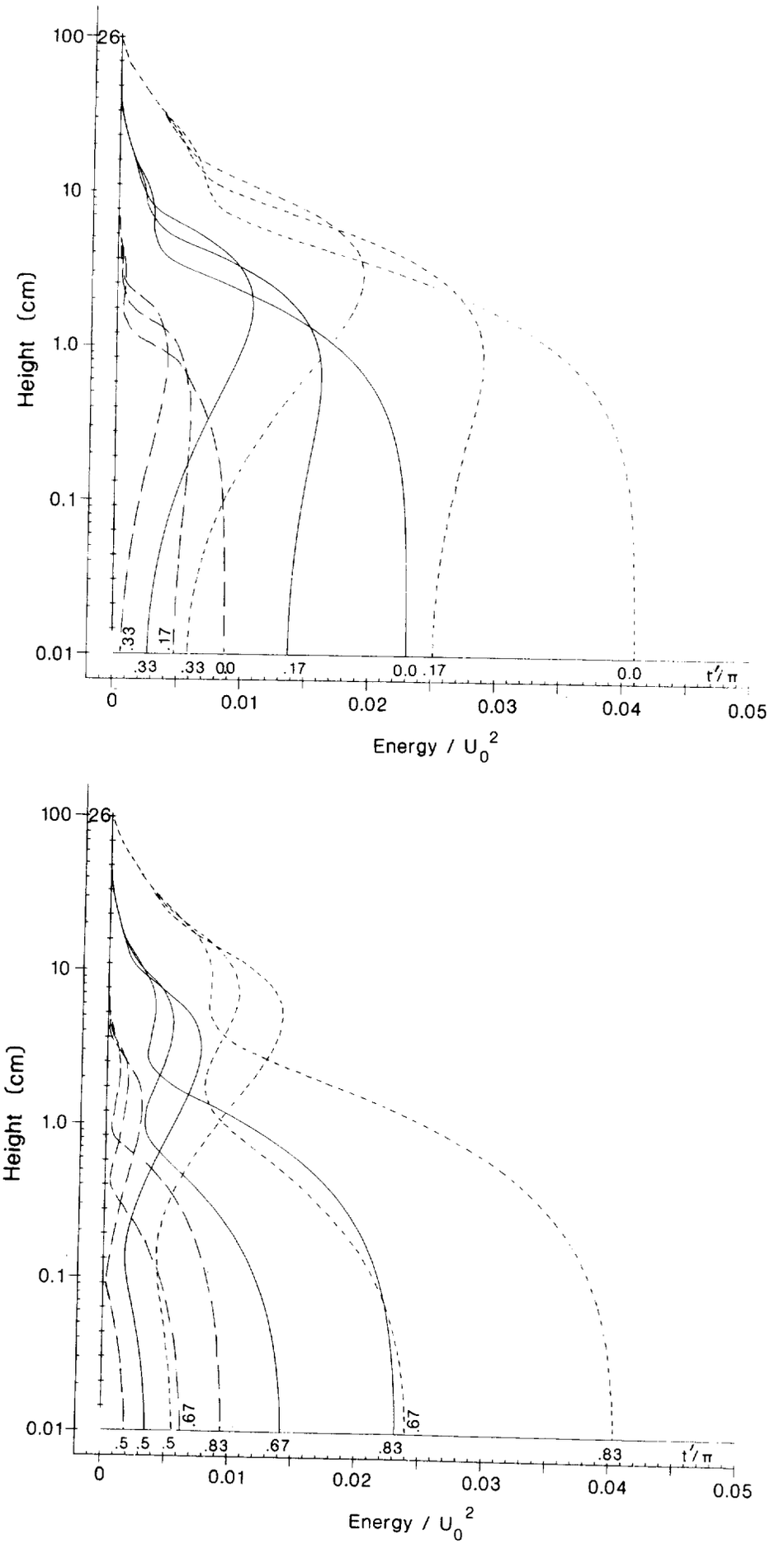

Figure 16a: Energy profiles.

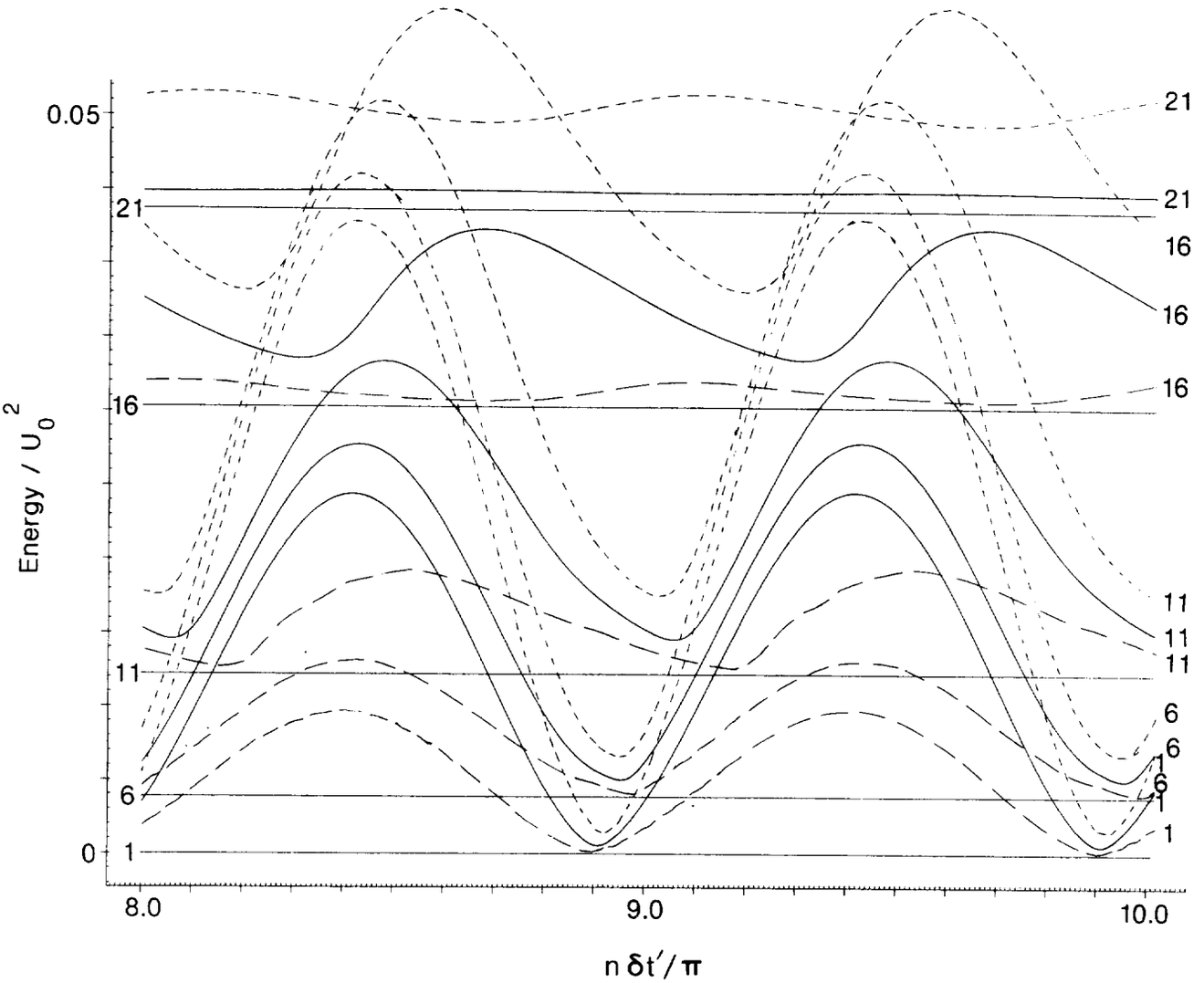

Figure 16b: Energy time series.

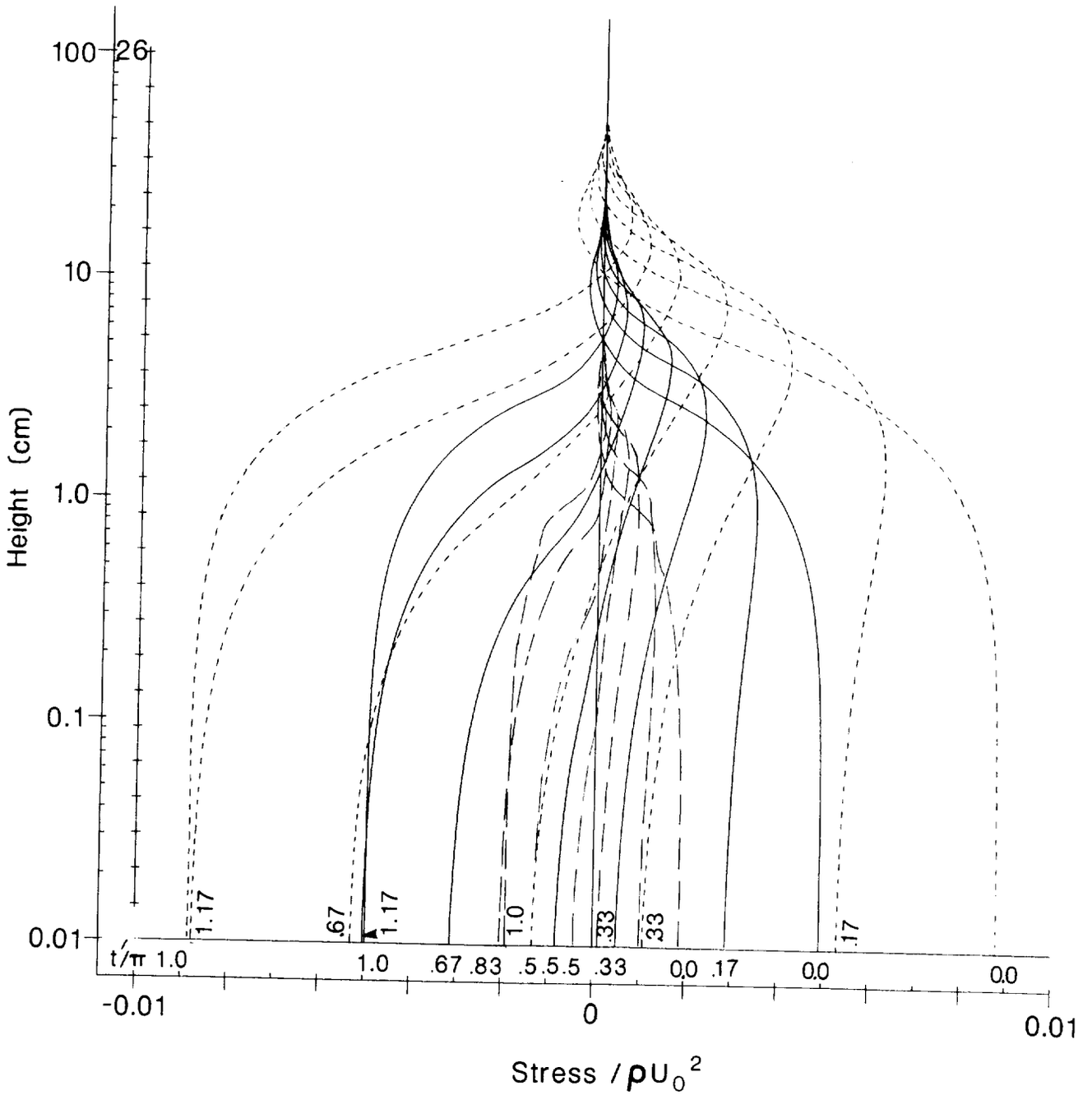

Figure 17a: Shear stress profiles.

Figure 17: The sensitivity of the model's shear stress values to a change in Von Karman's constant κ. Figure 17a compares profiles, and 17b time series, from solutions obtained with the values :

κ = 0.4, ——————————

κ + 50% = 0.6, — — — — — — —

and κ - 50% = 0.2. —— —— —— ——

For details of annotation see Figure 15.

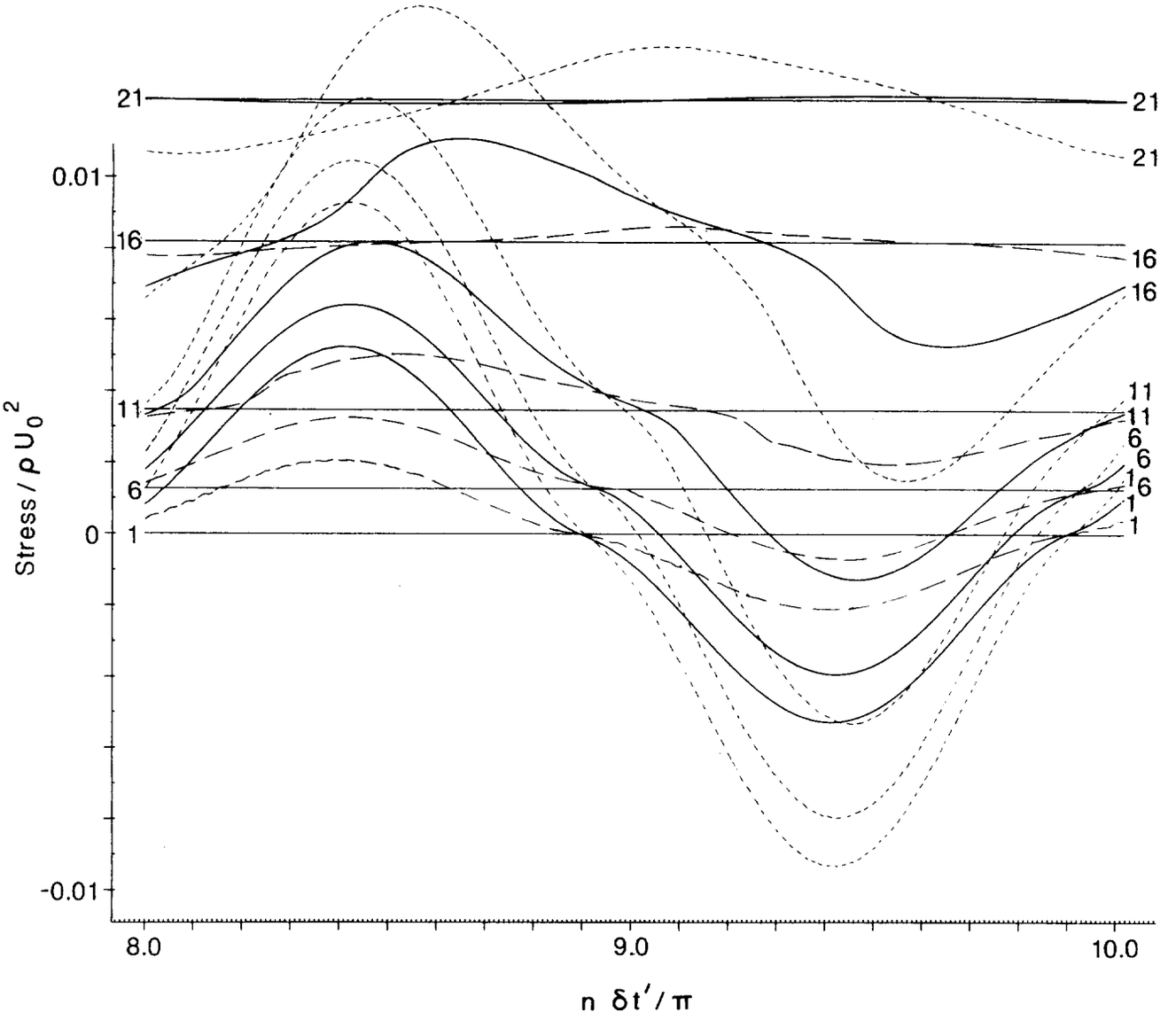

Figure 17b: Shear stress time series.

Figure 18: The comparison of energy values obtained by the model for an oscillatory flow of tidal period in shallow water, using different formulations for the dissipation term, namely :

$$(b')^{3/2} \simeq b'^{n+1}(b'^{n})^{1/2} \qquad \text{———————} \quad \text{(B1)}$$

and $$(b')^{3/2} \simeq 0.75\, b'^{n+1}(b'^{n})^{1/2} + 0.25\,(b'^{n})^{3/2} \qquad \text{– – – – – – –} \quad \text{(B3)}$$

Figure 18a compares profiles, while 18b compares time series.

The z values corresponding to the level indices used in 18b are as follows :

m	=	1	7	16	25	50	
z	=	0.10	0.42	3.54	29.42	1843.5	cm

The phase angles t' in Figure 18a have been reduced to lie in the interval $[0,2\pi]$.

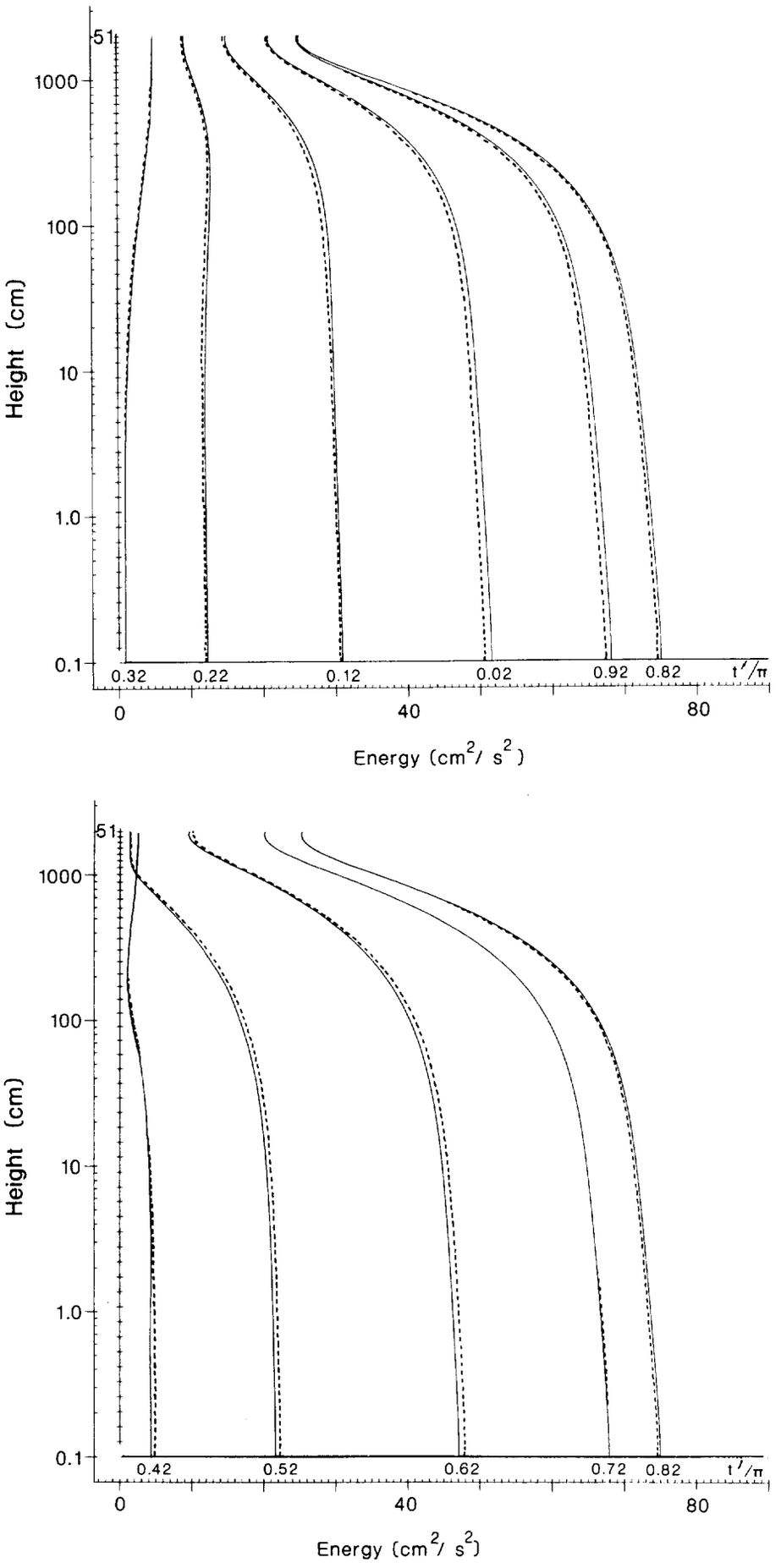

Figure 18a: Energy profiles.

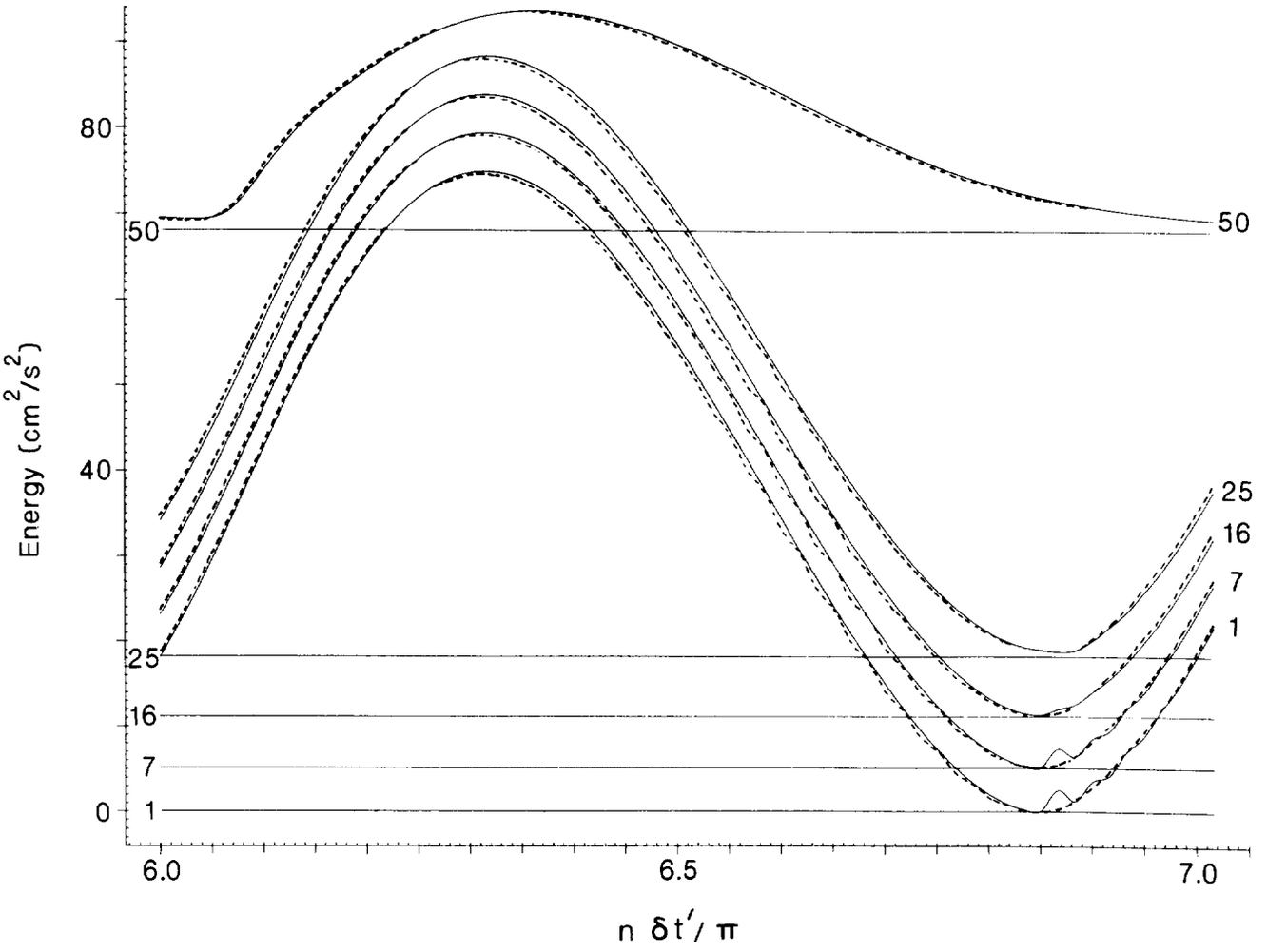

Figure 18b: Energy time series.

Figure 19: The comparison of defect velocity components from the present model with the results from Vager and Kagan's (V&K) model. Figure 19a contains the u and 19b the v component of velocity.

The z values equivalent to the level indices are :

m	Model z/z_1	V&K z_n
1	10^{-4}	10^{-4}
28	0.050	0.05
31	0.100	0.10
34	0.200	0.19
37	0.398	0.38
41	1.000	1.00

The present model's solution ————————————
Points taken from the Vager & Kagan's graphs × × ×
The 'smooth' curves joining the V&K points. — — — — — — —

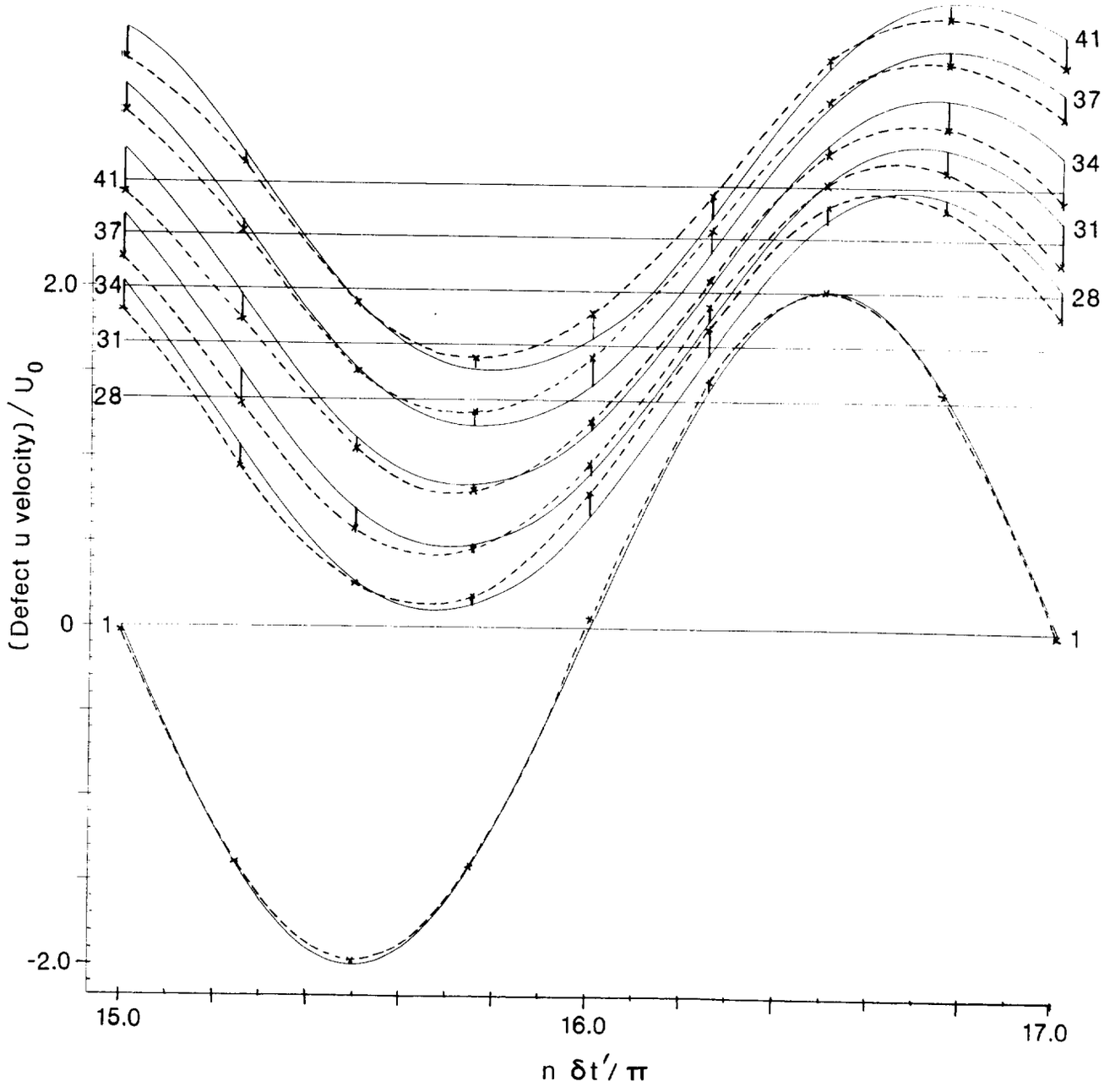

Figure 19a: Defect velocity, u component.

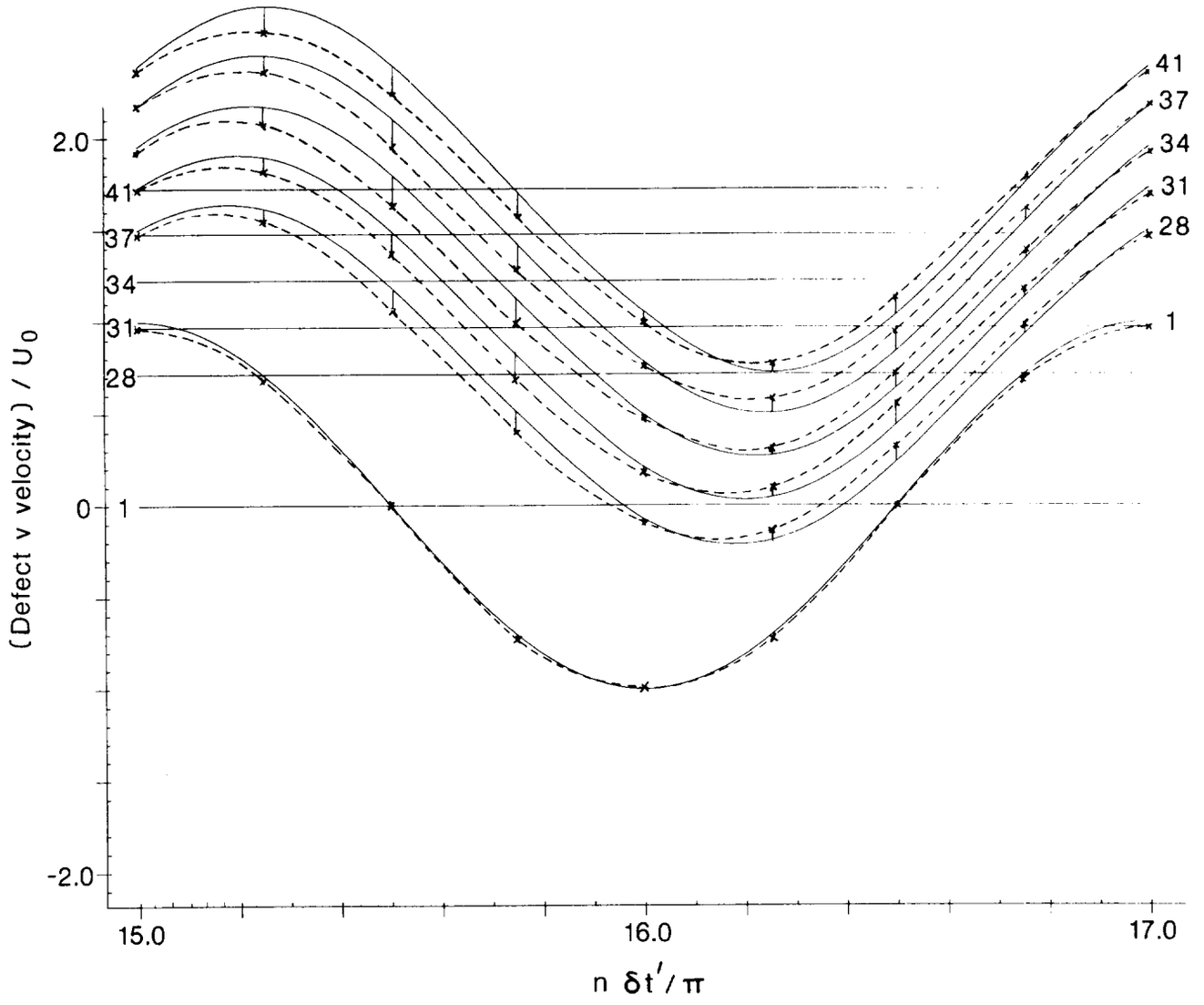

Figure 19b: Defect velocity, v component.

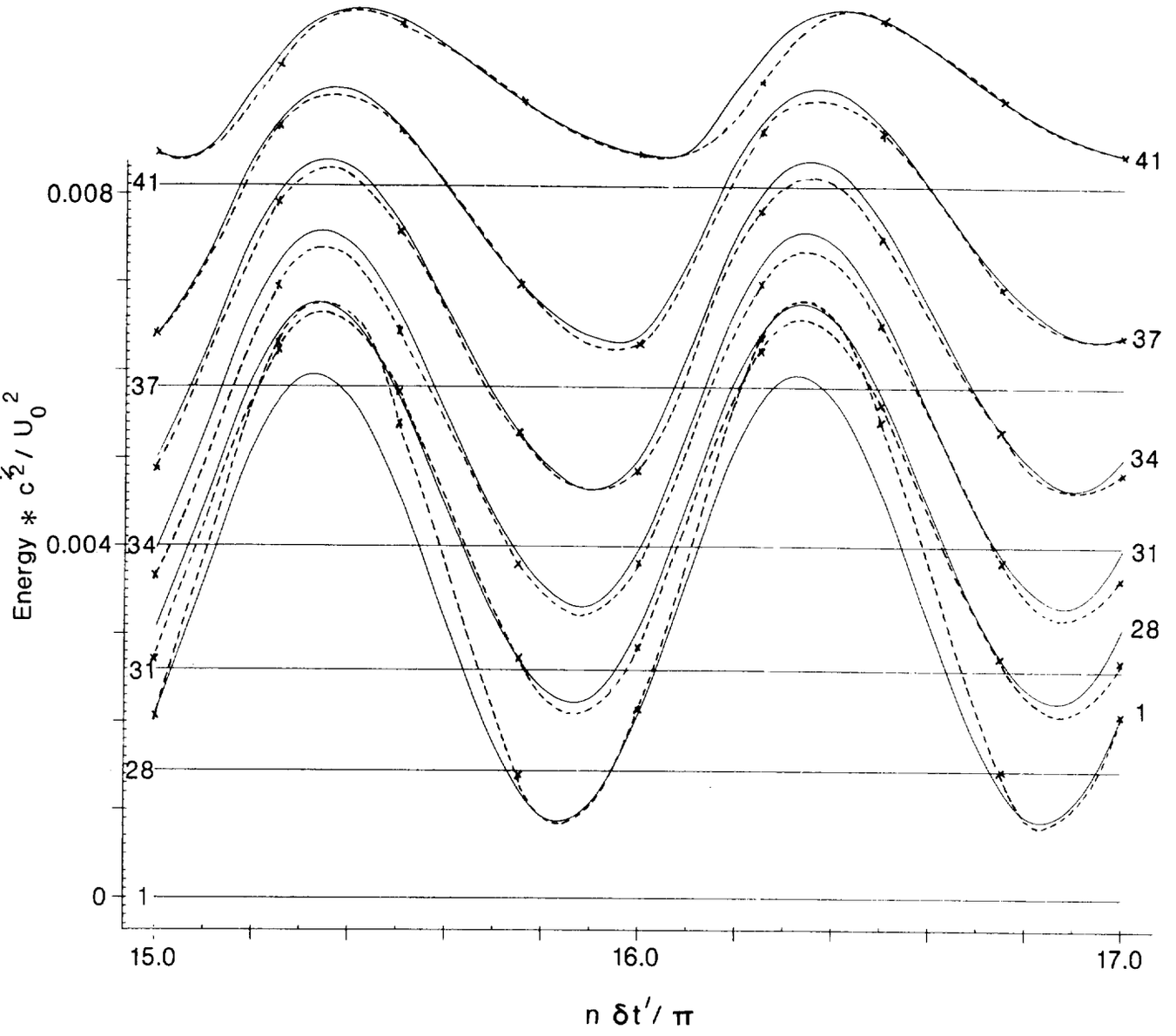

Figure 20: Comparison of the energy time series from the present model with the results from Vager and Kagan's model. Annotation details are as for Figure 19.

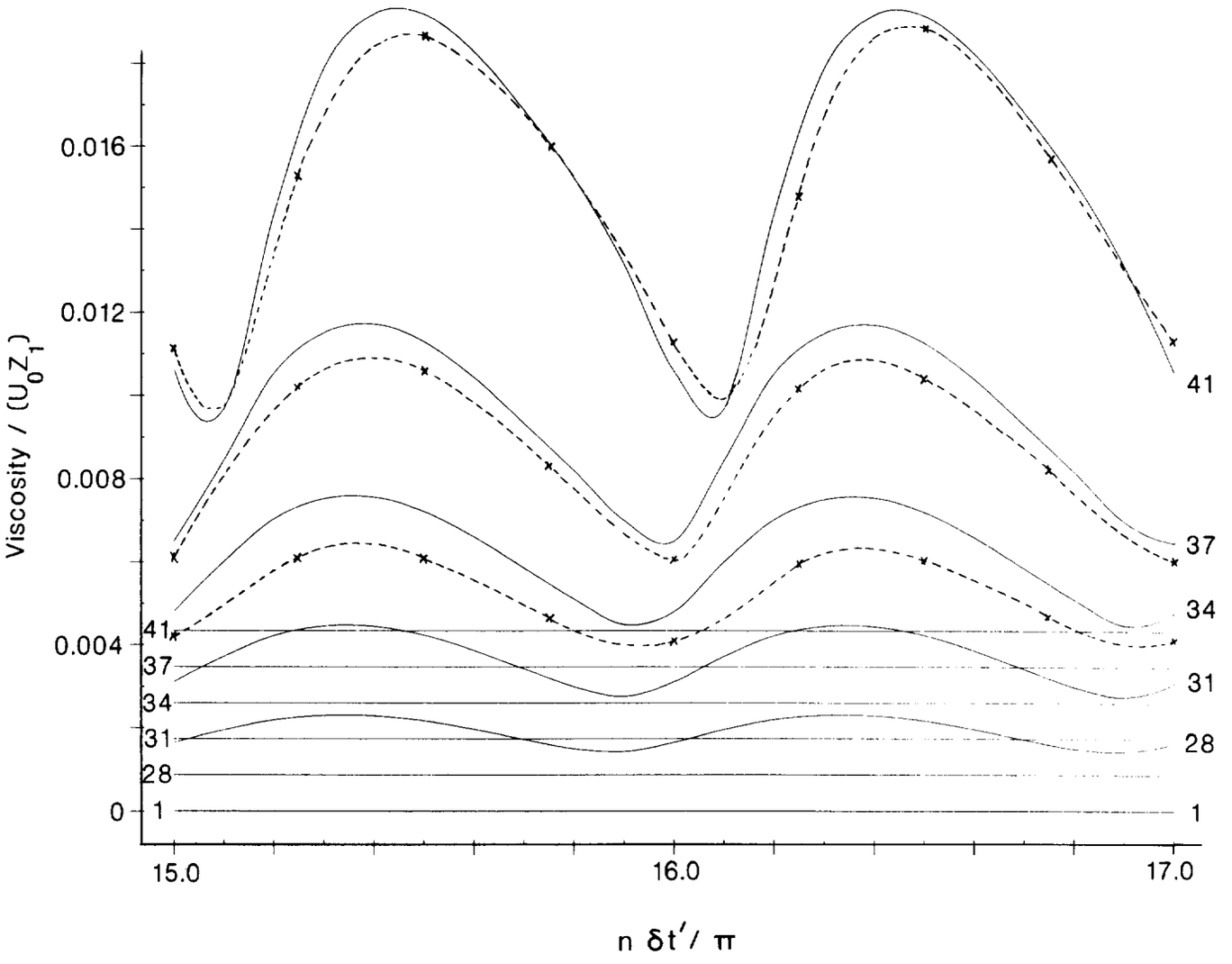

Figure 21: Comparison of eddy viscosity time series from the present model with the results from Vager and Kagan's model. Details of the annotation and indexing are as for Figure 19. Reliable comparisons were possible only for levels 34, 37 and 41.

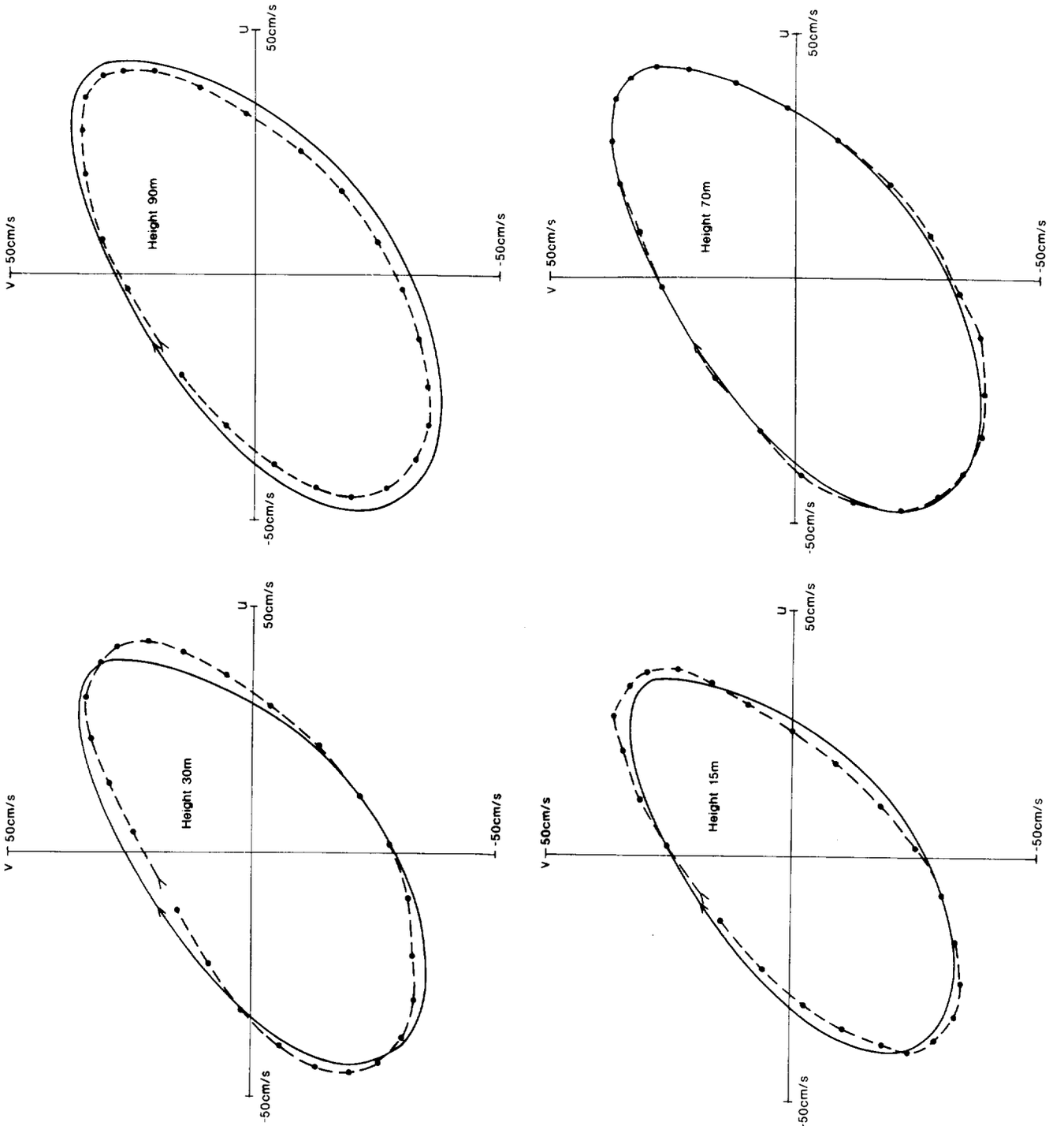

Tidal velocity ellipses.

Figure 22: Comparison of the model's velocity solution with the ensemble averaged velocities obtained from current meters deployed near the Scillies. The velocities at each meter level are plotted as ellipses over one cycle. The model's values plotted were obtained using constituents for (U,V) which matched the model and data at 70m as closely as possible.

Model's velocity solution (u,v) ——————

Velocities from current meter data ←— — —●— — —●— — —●—

The arrow drawn on each ellipse marks the position of the first point on the ellipse.

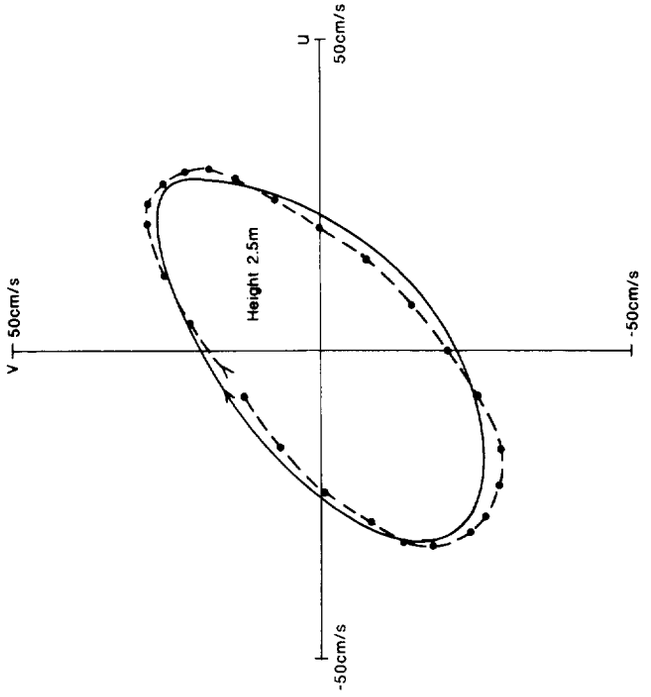

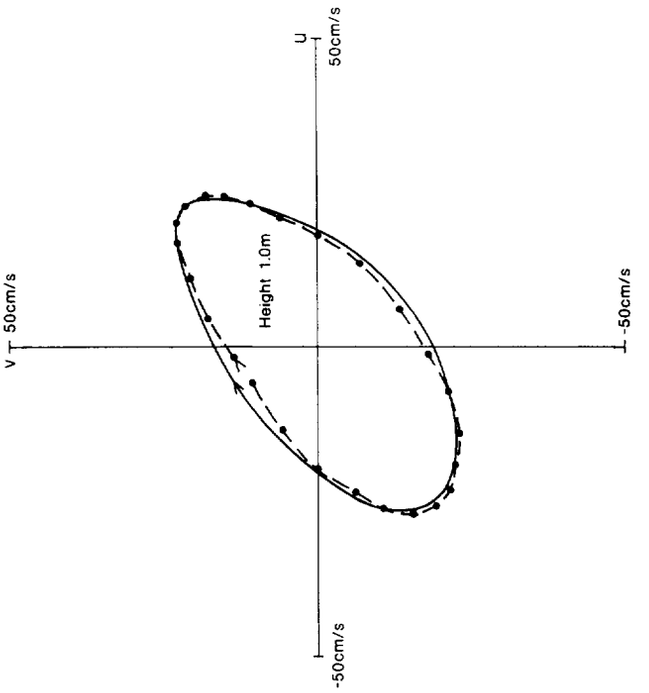

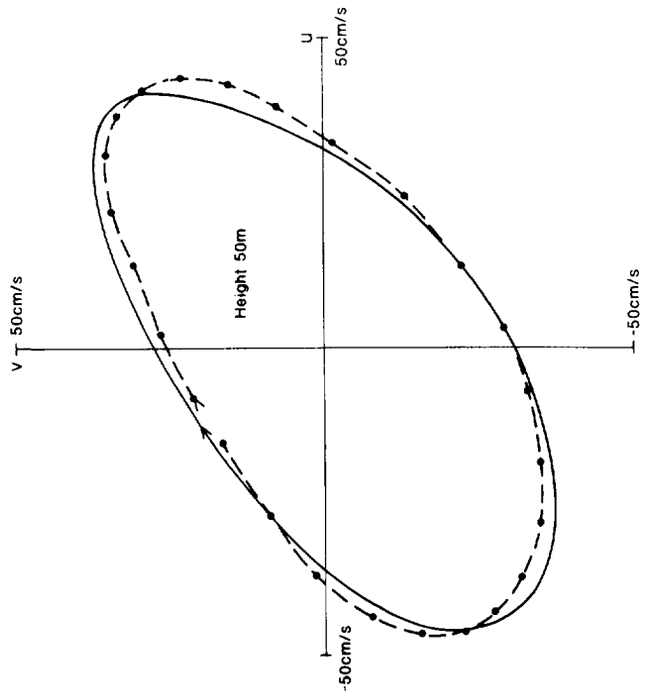

Figure 22: continued

Figure 23: Comparison of ellipse property profiles with those from current meter data, using the present model's solutions obtained for various values of z_o and two values of κ.

Since the direction of north and the start of the time series are arbitrary, the ellipse orientations (γ) and phases (ψ) can be shifted so that they are identical at 70m without any inconsistency. The adjustments made to each of the model's γ and ψ profiles are given in the table below.

In order to provide as much detail as possible, the graphs are drawn with offset origins.

Current meter data values				●
Model values using: κ	z_o cm	Adjustments: ψ_o	γ_o	
0.40	0.4	0.0	+0.3	———
0.40	0.1	-2.9	-1.8	.....
0.40	1.0	-0.4	+0.1	— — — —
0.35	0.4	-1.6	-0.8	+

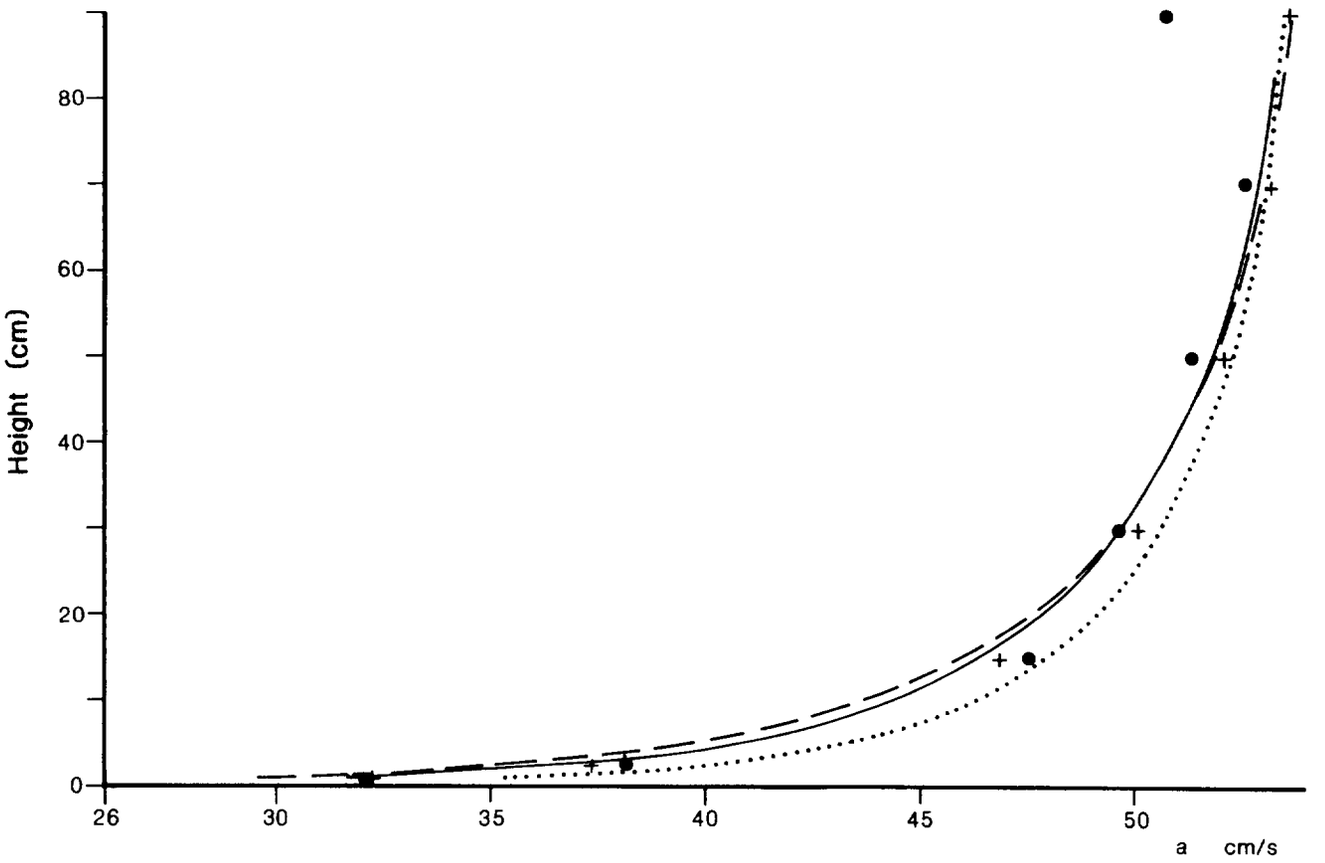

Figure 23a: Profiles of semi-major axes (a).

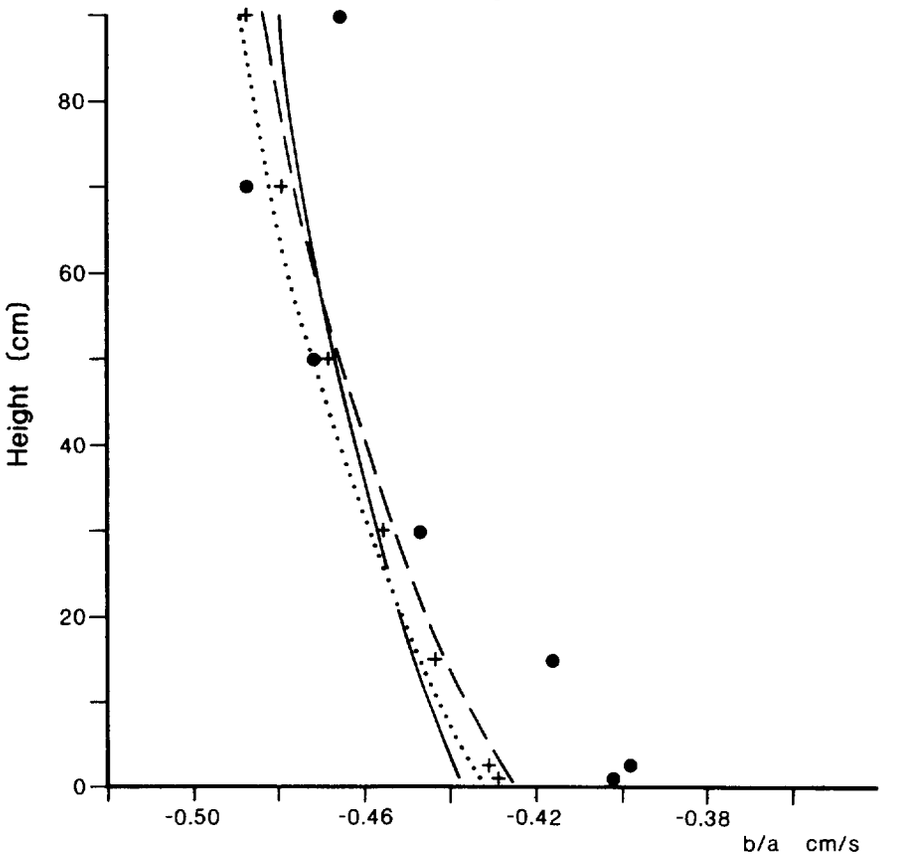

Figures 23b: Profiles of the ratio semi-minor / major axes (b/a).

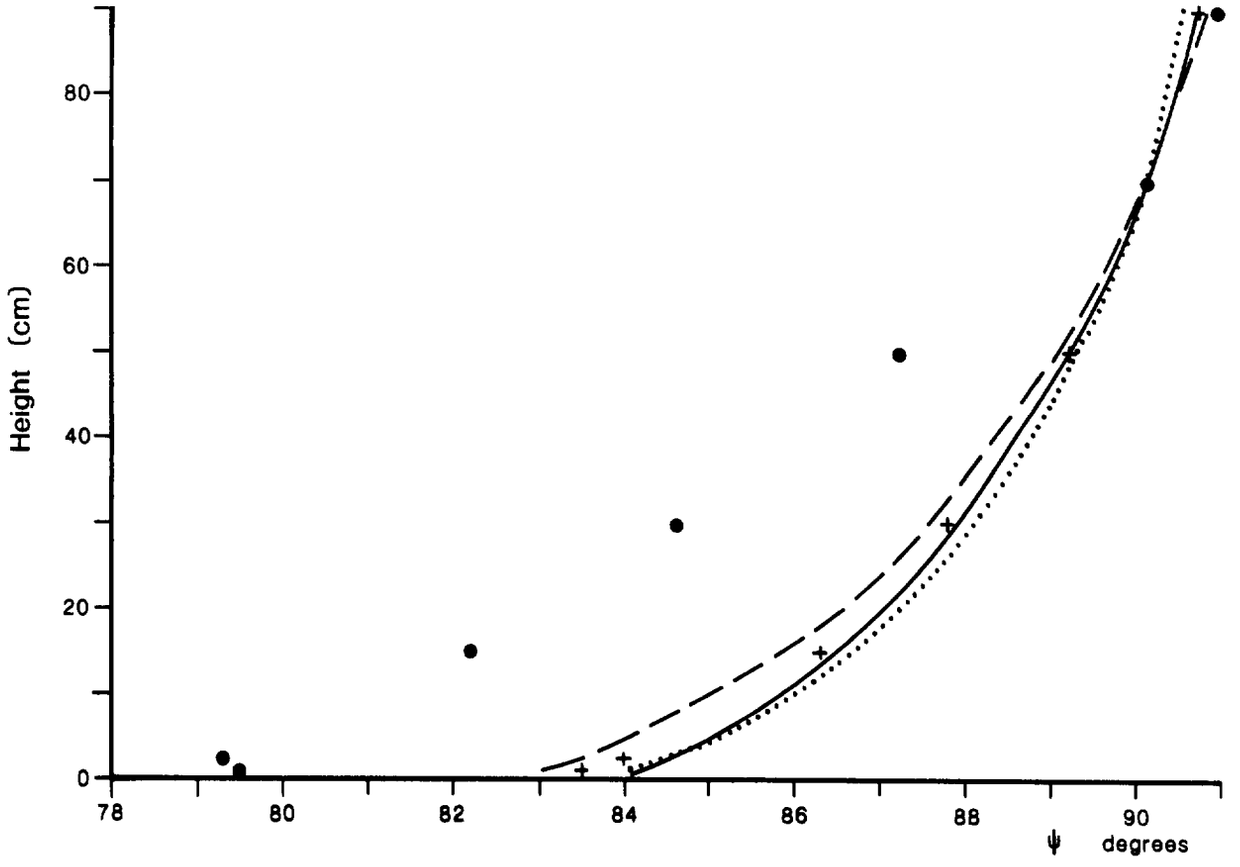

Figure 23c: Profiles of ellipse phases (ψ).

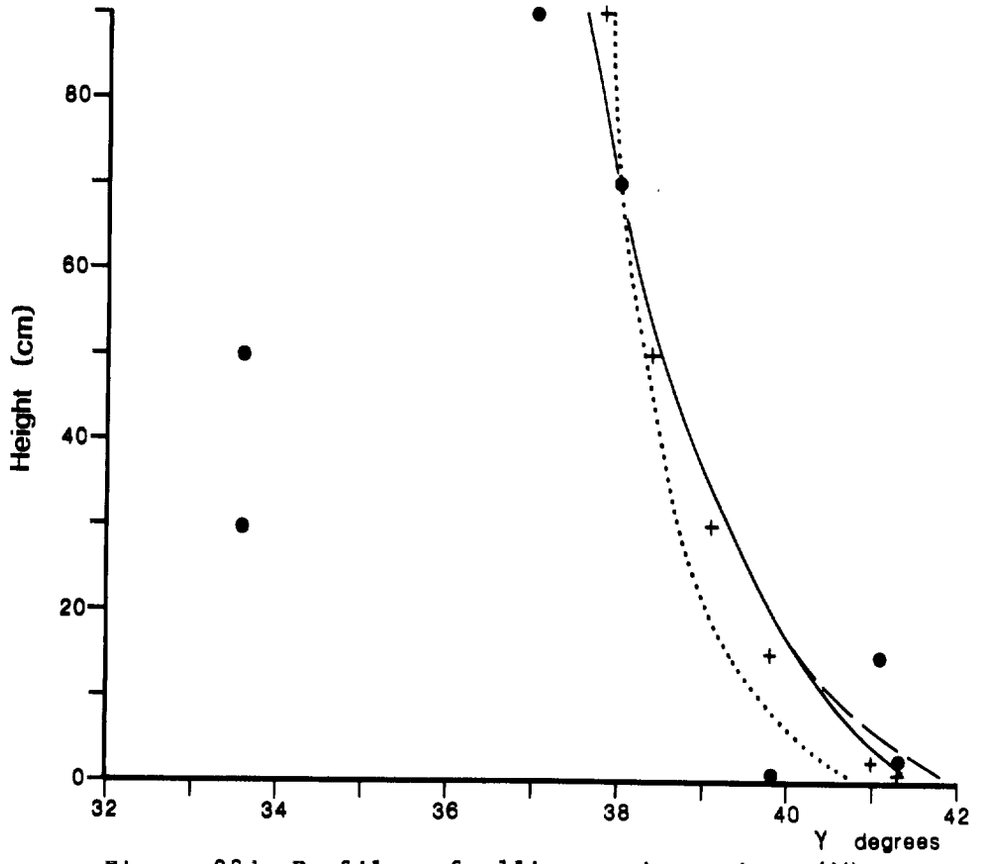

Figure 23d: Profiles of ellipse orientations (γ).